TECHNISCHE UNIVERSITÄT MÜNCHEN
Lehrstuhl für Steuerungs- und Regelungstechnik

Human-centered control design for haptic telepresence systems over communication networks

Iason Vittorias

Vollständiger Abdruck der von der Fakultät für Elektrotechnik und Informationstechnik der Technischen Universität München zur Erlangung des akademischen Grades eines

Doktor-Ingenieurs (Dr.-Ing.)

genehmigten Dissertation.

Vorsitzender:	Univ.-Prof. Paolo Lugli, Ph.D.

Prüfer der Dissertation:

1. Univ.-Prof. Dr.-Ing. Sandra Hirche

2. Univ.-Prof. Dr.-Ing. Eckehard Steinbach

Die Dissertation wurde am 10.10.2011 bei der Technischen Universität München eingereicht und durch die Fakultät für Elektrotechnik und Informationstechnik am 24.04.2012 angenommen.

Preface

This thesis has emerged from almost four years of work at the Institute of Automatic Control Engineering (LSR), Technische Universität München (TUM) where I stayed from 2008 until now. It was supported in part by the Alexander S. Onassis Public Benefit Foundation and by the German Research Foundation (DFG) within the Collaborative Research Center SFB453 on 'High-Fidelity Telepresence and Teleaction'.

First and foremost, I would like to express my gratitude to my advisor Prof. Sandra Hirche for the opportunity she gave me to work close to her, and for showing trust in my abilities. Her suggestions, her patient guidance along all my way, and her genuine interest on my improvement make her an unforgettable part of these years. I am also very grateful to the great administrative support I received in my institute, treated with professionalism and help in every matter I had. The LSR will always be an important step of my career and a paradigm for every research institute.

Special thanks go to my closest collaborators, Prof. Eckehard Steinbach and Julius Kammerl (LMT, TU München). Many research results presented in this thesis were inspired by fruitful discussions and joint work I had with them in three joyful years of collaboration. Their opinion always helped me think out of my box and go one step ahead.

Many heartfelt thanks go to all of my teammates, who always offered me assistance, whether for research or for my daily life in Munich. Special thanks go to the friend and colleague Tilemachos Matiakis, for his guidance at my early PhD steps, and to Markus Rank, for the unforgettable conference trips and his constructive feedback during my rehearsals; finally to my office-mates Andreas Schmid, Arman Kiani, Zheng Wang, Andrea Bauer, Daniel Althoff, Michael Scheint and Tianguang Zhang for the nice atmosphere in the offices we shared during my stay in LSR. Special thanks go to my colleagues Thomas Schauss, Carolina Passenberg and Angelika Peer for the useful and critical technical and theoretical comments and support. I also have to mention the stimulus I received from the students I supervised, especially from Hamza Ben Rached - his master thesis has been a valuable support. My friends in Munich, Harrys, Kimon, Theo, Panos and Akis have also been a great source of inspiration and funny moments.

Finally, nothing would be realizable without the deep love of my family, Niki, Spiros, Iakovos, Ewa, Antonis and Stefania, who supported me to begin my PhD, tolerated my absence and my lack of time all these years and still passionately support me at every step. Last but not least, I am very grateful to my girlfriend Christina for her love, her unforgettable patience hearing up my problems, and for the very happy moments she gave me during this challenging period of my life.

Munich, October 2011   Iason Vittorias

to Niki
...

Abstract

Telepresence systems allow a human operator to act in a remote, inaccessible, dangerous or scaled environment and receive feedback from it without physically being there. Applications range from underwater and space teleoperation to minimally invasive surgery and nano-manipulation. The haptic (motion and force) feedback system - additional to the auditory and visual modality - enables the realistic and efficient manipulation in the remote environment. Ideally, a telepresence system is transparent, i.e. the human cannot distinguish between direct and tele-interaction with the remote environment.

Stability and transparency of haptic telepresence systems over non-ideal communication networks are challenging control problems. The human operator and the remote environment are both unknown dynamical systems and parts of a global closed control loop. Additionally, the human operator plays a special role in the closed control loop, in that he/she a) is coupled with the telepresence system through energy exchange, affecting it with his/her dynamics, and b) perceives the remote environment through the telepresence system with the degree of transparency strongly influencing his/her evaluation thereof. Consequently, the human operator should be an inextricable component of the control design process. The global control loop is closed through a communication network with time delay and other network-induced unreliabilities, such as packet loss. Without further control measures this may degrade the transparency of the telepresence system and even destabilize it. An additional challenge are the limited network resources, e.g. in underwater or space teleoperation. The ultimate goal would be to mitigate this, without impairing the system stability or distorting the human user experience.

This dissertation provides a comprehensive control-design concept for telepresence systems over non-ideal communication networks by bringing the perspectives of stability, transparency, and network utilization together using a common point of reference: the human operator. A novel control framework is proposed, in which the exact modeling of dynamics is circumvented through the use of the theory of dissipative systems. We manage to guarantee stability with communication unreliabilities and to improve the transparency of the system despite having only approximate knowledge on the human operator's (or other subsystems') energetic behavior. Unique compared to existing literature is the utilization of the grip force of a human operator. Using this haptic measure, the human arm dynamics can be estimated online and used for the parametrization of the control mechanisms. Finally, with regard to the communication-related challenges, an efficient method of transmitting haptic data is developed considering human factors, such as the haptic discrimination abilities of the human and the task performance. Haptic data can be reduced significantly, without impairing the human's perception of the remote environment. The proposed methods are, throughout the thesis, extensively evaluated with experiments on telepresence systems with multiple degrees-of-freedom.

Zusammenfassung

Telepräsenzsysteme ermöglichen dem Menschen, in einer entfernten, unerreichbaren, gefährlichen oder skalierten Umgebung zu agieren, ohne selbst vor Ort zu sein. Die vielfältigen Anwendungsmöglichkeiten erstrecken sich von der Teleoperation unter Wasser und im Weltraum bis hin zu minimal-invasiver Chirurgie und Nanomanipulation. Dabei ermöglicht erst die haptische Modalität (Bewegung und Kraft) - zusätzlich zur visuellen und auditorischen Modalität - die wirklichkeitsnahe und effiziente Manipulation in der entfernten Umgebung. Im Idealfall ist das Telepräsenzsystem transparent für den/die Bediener/in, d.h. er/sie kann nicht zwischen direkter und Tele-Interaktion mit der entfernten Umgebung unterscheiden.

Die Gewährleistung von Stabilität und Transparenz haptischer Telepräsenzsysteme über nicht-ideale Kommunikationsnetzwerke stellt dabei eine große Herausforderung für die Regelung dar. Der bedienende Mensch und die entfernte Umgebung sind Teilsysteme mit weitestgehend unbekannter Dynamik, welche Teil eines global geschlossenen Regelkreis sind. Eine besondere Rolle nimmt dabei der bedienende Mensch ein, da er/sie a) durch Energieaustausch mit dem Telepräsenzsystem verkoppelt ist und dessen Dynamik beeinflusst, und b) über das Telepräsenzsystem die Umgebung sensorisch erfasst und die empfundene Wirklichkeitsnähe stark von der Wahl der Regelungalgorithmen abhängt. Aus diesem Grund ist der Mensch ein unverzichtbares Element beim Regelungsentwurf. Darüber hinaus ist der geschlossene Regelkreis mit Zeitverzögerung und anderen kommunikationsnetzinduzierten Unsicherheiten, wie z.B. Paketverlust, behaftet, was ohne geeignete Regelungsmechanismen die Stabilität und Transparenz des Systems gefährdet. Zusätzlich stellen begrenzte Kommunikationsnetzresourcen, wie sie z.B. unter Wasser oder im Weltraum gegeben sind, eine weitere Herausforderung dar. Aus diesem Grund ist die effiziente Übertragung haptischer Daten unter der Berücksichtigung von Stabilität und menschlicher Wahrnehmung von großer Wichtigkeit.

Diese Dissertation stellt ein umfassendes Regelungsentwurfskonzept für Telepräsenzsysteme über nicht-ideale Kommunikationsnetze vor, wobei die Kriterien Stabilität, Regelungsperformanz und Kommunikationsnetzauslastung im Bezug auf den Menschen evaluiert werden. Ein neuartiges Regelungskonzept wird vorgestellt, welches auf die exakte Modellierung des Menschen (oder anderer Teilsysteme) mittels der Theorie dissipativer Systeme verzichtet. Für den Regelungsentwurf ist nur approximatives Wissen über das Energieverhalten der Subsysteme ist erforderlich, um die Stabilität des Telepräsenzsystems mit Kommunikationsunsicherheiten zu garantieren und dessen Transparenz zu verbessern. Einzigartig im Vergleich zur bisherigen Literatur, ist die Verwendung der Greifkraft des bedienenden Menschen zur Schätzung der Dynamik des menschlichen Armes, welche zur Parametrierung der Regelungsmechanismen herangezogen werden kann. Des Weiteren wird eine effiziente Methode zur Übertragung haptischer Daten vorgestellt, bei der menschliche Faktoren wie die haptisch Unterscheidungsfähigkeit des Menschen und die Aufgabenleistung berücksichtigt werden. Damit kann die Menge der zu übertragenden haptischen Daten maßgeblich reduziert werden ohne die Transparenz des Systems zu beeinträchtigen. Die vorgeschlagenen Ansätze sind in Experimenten mit Telepräsenzsystemen mit mehreren Freiheitsgraden umfangreich evaluiert worden.

Contents

List of Figures

List of Tables

Notations

Abbreviations

CAN	Controller Area Network
CD	Collision Detection
CPU	Central Processing Unit
CSMA	Carrier Sense Multiple Access
DoF	Degree of Freedom
GAS	Globally Asymptotic Stable
GST	Generalized Scattering Transformation
HLS	Hold Last Sample
HSI	Human System Interface
I/O	Input Output
IF-OFP	Input Feedforward Output Feedback Passive
IFP	Input Feedforward Passive
IP	Internet Protocol
ISO	International Organization for Standardization
ISP	Input Strict Passive
JND	Just Noticeable Difference
LCWV	Locally Computed Wave Variables
LTI	Linear Time Invariant
MAC	Medium Access Control
SISO	Singe Input Single Output
ST	Scattering Transformation
OFP	Output Feedback Passive
OSP	Output Strict Passive
OP	Human Operator
TCP	Transport Control Protocol
TPTA	Telepresence and Teleaction
TO	Teleoperator
UDP	User Datagram Protocol
VSP	Very-Strongly Passive
WV	Wave Variables
ZSD	Zero-State Detectable

Conventions

Scalars and *Vectors* are denoted by upper and lower case letters. *Matrices* are denoted by upper case letters.

x	scalar/vector
X	matrix
$f(\cdot)$	function
$\dot{x}, \ddot{x}$	equivalent to $\frac{d}{dt}x$, $\frac{d^2}{dt^2}x$
$\|\cdot\|$	Euclidian norm
$\lambda(\cdot)$	eigenvalue

Subscripts and Superscripts

x_h	value x associated with the human
x_e	value x associated with the environment
x_t	value x associated with the teleoperator
x_l	value x associated with the left-hand side
x_r	value x associated with the right-hand side
x_m	value x associated with the master
x_s	value x associated with the slave
x^d	desired value x
x'	stands for $x(t')$
$\overline{x}$	mean of x
$\hat{x}$	estimate of x
$x_{min}(\cdot)$	stands for minimum
$x_{max}(\cdot)$	stands for maximum
$(\cdot)_{\mathbf{t}}$	translational part
$(\cdot)_{\mathbf{o}}$	orientational part

Symbols and Abbreviations

Unless otherwise denoted:

b	characteristic impedance
$b_{(\cdot)}$	damping
$B(\cdot)$	inertia matrix
$C(\cdot)$	centrifugal and Coriolis forces matrix
$D(\cdot)$	damping term matrix
$\mathbf{D}_{(\cdot)}$	control gain matrix
d_{min}	minimum damping term
e	error
E	energy
f	force
g	gravity forces
$g_{11,12,21,22}$	scaling matrix parameters
G	scaling matrix
I	stimulus intensity
$J(\cdot)$	performance index
J	manipulator jacobian
J_A	analytical jacobian
k	deadband parameter
$k_{(\cdot)}$	stiffness
K	stiffness matrix
$\mathbf{K}_{(\cdot)}$	control gain matrix
m	mass
M	inertia matrix
$\mathbf{M}_{(\cdot)}$	control gain matrix
$\mathbf{P}$	impedance parameters matrix
P	dissipativity matrix
P_{in}	power input
q	generalized coordinates
$\mathcal{Q}_{(\cdot)}$	quaternion
Q	dissipativity parameter
R	dissipativity parameter
$R(\cdot)$	Rayleigh dissipation function
R_θ	rotation matrix
S	dissipativity parameter
s	independent variable in the Laplace domain
t	time
T	round trip time delay
T_1	forward channel time delay
T_2	backward channel time delay
T_s	sampling time

u   flow vector

u system's input

$u_{l,r}$ transformed variable on left/right hand-side

v   linear velocity vector

V storage function

x position

$\dot{x}$ velocity

$\ddot{x}$ acceleration

x   fused multi-DoF vector

y   effort vector

y system's output

Z mechanical impedance

α velocity-proportion for deadband

$\gamma_{(\cdot)}$ small gain

δ IFP-property parameter

Δ_x deadband

ϵ OFP-property parameter

$\boldsymbol{\epsilon}$ quaternion parameter

θ transformation angle

κ Weber constant

$\lambda(\cdot)$ eigenvalue

$\xi_{11,12,21,22}$ general scattering transformation matrix parameters

Ξ generalized scattering transformation matrix

Σ system

$\tau_{(\cdot)}$ torque

$\upsilon_{l,r}$ backward channel transformed variable on left/right hand-side

ϕ velocity-adaptive deadband parameter

ω angular frequency

$\boldsymbol{\omega}$ angular velocity vector

$\Omega_{(\cdot)}$ multi-DoF deadband matrix

1 Introduction

1.1 Haptic telepresence systems

"People are living their lives remotely from the safety of their own homes via robotic surrogates – sexy, physically perfect mechanical representations of themselves" [112].

1.1.1 Vision and challenges

In the year 2011, the sentence above may sound fictional, and is indeed, as it is cited from the film 'Surrogates' [112]. Seen from another point of view though, it might only be one slightly exaggerated scenario of the evolution that communication and interaction means will take in the upcoming future. A short historical survey will give further insight to that. Graham Bell in 1875 developed the first acoustic telegraph which consisted the basis of the nowadays widely used voice-telephony. Only four years later, in 1879, the first extensions of it showed up as fictional ideas; the telephonoscope (transmits light as well as sound) was conceptually presented. It was some decades later, in 1920s, when the first video-phone was experimentally developed and some more decades until it finally really entered the market. Today, communicating by use of visual and auditive media seems very natural. Having successfully transmitted two of the five human modalities by using technical media, it no longer seems fictional to extend this concept by augmenting it with another human modality, the haptic one (motion and force). It is only a matter of time, if the trend stays the same, until the fictional and experimental concepts turn out to be everyday habit.

Multimodal telepresence (or teleoperation) systems make use of robotic and other technical media to allow a human to operate into a remote, scaled or even dangerous area without physically being there. A human operator manipulates a human system interface (HSI) and commands a remote executing robot, the teleoperator (TO). While the teleoperator interacts with the remote environment, the multi-modal sensor data - amongst them haptic signals - are fed back and displayed to the operator. A communication network realizes this transmission of the command and sensor signals between the operator and the teleoperator side, see Figure 1.1 for an illustration. The haptic feedback system - additional to the auditory and visual modality - enables the realistic and efficient manipulation in the remote environment. Whether this will be the future "telepresence-call" or not is yet to be seen. However, multimodal telepresence systems have already been used in a wide range of scenarios [143]. In space or underwater exploration the exposition of the human to a dangerous or unreachable environment is avoided [136]. Dangerous repairs on spacecrafts can for example, be performed by teleoperating a robot from the inside the space-shuttle or from earth, see for example the on-orbit servicing concepts in [135, 156] illustrated also in Figure 1.2(b). In minimally-invasive surgery the barrier exists on the skin of the human
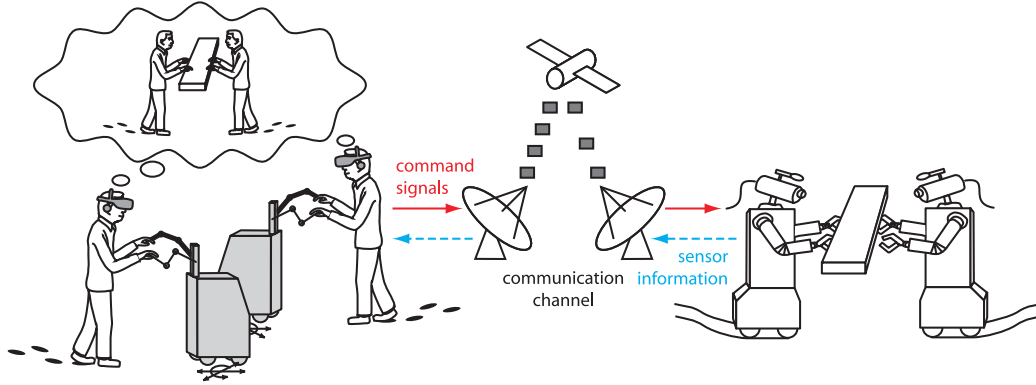
Fig. 1.1: A multimodal telepresence system over communication channel.

body, which restricts the available space and degrees of motion available for the surgeon. Teleoperation systems are employed for that [53, 54] leading to less pain and quicker recovery of the patients, see Figure 1.2(a). Moreover, in telesurgery, an operation is made possible even when the specialist is not located at the site of the patient [138].

Nevertheless, haptic telepresence systems are still highly challenging from the control point of view. Through the command and feedback signals energy is exchanged between the HSI and the teleoperator thereby closing a global control loop through the communication network. Naturally, the transmission of the command and sensor signals is afflicted with time delay. Without further control measures the telepresence system is unstable, resulting in a severe hazard for the human and the environment. The Internet is a very attractive medium for the transmission of the haptic information as it provides communication with low cost, ease of access, worldwide coverage and high flexibility. However, it introduces further destabilizing effects such as time-varying delay and data losses. Finally, the human feeling of presence is very sensitive, thus it is highly challenging for a human operator to feel like really interacting with the remote side. It is obvious, that each subcomponent of the global control loop affects the realism of the haptic telepresence systems. A telepresence system will be called *transparent* if the human operator actually feels exactly what is happening on the remote site as if the technical equipment was not present. Robust stability vs. high degree of transparency has been a challenging trade-off until today.

Human knowledge is of utmost importance in this context. First of all, in order to understand the human factors that can degrade the transparency feeling of the system and explore them to further improve the design. Secondly, in order to understand how a human operator is incorporated in the closed-loop and how his/her dynamics and mechanical energy exchange affect it. Although most of the works on haptic telepresence systems consider and intensively concentrate on all other subcomponents included in this global loop, i.e. robotic manipulators, haptic displays, controllers etc., the human operator has been poorly studied in most of the works, as will be seen later. We believe that the human operator should be an inextricable component of the control design.

We envision true immersion in a remote environment through the transmission and realistic display of multimodal data over communication networks. To achieve that, we acknowledge the importance of the human as part of the closed-loop. This thesis focuses on *haptic* telepresence systems with communication unreliabilities and examines stability,

(a) DLR's telesurgery system. Image courtesy of [54].

(b) TUM's and DLR's joint on-orbit-servicing experiment. Image courtesy of [156].

Fig. 1.2: Teleoperation systems find a wide range of application, from telesurgery with haptic-feedback in (a) to on-orbit servicing in space and under heavy time delay constraints in (b).

transparency and efficiency of the design having one common reference point: the human operator. By considering the importance of the in-the-loop human, coupled with the technical system, a *human-centered* design is sought. State-of-the-art knowledge of both his/her dynamics but also his/her perceptual characteristics is considered in all phases.

1.2 State-of-the-art

Stability over communication networks

Time-delayed teleoperation appeared in early 60ies, initially, with no force-feedback. It was then shown that time delays can be a destabilizing factor for a force-reflecting teleoperation system and stability can only be achieved by severely reducing the bandwidth of the control loop [39, 169, 9]. The development of high-fidelity, force-reflecting teleoperators, and the introduction of passivity-based algorithms in the late 1980s inspired researchers to further investigate the utilization of force-feedback. For instance, Hannaford *et al.* [57] conducted a series of experiments with and without force feedback in teleoperation systems. They reported a positive effect in task-completion time when force feedback was employed in the control loop. However, force-feedback over modern packet-switched networks, such as the Internet, would be unfeasible have not been for proper control methods that explicitly dealt with effects such as the time delay and packet loss that will be analyzed later on.

In the last two decades several methods to stabilize haptic telepresence systems with time delay have been presented; for an overview of the control challenges and a survey on current approaches see [37, 80], and [5] for a comparison of control schemes. The control architectures can be categorized based on the number and type of signals transmitted between the operator and the teleoperator side. Early approaches consider a position/force architecture [149, 40], where the position is sent to the teleoperator, the environment force is transmitted back to the HSI. In four channel architectures, see [98] for the generic definition, velocity and force information is transmitted in both directions. Ideal transparency is achieved by dynamic filters [60, 61], but only for zero delay. By proper definition of the control parameters this control scheme can be simplified to a three channel architec-

ture [60]. In order to cope with the changing environment dynamics adaptive schemes are considered in [183, 184], based on a position/force four channel architecture. Variable structure control with an impedance controller at the HSI, and a sliding mode controller to obtain robust stability is applied in [125].

The considered approaches have to assume an upper bound for the time delay - some even assume bounded environment parameters or bounds on the deviation from a nominal environment or human dynamics model [21] to provide more aggressive network control and coupling parameters. Tognetti in [165] indicates that the high variability, adaptability, and complexity of the human as long as the different hand configurations, use of different muscles and magnitudes of motion might require different configurations of the control system. Therefore, he used human impedance/admittance dynamic limits in a two-port telepresence design and a virtual coupling to guarantee stability via the Llewelyn's criterion. However, he could not circumvent the highly nonlinear human arm dynamics and additionally, his suggested work requires proper tuning to treat with the high intersubject variability. Generally speaking, in packet-switched communication networks, a bound on the delay is not reasonable. Limiting the range of possible environments is also not desired, whereas limiting the human dynamics is difficult. The well-known passivity paradigm, in contrast to model-based approaches, targets these challenges. From the approaches seen so far, it is the most powerful concept in telepresence systems analysis and synthesis as it is neither requiring bounded human/environment dynamics nor a bounded time delay.

Energy-based approaches

Over the last 20 years, control approaches based on the passivity framework and the scattering transformation have been developed in order to stabilize the teleoperation system in the presence of communication unreliabilities. All were based on one assumption, that the human operator behaves in a passive way. Inspired by power transmission lines, the scattering transformation is proposed in [4] where arbitrary large constant time-delay is addressed. This is the first time the passivity paradigm is applied to haptic telepresence systems and in the sequel it emerged to one of the most preferred tools. A network-theoretic equivalent approach was the outcome of the work in [118] where notations such as the 2-port systems passivity first appear in the teleoperation context. This seminal work contributed a lot to an easier and more digestible approach to guarantee stability of the time-delayed system. Network-theoretic inspired techniques, such as impedance matching were also made possible and achieved higher transparency at the cost of some tracking error.

In [140] a new passivity-based stabilization strategy is proposed. Instead of a priori guaranteeing the passivity of the system under all circumstances, they introduce a passivity observer that activates dissipating elements on demand to enforce passivity between the interconnected components of a teleoperation system. Sampled-based systems based on the same argument are studied in [1], whereas the time domain approach was further elaborated for time-delayed haptic telepresence systems in [6]. The same concept is also applied in purely position-transmitting teleoperation architectures in [7]. A energy-based concept similar to the passivity-paradigm is proposed in [157] to stabilize interconnected robotic systems observing their energy, using the notion of port-controlled Hamiltonian

systems. To allow for the highest transparency possible in this setting [44, 146] use a two-layered structure with a passivity/stability and a transparency layer.

In general, energy-based approaches appear rather promising as they avoid the exact modeling of the human operator or the environment dynamics. They paved the way for novel methods to address the further communication-related challenges. A packet loss compensation strategy is presented in [70], and time-varying delay is studied in [113, 22]. The scattering transformation approach has been further extended to stabilize with packet loss, see e.g. [9, 70] and with time-varying time delay [179] by guaranteeing a small gain property in the network loop. An extensive comparison study is presented in [137].

Considering the human perception

Although stability, even considering transparency, might seem sufficient for a successful haptic telepresence design, practically further significant challenges will appear. A high degree of telepresence is desired to enable a human operator to safely and successfully conduct teleoperation tasks. In recent years, much research has focused on the added value of haptic feedback for task performance and transparency [175, 31]. Although most of the approaches managed to achieve stability, even in the most unreliable communication networks without requiring bounds on the time delay, they included a very generic human model, i.e. passivity, that rendered a conservative control performance which in turn affects the human perception. High transparency is still a goal to be achieved in haptic telepresence but stability and telepresence (transparency) are generally conflicting tasks [56]. Incorporating knowledge of the human dynamics or perceptual system can relax the passivity conservatism; we will treat with that in Chapter 3.

Finally, data transmission and the efficient use of the communication resources is a very interesting area; not only have redundant data to be discarded in order not to congest the communication network, but this has to be done in stable and transparent way as well. Hirche *et al.* developed haptic data reduction mechanisms in [68, 69, 73, 71, 76] that aim to guarantee both stability, as they are used in a haptic control loop, and transparency, as the human-perception is taken into consideration. For a more thorough analysis and literature overview of this area the reader is referred to Chapter 4 which elaborates this topic.

1.3 Major contribution and outline of the dissertation

In this work, the focus is only on the haptic modality of the telepresence system. A key component of all the techniques discussed throughout this thesis is the human, which is involved at all design and evaluation phases of the telepresence system. We do not seek a pure model-based design, nor is the passivity-induced conservatism satisfying from the performance point of view. Thus, both the human operator dynamics and his/her energetic-behavior, but also its perceptual characteristics and human haptic discrimination factors are seriously taken into consideration to guarantee not only a stable, but resource-friendly and transparent telepresence systems. We acknowledge the importance of this human knowledge in the closed-loop and therefore, design both the control architecture
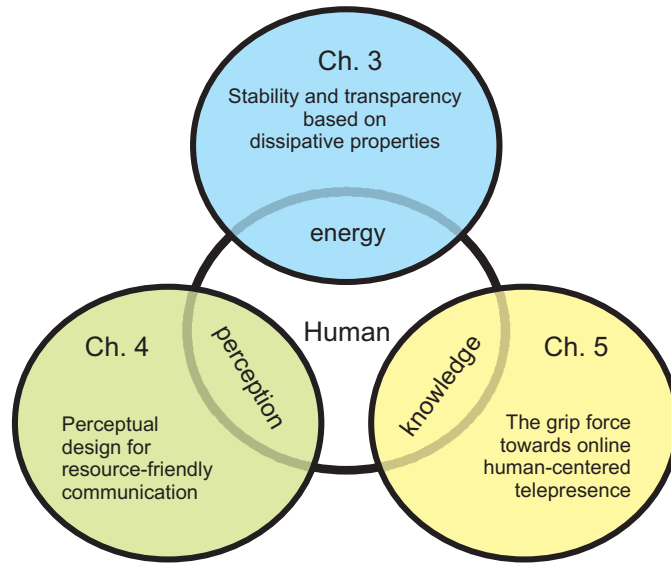
Fig. 1.3: Outline of the thesis: human-centered control design for stability, efficiency and transparency.

as well as the communication network in a human-centered manner; the role of human is graphically illustrated on Figure 1.3 in the thesis outline.

The key deliverables of this thesis are:

- a modular framework, based on the - for the first time used in this context - *dissipativity theory* to guarantee stability in the control design of a teleoperation system over a communication network and in parallel improve its transparency, despite having knowledge of just the energetic behavior of the human, the environment and/or the robotic manipulators;

- a set of data-reduction techniques to guarantee an efficient use of communication resources by considering the perceptual characteristics of the human and, therefore, avoid impairing his feeling;

- techniques and ideas on how to acquire human dynamics knowledge online by using the grip force measurement in order to estimate the human arm impedance and use it in an augmented teleoperation system to improve the telepresence realism.

The Chapter 2 sets the stage for the innovation chapters that will follow. It provides the needed control background to treat with the stability challenges, as well as human- and communication-related discussion.

In Chapter 3 a general control design framework to guarantee stability of haptic telepresence systems over communication networks is presented. The framework is considering communication unreliabilities such as time delay and packet loss that can destabilize the system. Novel enough is the employment of the theory of dissipativity, for first time used in telepresence systems. It allows, first of all, to break the passivity-induced conservatism barrier by keeping all the advantages of passivity-based approaches and, secondly, it leads to significant control performance improvement. It further allows for systems that presents

some lack/excess of passivity to be studied. Exact modeling, of the usually unknown human operator and environment dynamics, is avoided by requiring only approximate knowledge (energetic behavior) about the human/environment and/or the robotic manipulators.

In Chapter 4, a discussion on the characteristics of the human haptic perception is given and, based on that, four haptic data-reduction schemes are discussed. The deadband-based data reduction scheme allows for imperceivable data reduction of the haptic data by using the psychophysical law of Weber. An extension of this approach is proposed, considering the relative hand movement of the human which allows for further data reduction. Psychophysical studies with human subjects evaluate that the perception of the human operator is impaired when his/her interaction speed is increasing, giving thus room for further reduction rates. Psychophysical experiments validate the results. Besides that, a teleoperation architecture is given where perceptual deadband-based reduction can be applied also to systems with time delay. Finally, the haptic data reduction algorithm is extended in a multi-dimensional framework to treat with the challenge of both increasingly degrees-of-freedom in nowadays robotic systems as well as with the non-isotropy of the human perception in multi/-dimensional/-modal spaces.

Finally, in Chapter 5, driven by the findings of Chapter 3, the haptic system is augmented with one extra degree-of-freedom, namely the human grip force, which is utilized for a more realistic and transparent human-robot interaction in the setting of haptic telepresence systems. Particularly, it is shown, that the grip force intensity correlates with the human arm impedance. An easy online recognition of a tighter or looser grip can therefore be employed for the otherwise difficult estimation of the human arm impedance. Taken this human knowledge, we illustrate how the maximum displayable stiffness of a haptic device can be increased. Besides that, and in combination with the findings of Chapter 3, this human knowledge is used to enhance the control performance even with the presence of communication unreliabilities.

The thesis is concluded in Chapter 6 with a summary and a discussion about future directions.

2 Background

A haptic telepresence system basically consists of the following components:

- the human system interface (HSI), also called master manipulator, a robotic equipment able to display forces;

- the human operator, who manipulates the HSI and commands the remote executing robot,

- the telerobot (TO), also called slave manipulator, which is equipped with haptic sensors (motion, forces) to be fed back and displayed to the human operator on the HSI,

- the environment, which is an unknown system that the operator wants to interact with and explore. Finally,

- the communication network, which realizes the transmission of information and data and brings the two sites, local and remote, together.

Before we examine each component separately, the overall system architecture is illustrated on Figure 2.1. Exemplarily, in this architecture, velocity is transmitted in the forward channel and force sensed by the TO is fed back. The human operator moves his/her arm holding on to the HSI with the velocity $\dot{x}_h$ and applies the force f_h. The velocity is transmitted and a desired teleoperator velocity $\dot{x}_t^d$ is given as an input to the remote robot. It then interacts with the environment collecting force/torque measurements which are indicated by f_e. Consequently, those are fed back through the communication channel to display a desired force f_h^d to the human.

2.1 The role of human in haptics

The role of human in haptic systems is twofold. The human can not only perceive the haptic feedback offered - similar to other modalities - but also, in response, physically act upon an environment to alter it. The haptic modality is, hence, bilaterally communicated through the system. The human acts (motor skills), and affects the telepresence system with his/her dynamics, and perceives (sensory skills) through the same system, hence, evaluates the degree of realism of the system. This something totally different from the modality communication we are used so far, e.g. the visual communication is unilateral.

Understanding the human haptic behavior involves multiple fields such as mechanics, neuroscience, psychophysics, and motor control. At this part, only the physical mechanical modeling of the *human arm* will be discussed, accompanying the control design process of the next chapters. The human perceptual characteristics will be reviewed in Chapter 4.
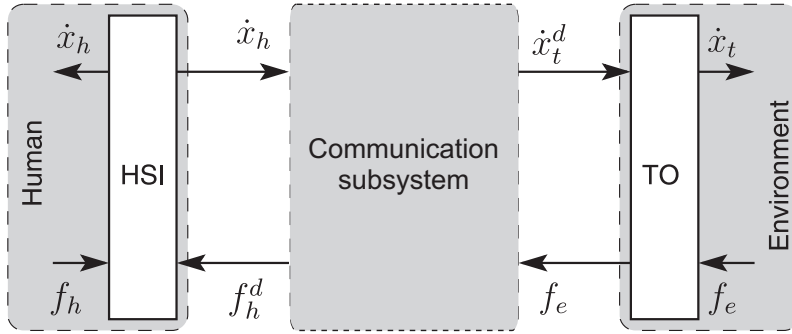
Fig. 2.1: The system architecture of a haptic telepresence system over network

2.1.1 Human arm models

The human arm is an amazingly complex system of muscles, bones, nerves and other tissues. It is so dexterous and reconfigurable, that researchers have reported many different dynamic behaviors depending on variations in arm configurations, grip forces, and application environment. Besides that, they depend on intentional and physiological aspects and vary from operator to operator. The difficulty to institute a "one-fits-all" model is obvious. Therefore, in robotics, research is usually not as concerned with the complex neuromuscular interactions within the human arm, but rather the development of a simple model that represents the effective arm dynamics as an input/output relationship.

Structured models

The role of mechanical impedance in human motor control has long been recognized in the fields of biomechanics and in robotics. Studies in biomechanics have shown that humans have the ability to actively vary both the magnitude and direction of their limb impedance, see Figure 2.3 for an illustration of the limb impedance. This capacity is employed strategically by the neural system to more successfully and efficiently perform motor control tasks [45, 163]. In robotics, the concept of impedance control dates to the 1980s and was applied to software implementations of variable stiffness and damping [142]. Subsequent research led to the use of hardware-based impedances such as series-elastic actuators for dynamic tasks like walking and running [131]. Most recently, efforts to create human-safe robots have spurred interest in impedance-based control methods and in the development of variable impedance hardware [185].

Several researchers have experimentally determined values for the human hand impedance as a function of the direction of motion in the horizontal plane and as a function of arm configuration [114, 43, 167, 34]; see [151] for an overview thereof. Mussa-Ivaldi *et al.* [114] delivered small displacements to the hand while a test subject maintained a particular posture. The force on the hand was measured and the stiffness was calculated from the force and displacement data. They concluded that the neuromuscular behavior of the arm is predominately spring-like. Flash and Mussa-Ivaldi [43] investigated the interactions between the geometrical, mechanical, and neural factors that determine arm behavior. They found that the hand stiffness is strongly dependent on the arm configu-
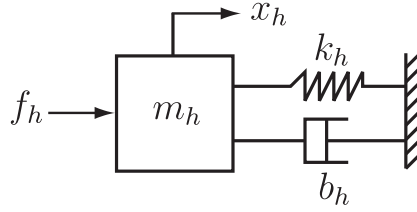
Fig. 2.2: A mass-spring-damper model.

ration. Gomi *et al.* [50] concluded that experimentally determined human-arm stiffness values vary greatly between subjects, tasks, experimental apparatuses, and perturbation patterns.

In the teleoperation context, the human arm is modeled as an impedance for the purposes of designing a teleoperation control architecture in [94]. The mass, damping and stiffness values for single degree-of-freedom linear model are experimentally determined. Lawrence [97] also suggested modeling the human as an impedance for the purposes of illustrating a telemanipulation architecture. This human impedance, Z_h, is given by the equation

$$Z_h(s) = \frac{f_h}{x_h s} = \frac{m_h s^2 + b_h s + k_h}{s},\tag{2.1}$$

where $s = j\omega$ is a complex variable, representing the Laplace domain; it will be omitted when not needed, m_h, b_h, and k_h are the mass, damping and stiffness of the human operator; f_h is the force acting on the human; x_h is the displacement of the human. The mass-spring-damper system shown in Figure 2.2 illustrates the model. Kuchenbecker *et al.* [95], used a similar mass-spring-damper model to characterize the human wrist during haptic interaction with various grasp forces, and Hajian and Howe [55] studied the mechanical impedance of the human finger. Higher order models can be employed, to better approximate the dynamics of the human arm, as for example the work of Speich *et al.* in [151], however, in this thesis only the second-order models are considered from the structured human arm models class.

A second-order linear time invariant model for the impedance of the human arm seems to have sufficient accuracy, however, in all above studies the user had some specific configuration and/or predefined grip. Besides that, at some studies the human does not apply any force but rather passively tries to preserve his configuration while forces or perturbations are applied on his arm. Humans significantly vary the impedance of their limbs during many manipulation tasks and during interactions with their environment. As long as the configuration or the experimental conditions change, *most of those models will no longer hold* making still the human arm modeling a very challenging task. Moreover, these operation conditions are not suitable for applications in which applying perturbations in real-time is not feasible, e.g. haptics or telerobotics. This fact, triggered human arm dynamics identification methodologies that run online, such the one seen in [111], where electromyogram signals collected from the upper-arm muscles are also used to identify dynamic parameters with the help of trained neural network. The impedance for elbow motion in horizontal plane was approximated with a second-order quasi-linear dynamic model using the upper-arm EMG signals, and the elbow angular position and velocity.
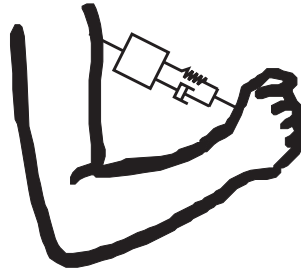
Fig. 2.3: The end-point characteristics of the human arm impedance modeled as a mass-spring-damper system.

In [67] a preliminary real-time measurement technique based on unperceivable controlled vibrations is used to estimate the user impedance. Structured human arm models will be employed at a later stage of our control design in Chapter 5.

Energy-based: Passivity

The dexterous, nonlinear and time-varying dynamics are not always sufficiently captured by the structured models presented above, especially simple LTI ones which are based on experimental time-constant conditions. The impedance of the human arm is highly adaptable; as task conditions change, the human arm impedance changes. Motivated by the large variation range of the human arm stiffness reported in literature, Hogan in his pioneering work in [78] provided a significant tool for teleroboticists, which is widely used until today in their research. It is there shown that *"despite active neuro-muscular feedback control, the human arm exhibits the impedance of a passive object"*. The muscular actuators and neural feedback driving the arm would surely constitute an active system, yet his experiments indicated that the impedance at the hand appears indistinguishable from that of a passive object. As will be seen later on in this chapter, the passivity property of the human arm is very useful to guarantee stability of the global haptic teleoperation system. It avoids an exact modeling of the human arm dynamics, and it is based only on observing its input/output energetic-behavior.

Tognetti in his work in [165], criticized how Hogan came to classify the human's arm impedance as passive. One must look further back to the testing he, Bizzi, and Mussa-Ivaldi performed in [114]. They set out to characterize the steady state spring like behavior of the neuromuscular system. They wanted to measure the force/displacement relationship for different postures of the arm-hand serial linkage when the hand is displaced from an equilibrium position. For each human subject and arm posture the resulting measured reaction force was expressed as a two-dimensional stiffness matrix. This matrix was then split into symmetric and anti-symmetric components, with the symmetric part representing the conservative spring like component and the anti-symmetric part representing any non-conservative reaction forces. From the assumption of a negligible anti-symmetric component and a positive definite symmetric component, Hogan derives the human acts as an element with a passive precognitive neuromuscular system.

The problem with this extension is that the human will not solely act in a precognitive manner when interfacing with haptic devices. Furthermore, it has been accepted that all

humans exhibit a pure time delay, either due to neuromuscular lags or reaction time. Once again, Hogan's analysis only dealt with the neuromuscular's steady state response and did not look into its dynamic response or lags. The problem is more extensively discussed in [165].

In our work, inspired by the passivity properties that a human arm does or may exhibit, we acknowledge for this problem, and do not take the passivity of the human arm for granted but rather keep the energy-based character of the passivity model, see Chapter 3; further research will evaluate that. In that way, a new class of semi-parametric human models is actually employed, in that we are able to distinguish between two models (based on the energetic behavior) without having to exactly characterize them.

2.1.2 Transparency evaluation

A high degree of telepresence is desired to enable operators to safely conduct a teleoperation task. However, it is hard to quantify the degree of telepresence, or the "feel" of the remote site available to the operator through the teleoperation system. A telepresent system will be called *transparent* if the human is unable to distinguish between direct and tele-interaction with the environment. Ideally he/she feels as if directly interacting with it [133, 180].

Despite the transparency definitions, which are usually based on an ideal system, the transparency evaluation is not an easy task. On that account we evaluate the transparency of the developed architectures and algorithms in this work using two ways: a) objective transparency criteria, which are based on measurable quantities and the transparency definitions above, and b) human factors, which are a main field of study in psychology, hence, by experiments done with human subjects, employing post-test questionnaires and subjective rating scales.

Other performance metrics evaluate the task performance of the operator for example in terms of task completion time and the operators effectiveness in completing the assigned task like the sum of squared forces, e.g., in [57]. These metrics are in contrast to the concept of transparency and are operator dependent.

Objective transparency criteria

When the teleoperator comes in contact with the environment, its positions and forces are related by the impedance Z_e of the environment

$$f_e = Z_e(x_e). \tag{2.2}$$

The operator's force on the HSI f_h and the HSI's motion x_h should have the same relationship, i.e. for the same forces $f_e = f_h$ we want the same motions $x_e = x_h$. This requires that the impedance Z_h transmitted to or "felt" by the human operator satisfies the transparency condition [97]

$$Z_h = Z_e. \tag{2.3}$$

Assuming the impedances are approximated by linear time-invariant systems, measures derived from this criterion are integral impedance error norms in the frequency domain as

will be applied in Chapter 4. In that way a performance index J can be defined

$$J(Z_1, Z_2) = \int\limits_{\omega_{min}}^{\omega_{max}} \frac{1}{|Z_1|} |Z_1(\omega) - Z_2(\omega)| \mathrm{d}\omega, \tag{2.4}$$

where ω_{max} and ω_{min} are the maximum and minimum frequencies of the manipulation bandwidth of the human operator. A similar fidelity measure was introduced in [171] using a weighted integral to account more for the low frequency components. However, the value of such a measure does not allow an intuitive interpretation, although it can serve as a perfect objective comparison tool.

In [26, 24] the Z-width concept is introduced as the dynamic range of perceptible impedances by the haptic device in virtual reality frameworks. Transparency can be thus measured by contrasting the highest perceptible impedance (normally corresponding to a high stiffness contact situation $Z_e \to \infty$) against the lowest one, which the haptic device can render (analogous to a free environment situation $Z_e = 0$). In a teleoperation context it was first used in [61] to express the dynamic range of the impedance transmitted to the operator as a measure for the level of transparency. However, it is quantified for the two extreme values of environment impedance, i.e. $Z_e = 0$ and $Z_e \to \infty$ only. Accordingly, transparency is good if $Z_h \to 0$ and $Z_h \to \infty$, respectively.

A criterion which incorporates human haptic perception limits was first introduced in [69, 72, 74] where the haptic telepresence system is called *perceived transparent* if the difference between the displayed impedance and the environment impedance is within the just noticeable difference $Z_h \in [Z_e - JND, Z_e + JND]$ (analogous for position and force errors). Both, transparency and perceived transparency are objective quality metrics.

Finally, transparency has been recently also tackled by energetic means in [6], where the concept of bilateral energy transfer is introduced. A transparent system straightforwardly conveys energies bilaterally without (passive or active) energy leaks. The transparency for port-Hamiltonian-based bilateral telemanipulation systems is studied in [145, 146].

Evaluation using human factors

The above measures are appropriate for qualitative comparisons of control schemes without however considering human perceptual limits. Psychophysics is a discipline within psychology that quantitatively investigates the relationship between physical stimuli and the sensations and perceptions they affect [47]. In the teleoperation context, it aids the measurement of the "feeling of presence" on the (remote) site and can therefore be used instead of the transparency evaluation metric defined above.

Regardless of the sensory domain, there are three main areas of investigation: absolute thresholds, discrimination thresholds and scaling. In this work, particularly in Chapter 4, the discrimination thresholds of the haptic sensation will be exploited for the design of efficient, imperceivable data reduction algorithms. Experimentation, on the other hand, seeks to determine whether the subject can detect a stimulus, identify it, differentiate between it and another stimulus, and describe the magnitude or nature of this difference [150]. Experimentations is hence also used to evaluate the transparency of a system

2.2 Communication networks for control

The communication network constitutes a significant component of a haptic teleoperation system as a global control loop is closing through it. However, the communication network is a dynamical system itself, and as such, without further control measures the intrinsic communication unreliabilities can render the haptic telepresence system unstable and of course affect its performance. In this section, a careful look at the structure of communication networks and based on similar work in [69, 105, 20], will help understand some concepts and aid the design of stabilizing control architectures and efficient transmission algorithms later on in this thesis. However, the low-level protocol design is not considered in this work. The reader is encouraged to refer to [8] for a general overview on networks specifications, analysis and design approaches developed for networked controlled systems (NCS) such that stability and performance are preserved.

The OSI model

For better modularity, nowadays networks are developed in separate layers, with each one of them performing some specific functions, ideally independently from the other layers. These layers are arranged logically from the bottom to the top. Each one of them utilizes the services provided from the layer below and provides it's services to the layer above. The most common model for networks is the OSI (Open Systems Interconnection) reference model developed by ISO (International Organization for Standardization). The OSI model comprises 7 layers (from the bottom to the top: physical, data link, network, transport, session, presentation, application) and dictates which specific functions each layer should implement. The control systems relevant characteristics are defined mainly by the second layer, or more precisely a sublayer of the second layer on which the medium-access-control (MAC) protocol is implemented. The MAC (sublayer) protocol is responsible for the network resource allocation among the various nodes attempting to communicate at each time instant and defines the blocking time, i.e. the time that each message has to wait until the necessary network resources are available before it is transmitted. Moreover, it is responsible for the action to be taken in case of buffer overflow or message corruption which can lead to packet loss. Higher layer protocols may also affect the time delay and the packet loss. This happens when a packet that is lost is requested to be retransmitted by a higher layer protocol.

In general, to treat with the wide variety of communication possibilities, we will focus on three key characteristics for teleoperation systems; the effective

- time delay,

- packet losses,

- and data rate.

Consequently, two layers of the OSI model are of interest, the data link (second) layer, which controls the information transmission and determines the characteristics of delays and packet dropouts of networks and the transport (fourth) layer, which determines the

effective effects of these issues. However, further in this work, no consideration or design is happening on the second layer. Moreover, we will refer only to Ethernet-based communication, due to its increased availability, infrastructure (e.g. the Internet), modularity and speed. Other communication networks, such as the controller area network (CAN) by Robert Bosch GmbH [28] are not considered as they achieve too low data rates for the realization of a telepresence system [101].

Time delay

Along the path across the network the packet suffers from several different types of delay. The most important of these delays are the queuing delay, the transmission delay, and the propagation delay; together, these delays accumulate to the total network induced delay [69].

The queuing delay results from the fact that the packet may have to wait in the input buffers and also in the output buffers of the routers due to other traffic using the same path. The queuing delay may substantially vary over the time depending on the traffic intensity along the path and the routing policies, it is the most significant portion of the overall delay.

The transmission delay is the amount of time required for the routers to push out the packet onto the outgoing links. It is a function of the packet's length and the bandwidth of the traversed links. As the path in a dynamically routed network may vary over time and such the experienced link bandwidth, the transmission delay may vary even in the case of fixed packet length. Generally, the amount of data transfered within one packet in haptic telepresence application is very low, such that this type of delay is an assumingly small partition of the overall delay.

The propagation delay depends purely on the characteristics of the physical medium and the distance between the source and the destination. As the path through the network may vary, a slight variation of this delay portion is possible. In summary, the time-varying delay experienced by the data packets consists of a deterministic component, the minimum time delay determined by the minimum accumulated propagation and transmission delay for a dedicated path. The delay variation, mainly introduced by the queuing delay along a path, is very difficult to model. Stochastic models are generally used to model the network delay variation.

Remark 2.2.1 Time-varying delay is in the literature commonly characterized by the parameters latency and jitter. The notion of latency describes the expected value of the time delay. The variability of the delay (not necessarily the delay variance) is commonly termed jitter.

Packet loss

Packet loss occurs when one or more packets of data traveling across a computer network fail to reach their destination. Packet loss is distinguished as one of the three main error types encountered in digital communications; the other two being bit error and spurious packets caused due to noise. Packet loss can be caused by a number of factors, including signal degradation over the network medium due to multi-path fading, packet drop because

of channel congestion, corrupted packets rejected in-transit, faulty networking hardware, faulty network drivers or normal routing routines.

The most simple models assume an uncorrelated probability of packet loss. As before for the time-varying delay, these model cannot describe the observed busty packet losses as they often occur in packet switched networks. Therefore models with correlated probability are appropriate such as the well-known Gilbert model which is based on a two-state hidden Markov model [181]. Here the loss probability of a packet is influenced by the state of the previous packet.

2.2.1 The data link layer

The data link layer provides the functional and procedural means to transfer data between network entities and to detect and possibly correct errors that may occur in the physical layer.

Ethernet

Ethernet is known as the most popular communication network and has the widest application domains [82]. In general, Ethernet can be categorized into two types: (i) hub-based Ethernet, which is commonly used for data exchange. It uses CSMA/CD (carrier sense multiple access with collision detection) mechanism for resolving contention on the communication medium, (ii) switched Ethernet with CSMA/CA (carrier sense multiple access with collision avoidance) mechanism, which is implemented in manufacturing and control environments. In the former, a transmitting node first listens to the network to determine whether any other node on the network is occupying the medium. If the network is busy, the transmitting node waits until it becomes idle and continues the transmission. The latter acts to prevent collisions before they happen by checking whether the network is clear, i.e. no other node is transmitting at the time. If the network is clear, the packet is sent. Otherwise, the transmitting node waits for a randomly chosen period of time, and then checks again to see if the network is clear. Consequently, Ethernet is a *non-deterministic* protocol. Its network-introduced delay is random and highly depends on the traffic condition. However, Ethernet is cost-effective and has high bandwidth, popularity as well as versatility. This leads to a steady development and improvement of Ethernet technology for the application of complex control systems and telepresence systems, see [124, 30, 69].

Wireless Ethernet

In wireless networks the communication medium is by default a common bus, namely the air. The quality of the communication channel is affected by many parameters, including the distance of the communicating nodes and the interference with other networks, making thus hard to guarantee a standard communication quality, especially if the nodes are moving. The wireless medium inherently has higher error rates. Due to the nature of the communication channel additional restrictions apply in the implementation of MAC protocols. Collision detection is impossible, since wireless transceivers cannot send and receive at the same time, meaning that a node cannot listen if a collision occurs when it is

transmitting. The above are only some of the additional challenges that have to be faced in wireless networked control systems, for a more detailed discussion see [174].

2.2.2 Transport protocol - Effective delay and packet loss

The network topology, the routing policy and the traffic volume determine the transmission quality. However, the effective delay and loss seen by the processes in the end-systems, i.e. the HSI and the teleoperator, are further influenced by the transport protocol applied as discussed in [69]. The transport protocol provides the logical communication between the processes in the end systems. In IP based networks two protocols are available, namely the TCP (Transmission Control Protocol) and the UDP (User Datagram Protocol).

The TCP provides a reliable service as it detects packet loss and resends the data resulting in a significantly increased delay for the affected packet. Furthermore, the congestion control of TCP, i.e. the sending rate adaption known as window behavior may result in increasing delay. As the protocol overhead is high in relation to the small packet loads common in haptic telepresence systems the additional traffic induced by TCP is high. In summary the TCP trades increased jitter, higher latency to zero packet loss. The UDP is an unreliable protocol as it does not recover packet loss. As no implicit congestion control or other services are provided the protocol overhead is comparably low. The UDP does not significantly change the transmission characteristics seen by the processes in the end systems compared to the network induced characteristics. For a comparative view of those two protocols see Table 2.1.

The network traffic of closed loop control systems operated over a network is characterized by high packet transfer rates in the range of the sampling rate of the end systems HSI and teleoperator. The packet rate is not exile in general, hence the rate adapting congestion control of *TCP is not appropriate*. The packet loads in such systems are comparably small, as a result the additional traffic induced by the protocol overhead of TCP is high. The resend algorithm of TCP is useless in such *time critical applications*. For these reasons in networked telepresence systems the UDP is preferred over the TCP with its inferior real time characteristics, see also [41] for further arguments. The following considerations assume the communication over an IP based network with the UDP as transport layer protocol.

2.3 Control background

Haptic telepresence systems behave mainly as robots exchanging mechanical energy with the human and are hence posing significant challenges from the control point of view. Through the command and feedback signals energy is exchanged between the HSI and the teleoperator, thereby, closing the global control loop. From a control theoretic point of view the main goal of haptic teleoperation is twofold:

- *Stability:* Maintain stability of the closed-loop system irrespective of the behavior of the operator or the environment.

	TCP	UDP
Ordering	TCP rearranges data packets in the order specified	UDP does not order packets. If ordering is required, it has to be managed by the application layer
Data reliability	There is absolute guarantee that the data transferred remains intact and arrives in the same order in which it was sent	There is no guarantee that the messages or packets sent would reach at all
Error checking	Yes	No
Header size	20 bytes	8 bytes
Usage	In non-time critical applications	In applications that require fast transmission of data
Streaming	Data is read as a byte stream, no distinguishing indications are transmitted to signal message (segment) boundaries	Packets are sent individually and are checked for integrity only if they arrive. Packets have definite boundaries which are honored upon receipt, meaning a read operation at the receiver socket will yield an entire message as it was originally sent.
Weight	TCP requires three packets to set up a socket connection, before any user data can be sent. TCP handles reliability and congestion control.	There is no ordering of messages, no tracking connections, etc. It is a small transport layer designed on top of IP.

Tab. 2.1: A comparative view of the two Internet protocols, TCP and UDP.

- *Telepresence:* Provide the human operator with a sense of telepresence, with the latter regarded as transparency of the system between the environment and the operator.

Energy-based control approaches are a strong tool to face these challenges, see also Section 1.2, and consist the basis of the work presented in this thesis. They are therefore discussed below.

2.3.1 The passivity framework

The passivity formalism represents a mathematical description of the intuitive physical concepts of power and energy, see [93, 147], and is related to the more general framework of dissipative systems [173]. It provides a simple, robust, and powerful tool to analyze the stability of a system, solely based on input-output properties, hence without the exact knowledge of the internal state models. Passivity can be therefore applied to a large variety of systems, for example linear, nonlinear, continuous time, discrete time, distributed, or even non casual systems. It provides sufficient, but not necessary, input/output stability conditions.

Until the work of Popov [130], passivity was a network theory concept dealing with rational transfer function which can be realized with passive resistances, capacitances and inductances. Such transfer functions are restricted to have relative degree larger than one. They are called *positive real* because the real parts are positive for all frequencies, that is, their phase lags are always less than 90 degrees. A key feedback stability result from the 1960's, which linked passivity with the existence of a quadratic Lyapunov function for a linear system, is the Kalman-Yakubovich-Popov (KYP) lemma also called *Positive Real Lemma*. It has spawned many significant extensions to nonlinear systems and adaptive control. As in the following of this work, nonlinear systems are considered, the reader is encouraged to look into [93] for more details on these lemmas.

Remark 2.3.1 Passivity is often equated with stability. However, passivity itself does not require any internal models or even the specification of states. And without knowledge of the states, the very notions of equilibrium points, converge, and even stability are in question [116]. This connection will be discussed later on in this chapter.

The systems we consider in the following are continuous time, non-linear time invariant dynamical systems described by the equations

$$\Sigma : \begin{cases} \dot{x} = f(x, u), & x_0 = x(t = 0), \\ y = h(x, u), \end{cases} \tag{2.5}$$

$x \in \mathcal{X} \subset \Re^n$, $u \in \mathcal{U} \subset \Re^p$, $y \in \mathcal{Y} \subset \Re^q$ are the state, input and output vectors respectively, and $f(0, 0) = h(0, 0) = 0$. The function $f : \Re^n \times \Re^p \to \Re^n$ is locally Lipschitz, $h : \Re^n \times \Re^p \to \Re^q$ is continuous.

Passive systems

Intuitively, a passive system will absorb more energy than it produces.

Definition 2.3.2 We consider a system of the form (2.5) with the same input and output dimension $p = q$, i.e. a square system. The system is said to be passive in $\mathcal{X}$ if there exists a continuously differentiable positive semidefinite function $V(x)$, $V(0) = 0$, such that for all $x \in \mathcal{X}$

$$V(x(T)) - V(x_0) \leq \int_0^T u^T y \, dt \tag{2.6}$$

for all $u \in \mathcal{U}$ and all $T \geq 0$ such that $x(t) \in \mathcal{X}$ for all $t \in [0, T]$. The function $V(x)$ is called the storage function.

If the storage function $V(x)$ is differentiable, we can write (2.6) as

$$\dot{V}(x(t)) \leq u^T y. \tag{2.7}$$

Passivity, therefore, is the property that the rate of increase of storage (energy) is not higher than the scalar product between the input and the output (power). In other words a passive system cannot store more energy than is supplied to it from the outside, with the difference being the dissipated energy.

Definition 2.3.3 The system (2.5) is said to be *lossless* if the equality in (2.6) is true:

$$V(x(T)) - V(x_0) = \int_0^T u^T y \, dt. \tag{2.8}$$

When regarding the system (2.5) only as an input-output mapping $T : u(\cdot) \mapsto y(\cdot)$, i.e ignoring its states, passivity can be also defined in a purely input-output sense, by ignoring the storage function. In order to avoid unnecessary confusion, without loss of generality, when referring to input-output behavior the initial state is considered to be zero, i.e. $x(0)$, $V(x_0) = 0$. Considering further that $V(x) > 0$, the passivity inequality (2.6) can accordingly be written

$$\int_0^T u^T y \geq 0. \tag{2.9}$$

Geometrically, this means that the u-y curve of the input-output mapping must lie in the first and third quadrants, as shown in Figure 2.4(a). A resistor for example, see Figure 2.4(b), which is a very common element, will be passive if its characteristic lies in the first and third quadrant as indicated in Figure 2.4(c).

Remark 2.3.4 Only for specific choices of the input and output variables, such as velocity and force or current and voltage, will the power correspond to a physical power.

Example 2.1 (Integrator as a passive system)
An integrator is the simplest storage element:

$$\dot{x} = u$$
$$y = x$$
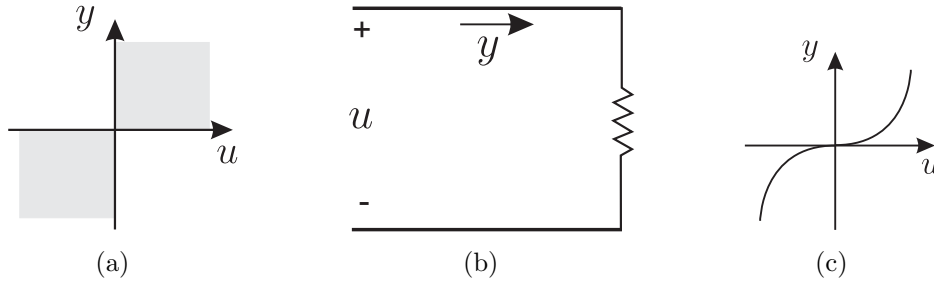
Fig. 2.4: (a) The u-y characteristic of a passive system lies in the first-third quadrant. (b) A resistor is a common passive element. (c) The characteristic of a a passive nonlinear resistor

The system is passive (lossless) with $V(x) = \frac{1}{2}x^2$ as a storage function because $\dot{V} = uy$.

$\square$

Remark 2.3.5 As passivity is a system input-output related concept, the passivity property is not invariant to the choice of the output.

Example 2.2 (Mass-spring-damper system)
Consider a mass-spring-damper system Σ, with an external force acting on the mass considered as the input u as shown in Figure 2.5. The state equations for the mass position x and velocity v are

$$
\begin{aligned}
\dot{x} &= v \\
\dot{v} &= -\frac{k_\Sigma}{m_\Sigma}x - \frac{b_\Sigma}{m_\Sigma}v + \frac{1}{m_\Sigma}u
\end{aligned}
$$

where $k_\Sigma > 0$ is the spring constant, $m_\Sigma > 0$ is the mass, and $b_\Sigma > 0$ is the viscous friction coefficient. The energy is

$$
E = \frac{1}{2}m_\Sigma v^2 + \frac{1}{2}k_\Sigma x^2
$$

and its rate of change is

$$
\dot{E} = uv - b_\Sigma v^2 \le uv.
$$

Thus, when the velocity is considered as the output, the mass-spring-damper system is passive. Its storage function is the energy E and the supply rate is the input power uv. However, the same system is *not passive* if the position x is taken to be the output $y = x$.

$\square$

Example 2.3 (Robot manipulator) [152]
The nonlinear dynamic equations for an m-link robot take the form

$$
B(q)\ddot{q} + C(q, \dot{q})\dot{q} + g(q) = u \tag{2.10}
$$
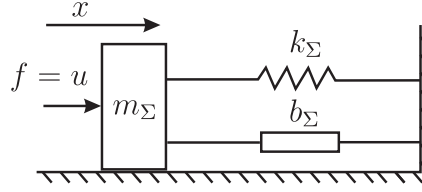
Fig. 2.5: A mass-spring-damper system can be shown to be passive with the force f as input and the velocity $v = \dot{x}$ as output.

where q is an m-dimensional vector of generalized coordinates representing joint positions, $u \in \Re^m$ the control input, and $B(q)$ is a symmetric inertia matrix that is positive definite for all $q \in \Re^m$. The term $C(q, \dot{q})\dot{q}$ accounts for centrifugal and Coriolis forces. The matrix C has the property that

$$\dot{B} - 2C \tag{2.11}$$

is a skew-symmetric matrix for all $q, \dot{q} \in \Re^m$, where $\dot{B}$ is the total derivative of $B(q)$ with respect to t. The term $g(q)$, which accounts for gravity forces, is given by $g(q) = \frac{\partial P(q)}{\partial q}$, where $P(q)$ is the total potential energy of the links due to gravity.

To prove the passivity property, let V be the total energy of the system, i.e., the sum of kinetic and potential energies,

$$V = \frac{1}{2}\dot{q}^T B(q)\dot{q} + P(q). \tag{2.12}$$

Then the derivative $\dot{V}$ satisfies

$$
\begin{aligned}
\dot{V} &= \dot{q}^T B(q)\ddot{q} + \frac{1}{2}\dot{q}^T \dot{B}(q)\dot{q} + \dot{q}^T \frac{\partial P}{\partial q} \\
&= \dot{q}^T \left\{ u - C(q, \dot{q})\dot{q} - g(q) \right\} + \frac{1}{2}\dot{q}^T \dot{B}(q)\dot{q} + \dot{q}^T \frac{\partial P}{\partial q},
\end{aligned}
$$

where we have substituted for $B(q)\ddot{q}$ using the equations of motion. Collecting the terms and using the fact that $g(q) = \frac{\partial P}{\partial q}$ yields

$$
\begin{aligned}
\dot{V} &= \dot{q}^T u + \frac{1}{2}\dot{q}^T \left\{ \dot{B}(q) - 2C(q, \dot{q}) \right\} \dot{q} \\
&= \dot{q}^T u
\end{aligned}
$$

the latter equality following from the skew-symmetry property. Considering as output the angular velocity $\dot{q}$ and as control input u the passivity (lossless) property follows.

$\square$

Passivity can be easily observed in LTI systems, without requiring knowledge of the state equations but only of the transfer function.

Lemma 2.3.6 [115] Consider a SISO LTI continuous-time system, and let $G(s)$ be the transfer function associated to the system. If (2.6) is satisfied then

$$Re[G(j\omega)] \geq 0 \tag{2.13}$$
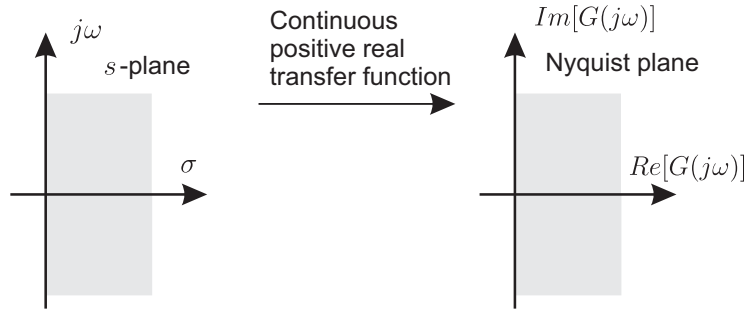
Fig. 2.6: Property of a passive SISO linear time-invariant continuous-time system.

for all real ω for which $j\omega$ is not a pole of G(s).

Corollary 2.3.7 [115] If a SISO LTI continuous-time system is passive then the following inequality holds

$$Re[G(s)] \geq 0, \;\; \text{whenever} \; Re(s) \geq 0. \tag{2.14}$$

In a graphical and intuitive way, this property of passive SISO LTI systems can be illustrated as in Figure 2.6. A continuous-time passive transfer function maps points in the right-half plane of the s-plane to the right-half plane in the Nyquist plot. The Nyquist plot of a passive system lies on the right-half plane, which means that an infinite gain proportional control can be introduced without destabilizing the system. In addition, positive real transfer functions do not have poles on the right-half-s-plane and their poles lying on $Re(s) = 0$ are simple with positive real residues.

System connections

One of the nicest features of passivity is its ability to connect two passive elements into a single passive unit, therefore allowing for reasoning about the stability of a closed-loop by studying individual components. This occurs if the connection is made in either a feedback or parallel configuration and it is very useful as many passive elements can be combined in this fashion without loss of the global stability properties.

Theorem 2.3.8 [147] Suppose that a system Σ_1 and a system Σ_2, both of the form (2.5) are passive. Then the two systems, one obtained by the parallel interconnection, and the other obtained by the feedback interconnection are both passive.

Proof: By passivity of Σ_1 and Σ_2, there exist $V_1(x_1)$ and $V_2(x_2)$ such that $V_i(x_i(T)) - V_i(x_i(0)) \leq \int_0^T u_i^T y_i \, \mathrm{d}t$, $i = 1, 2$. Define $x := (x_1, x_2)$ and $V(x) = V_1(x_1) + V_2(x_2)$ and note that $V(x)$ is positive semidefinite.

For the parallel interconnection, see Figure 2.7(b), the output is $y = y_1 + y_2$, so that

$$V(x(T)) - V(x(0)) \leq \int_0^T (u^T y_1 + u^T y_2) \, \mathrm{d}t = \int_0^T u^T y \, \mathrm{d}t.$$
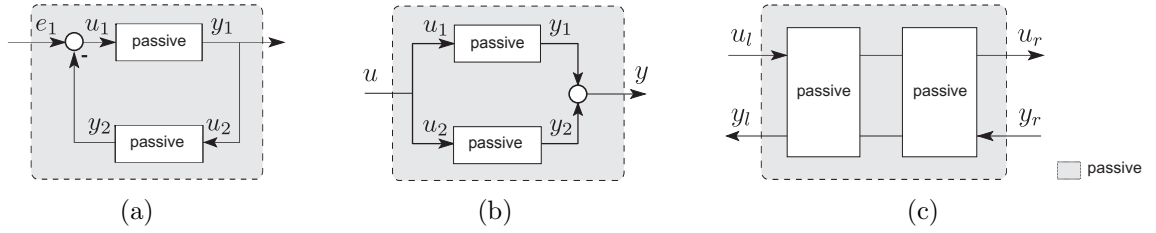
Fig. 2.7: The fundamental passivity results for interconnected systems. (a) Feedback interconnection. (b) Parallel interconnection (c) Cascade interconnection.

This proves that the parallel interconnection is passive.

For the feedback interconnection, see Figure 2.7(a), we have

$$V(x(T)) - V(x(0)) \le \int_0^T (u_1^T y_1 + u_2^T y_2) \, \mathrm{d}t.$$

Substituting $u_2 = y_1$ and $u_1 = e_1 - y_2$ we obtain

$$V(x(T)) - V(x(0)) \le \int_0^T e_1^T y_1 \, \mathrm{d}t = \int_0^T u^T y \, \mathrm{d}t.$$

which proves that the feedback interconnection is passive. ∎

In Chapter 4 we will use two-port elements to construct a teleoperation system consisting of passive elements. To facilitate the development of the systems we proceed with some additional definition. First, we define a major direction, along with positive power will flow, from left to right. Next we establish two-port elements, which provide a separate interaction port on both their left and right side. Positive power will enter a two-port element from the left and exit to the right. The total power input for a two-port element is given as

$$P_{in} = \dot{V} = u_l^T y_l - u_r^T y_r \tag{2.15}$$

where we have labeled the left port with 'l' and the right one with 'r', see Figure 2.7(c). Notice the power for the right port is negated as it is exiting the system. This sign definition allows for the simple cascading of elements to insure the closure properties of passivity. It implies that a simple cascaded sequence of passive two-port elements is also passive [118, 116].

Example 2.4 (Passive haptic telepresence) [69]
The passivity concept has been firstly applied to haptic telepresence systems in [4], and has in the sequel emerged to one of the most preferred tools in haptic telepresence control. In order to apply the passivity concept to haptic telepresence systems it is decomposed into the interconnected subsystems human, HSI, communication channel, teleoperator, and environment, as visualized in Figure 2.1. The human and the environment are represented by one-ports, the HSI, the bilateral communication channel and the teleoperator by two-ports.

Following the stability arguments from [4] the unit of interconnected HSI, communica-

tion channel and teleoperator has to be passive as well as the environment. Note, that according to [25] the passivity of the system in contact with an arbitrary, passive environment is not only a sufficient, but also a necessary condition for stability. The human operator naturally produces energy to interact with the system, however, the input energy is assumed to be bounded, and the above passivity arguments remain intact.

For passivity reasons the appropriately locally controlled HSI and teleoperator exchange the power variables velocity and force [4] (flow and effort in a system theoretic context). The mapping from velocity to force is generally passive, further the local control laws can easily be designed such that passivity property of HSI and teleoperator is always preserved [4, 118, 116]. Ignoring, for the time being, the communication induced delays and packet losses, the haptic telepresence system consists thus of two-port interconnection of passive systems, is thus in overall passive and stable.

2.3.2 Dissipative systems - Excess and shortage of passivity

The passivity formalism has been successfully used for a long time in control. It is however considered a conservative condition to guarantee the stability of a system. A system can be stable without being passive, in other words it can be stable even if it is less than passive. On the other hand some systems can also be more passive, especially after some passivity-based control method [121], therefore the question that is posed is whether such a system can have an "excess of passivity" that another, possibly interconnected system, can make use of. To bridge this gap in the passivity framework analysis, we will discuss here the dissipativity framework, namely a class of systems that can be considered *more or less* passive. Sepulchre *et al.* first used the term excess and/or shortage of passivity in [147], and it will be also adopted in our work.

The dissipativity formalism provides - just like the passivity one - a simple, robust, and powerful tool to analyze the stability of a system based on its *input-output* properties, hence without the exact knowledge of an internal state model. It is a mathematical description of the intuitive physical concepts of energy and represents a generalization of the passivity concept widely used in robotics. Roughly speaking, a dissipative system is defined as one that cannot supply to the environment a larger amount of energy than the one the environment supplies to it. Additionally, dissipativity provides a modular approach for showing the stability of an interconnected system: the dissipativity properties of its components and the interconnection structure is sufficient.

Dissipative systems

Definition 2.3.9 [66, 105] A dynamical system (2.5) is called (Q, S, R)-dissipative if there exist a positive semi-definite function $V : \Re^n \rightarrow \Re_+$ such that for each admissible u and each $t \geq 0$

$$V(x(t)) - V(x(0)) \leq \int_0^t \left[\begin{array}{cc} u^T & y^T \end{array} \right] P \left[\begin{array}{c} u \\ y \end{array} \right] \mathrm{d}\tau, \qquad (2.16)$$

with dissipativity matrix

$$P = \left[\begin{array}{cc} Q & S \\ S^T & R \end{array} \right]$$

where $P \in \Re^{p \times p}$, $Q \in \Re^{q \times q}$ and $S \in \Re^{p \times q}$.

The dissipativity matrix P can be restricted, without loss of generality, to the set of matrices that are not positive-semidefinite or negative-definite. The matrix P is not unique for each system. For example it is straightforward to see that if a system (2.5) is (Q, S, R)-dissipative with a matrix P, then it is also (Q, S, R)-dissipative for every matrix P' satisfying $P' \succeq P$. If this holds with strict inequality, i.e $P' \succ P$, then P' is more conservative than P, in the sense that it defines a larger class of systems than P, i.e. is less restrictive than P. This is inferred, as if a system satisfies the dissipativity inequality (2.16) with the matrix P then it also satisfies it with the matrix P', however, the opposite does not hold [105].

A special case of (Q, S, R)-dissipative systems are input-feedforward-output-feedback-passive (IF-OFP) systems. In IF-OFP systems the number of the inputs is equal to the number of the outputs, i.e. $p = q$ holds, and the dissipativity parameters are $Q = -\delta I$, $R = -\epsilon I$, $S = \frac{1}{2}I$, δ, $\epsilon \in \Re$.

Definition 2.3.10 The system (2.5) is said to be *Output Feedback Passive (OFP)* if the number of inputs is equal to the number of outputs ($p = q$) and there exists a continuously differentiable positive semidefinite function $V(x)$, $V(0) = 0$, such that for all $x \in \mathcal{X}$

$$V(x(T)) - V(x_0) \leq \int_0^T u^T y - \epsilon y^T y \, dt \qquad (2.17)$$

for some $\epsilon \in \Re$, $u \in \mathcal{U}$ and all $T \geq 0$ such that $x(t) \in \mathcal{X}$ for all $t \in [0, T]$.

Definition 2.3.11 The system (2.5) is said to be *Input Feedforward Passive (IFP)* if the number of inputs is equal to the number of outputs ($p = q$) and there exists a continuously differentiable positive semidefinite function $V(x)$, $V(0) = 0$, such that for all $x \in \mathcal{X}$

$$V(x(T)) - V(x_0) \leq \int_0^T u^T y - \delta u^T u \, dt \qquad (2.18)$$

for some $\delta \in \Re$, $u \in \mathcal{U}$ and all $T \geq 0$ such that $x(t) \in \mathcal{X}$ for all $t \in [0, T]$.

We quantify the excess or shortage properties with the notation IFP(δ) and OFP(ϵ). According to our convention, positive sign of δ and ϵ means that the system has an excess of passivity. Conversely, negative sign of δ and ϵ means that the system has a shortage of passivity [147]. If $\delta > 0$ the IFP concepts coincides with the Input Strict Passivity (ISP) introduced by Hill and Moylan [65, 66]. Respectively, OFP systems with $\epsilon > 0$ coincide with the Output Strict Passive (OSP) systems. For completeness we mention here also the very-strongly passive (VSP) systems, which are simply both ISP and OSP and their

storage function has to satisfy [65, 66]

$$V(x(T)) - V(x_0) \leq \int_0^T u^T y - \delta u^T u - \epsilon y^T y \, dt \tag{2.19}$$

for some $\delta, \epsilon > 0$. The IFP and OFP properties of a system will be extensively used in Chapter 3.

Remark 2.3.12 Note that in the case of multi-input-multi-output systems, $p, q > 1$, the described IFP and OFP properties (2.18), (2.17) may result in a conservative approximation of the input-output behavior as possibly individual supply rates can be assumed for every degree of freedom and the (Q, S, R) definition of dissipativity should be used instead. We will concentrate on isotropic supply rates, and thus IF-OFP systems, here for the sake of simplicity.

System connections

Similar to the system connection theorems for passive systems, the interconnection of dissipative subsystems is here of interest. It seems that feedback interconnections of IFP and OFP systems still exhibit IF-OFP properties as the two following lemmas show.

Lemma 2.3.13 [193] Consider the OFP(ϵ_1) system Σ_1 and the IFP(δ_2) system Σ_2. The negative feedback interconnection of Σ_1 and Σ_2 is OFP($\epsilon_1 + \delta_2$).

Proof: The system Σ_1 is OFP(ϵ_1) thus

$$V_1(x(t)) - V_1(x(0)) \leq \int_0^t u_1^T y_1 - \epsilon_1 y_1^T y_1 \, d\tau,$$

whereas for the IFP(δ_2) system Σ_2

$$V_2(x(t)) - V_2(x(0)) \leq \int_0^t u_2^T y_2 - \delta_2 u_2^T u_2 \, d\tau,$$

holds, where u_1, u_2 and y_1, y_2 are the respective inputs and outputs, see Figure 2.8(a). For the negative feedback interconnection of those two systems considering the compound storage function $V = V_1 + V_2$ gives

$$V(x(t)) - V(x(0)) \leq \int_0^t u_1^T y_1 - \epsilon_1 y_1^T y_1 + u_2^T y_2 - \delta_2 u_2^T u_2 \, d\tau$$

$$= \int_0^t (e_1 - y_2)^T y_1 - \epsilon_1 y_1^T y_1 + y_1^T y_2 - \delta_2 y_1^T y_1 \, d\tau$$

$$= \int_0^t e_1^T y_1 - (\epsilon_1 + \delta_2) y_1^T y_1 \, d\tau.$$
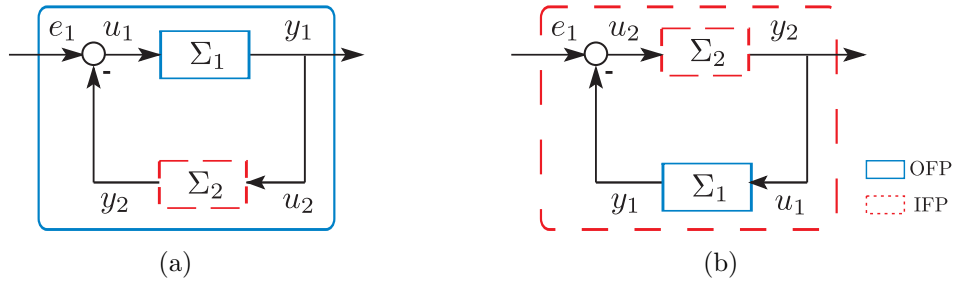
Fig. 2.8: The feedback interconnections of IFP/OFP systems exhibit IFP/OFP properties.

where $u_1 = e_1 - y_2$, e_1 being the input to the overall system, and $u_2 = y_1$ hold. The output of the overall system is y_1. The above lemma is illustrated in Figure 2.8(a). ■

Lemma 2.3.14 [193] Consider the IFP(δ_2) system Σ_2 and the OFP(ϵ_1) system Σ_1 with $\delta_2 \geq 0$ and $\delta_2 + \epsilon_1 \geq 0$. The negative feedback interconnection of Σ_1 and Σ_2 is $IFP(\kappa)$ with $\kappa = \min(\delta_2, \delta_2 + \epsilon_1)$.

Proof: The compound storage function gives

$$V(x(t)) - V(x(0)) \leq \int_0^t u_2^T y_2 - \delta_2 u_2^T u_2 + u_1^T y_1 - \epsilon_1 y_1^T y_1 \, \mathrm{d}\tau$$

$$= \int_0^t (e_1 - y_1)^T y_2 - \delta_2 (e_1 - y_1)^T (e_1 - y_1) + y_2^T y_1 - \epsilon_1 y_1^T y_1 \, \mathrm{d}\tau$$

$$= \int_0^t e_1^T y_2 + \begin{bmatrix} e_1 \\ y_1 \end{bmatrix}^T W \begin{bmatrix} e_1 \\ y_1 \end{bmatrix} \, \mathrm{d}\tau$$

$$\leq \int_0^t e_1^T y_2 + \lambda_{max}(W) \begin{bmatrix} e_1 \\ y_1 \end{bmatrix}^T \begin{bmatrix} e_1 \\ y_1 \end{bmatrix} \, \mathrm{d}\tau,$$

where, now, $u_2 = e_1 - y_1$, e_1 being the input to the overall system, $u_1 = y_2$ holds and

$$W = \begin{bmatrix} -\delta_2 I & \delta_2 I \\ \delta_2 I & -(\delta_2 + \epsilon_1) I \end{bmatrix}.$$

As $\lambda_{max}(W) = -\kappa \leq 0$

$$
\begin{aligned}
V(x(t)) - V(x(0)) &\leq \int_0^t e_1^T y_2 - \kappa e_1^T e_1 - \kappa y_1^T y_1 \, \mathrm{d}\tau \\
&\leq \int_0^t e_1^T y_2 - \kappa e_1^T e_1 \, \mathrm{d}\tau,
\end{aligned}
$$

holds. Thus, the system is IFP(κ) and $\kappa = \min(\delta_2, \delta_2 + \epsilon_1)$ as $\delta_2 \geq 0$ and $\delta_2 + \epsilon_1 \geq 0$. The above lemma is illustrated in Figure 2.8(b). ■

As in the passivity case, (Q, S, R)-dissipative systems can be also identified by the positive realness of a transfer function, for the LTI case; see [115, 51]. Here we will only refer to nonlinear systems and hence the lemma is not repeated here. However, a visualization of the LTI case will help understand and gain more insight into the IFP and
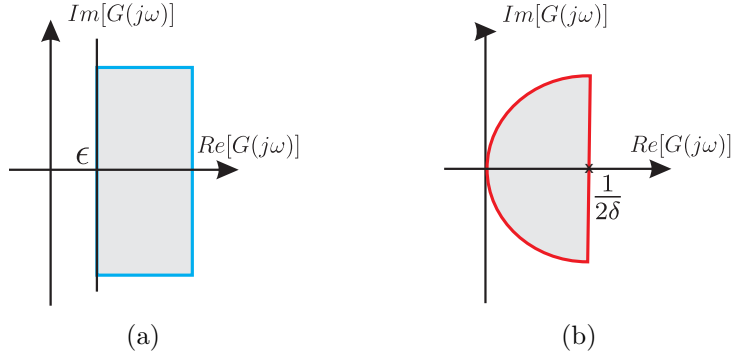
Fig. 2.9: Frequency-domain properties for dissipative LTI systems (a) OFP(ϵ) (b) IFP(δ).

OFP properties of a system. Figure 2.9 shows the characteristic of the Nyquist plot of $G(e^{j\omega})$ for the two different classes of dissipativity studied in this work, namely IFP and OFP systems.

2.3.3 Stability

The above presented frameworks, passivity and dissipativity, are discussed to guarantee stability of a system based on its input/output properties without requiring exact model knowledge.

Passive systems let stability in the sense of Lyapunov straightforwardly imply with one exception: The definition of passivity does not require that the storage function V is positive definite but it is satisfied also for positive *semidefinite*. As a consequence, in the presence of an unobservable unstable part of the system, they allow $x = 0$ to be unstable. This is excluded by zero-state detectability.

Definition 2.3.15 (Zero-state detectability and observability)
Consider a system with zero input, $\dot{x} = f(x,0)$, $y = h(x,0)$, and let $Z \subset \Re^n$ be its largest positively invariant set contained in $\{x \in \Re^n | y = h(x,0) = 0\}$. We say that the system is zero-state detectable (ZSD) if $x = 0$ is asymptotically stable conditionally to Z. If $Z = \{0\}$, we say that it is zero-state observable.

Remark 2.3.16 Equivalently, we can assume that if all system variables are represented in the energy storage function, such that bounded energy will also bound all states, passivity implies stability in the sense of Lyapunov.

Theorem 2.3.17 (Stability of OFP/IFP feedback interconnections) [147]
Assume that in the feedback interconnection a system Σ_1 is GAS and IFP(δ) and the system Σ_2 is ZSD and OFP(ϵ). Then $(x_1, x_2) = (0,0)$ is asymptotically stable if $\epsilon + \delta > 0$.
∎

The above result shows how the shortage of passivity in one system can be compensated for by the excess of passivity in the other system.

Finite gain $\mathcal{L}_2$-stability

Among the variety of stability notions we also consider finite gain $\mathcal{L}_2$-stability, which is another special case of quadratic dissipativity with $S = 0$, $R = I$, $Q = -\gamma^2 I$, $\gamma \in \mathcal{R}_+$.

Finite gain $\mathcal{L}_2$ stability implies that for each bounded input, the output is also bounded by the norm of the input signal scaled by a constant factor γ. When such a value exists, we are interested in the smallest possible one. The smallest possible value of γ is called the $\mathcal{L}_2$ gain of the system. Usually the exact value of γ can not be computed, but only a upper bound of it. In this case we say that the $\mathcal{L}_2$-gain of the system is smaller or equal to γ. An exception constitute LTI systems, where the $\mathcal{L}_2$-gain of a strictly stable system can be exactly computed, and it is shown to be the maximum gain of the transfer function over all frequencies, i.e $\gamma = \max|G(j\omega)|$ for all ω, where $G(j\omega)$ the transfer function of the system.

Definition 2.3.18 [93] A dynamical system Σ (2.5) is called finite-gain $\mathcal{L}_2$ stable if there exist a positive semi-definite function $V : \Re^n \to \Re_+$ such that for each admissible u and each $t \geq 0$

$$V(x(t)) - V(x(0)) \leq \frac{1}{2}\gamma^2 \int_0^t u^T u \, \mathrm{d}\tau - \frac{1}{2}\int_0^t y^T y \, \mathrm{d}\tau, \qquad (2.20)$$

The smallest possible value γ satisfying (2.20) is called the $\mathcal{L}_2$-gain of the system. An operator $\sigma : u(\cdot) \mapsto y(\cdot)$ with $u, y \in \Re^p$ the input and output respectively is called small gain operator if its $\mathcal{L}_2$-gain satisfies $\gamma_\sigma \leq 1$.

System connections

Finite gain $\mathcal{L}_2$-stability of a negative feedback interconnection can be concluded from the (Q, S, R)-dissipativity properties of its subsystems.

Corollary 2.3.19 [105] Consider the negative feedback interconnection of two systems Σ_1 and Σ_2. Assume that Σ_1 and Σ_2 are (Q, S, R)-dissipative with the dissipativity matrices Q_1, R_1, S_1 and Q_2, R_2, S_2 respectively. If

$$\hat{R} = \begin{bmatrix} Q_1 & S_1 \\ S_1^T & R_1 \end{bmatrix} + \begin{bmatrix} R_2 & -S_2 \\ -S_2^T & Q_2 \end{bmatrix} \prec 0, \qquad (2.21)$$

then the system is finite gain $\mathcal{L}_2$ stable. If further Σ_1, Σ_2 are zero state observable, the closed loop system is asymptotically stable.

As a more special case the, for IF-OFP systems, finite gain $\mathcal{L}_2$-stability of the negative feedback interconnection can be also concluded from the IF-OFP properties.

Proposition 2.3.20 [93] Consider two IF-OFP systems Σ_1 and Σ_2 with δ_i, ϵ_i, $i \in 1, 2$. The negative feedback interconnection of Σ_1 and Σ_2 is finite gain $\mathcal{L}_2$-stable if

$$\epsilon_2 + \delta_1 > 0 \text{ and } \epsilon_1 + \delta_2 > 0. \qquad (2.22)$$

Consequently, sufficient relationships to guarantee stability of interconnections between (Q, S, R)-dissipative, or IF-OFP in case $p = q$ were given and will aid the control design of Chapter 3.

Remark 2.3.21 A nice property of balancing shortage of passivity with excess of passivity between subsystems can be deduced. Clearly, the excess of passivity of one system can compensate for the shortage of passivity of the other if (2.21) holds. In the special case of IF-OFP systems (2.22) can be used instead, so some of the δ_i, ϵ_i can be negative if they are compensated by appropriate positive values. This property will be exploited in Chapter 3.

2.4 Discussion

In this chapter the necessary background knowledge required for the rest of this thesis is ordered. Three major areas can be distinguished, the human operator, the communication network, and the control-theoretic background on the stability of the systems.

The human operator is probably the most important and deciding element in a haptic telepresence system, both from the action as well as from the sensory point of view. Both aspects are considered, and the fundamental and up to now widely-used parametric mass-spring-damper modeling of the human arm who comes in contact with a haptic equipment is discussed. On the other hand, non-structured models such as e.g. the passivity-based human model can help the control design providing higher robustness. However, they have been criticized on empirical grounds and the do not allow for high distinguishability of the human, i.e. all humans are considered passive. All these aspects will be considered in the control design following in Chapter 3. Moreover, transparency, as a way of evaluating the haptic teleoperation realism, is addressed. The evaluation of haptic telepresence systems can happen in two ways, either by the given objective transparency criteria or experimentally, a field with a high scientific interest by psychologists, aiming at identification of significant human factors.

With respect to the communication network, things can be considered standardized as the Internet, or more general, packet-switched networks are well-established technologies nowadays. Therefore, the most important protocols that will influence the development of a haptic teleoperation system and will be also deployed in the experiments are studied; both the TCP and the UDP are observed under the scope of the very general OSI model and the choice of the UDP protocol as more appropriate is explained. The effective time delay and/or packet loss that the communication network implies in the application layer of a haptic telepresence system has to be considered, otherwise stability of the system is endangered. Bandwidth-related issues were not discussed here, although they consist a key part of this thesis; they will be exploited extensively in Chapter 4.

Finally, stability is the main focus of interest from the control point of view. Acknowledging for the difficulty of stability for a system where a highly unknown dynamic environment and a human with very complex dynamics are in the loop, initiated the passivity framework discussion. As will be seen later it is a very useful tool for studying the stability of a system over network and has been widely used in haptic teleoperation approaches over the years. However, it has been criticized for its conservatism results in terms of control

performance. Hence, systems with excess and shortage of passivity are considered and the dissipativity framework is illustrated. It is, to the best of the author's knowledge, poorly discussed in the literature, at least in the context of robotics. It is hoped, hence, that this background section can even aid the development of system in the wider area of robotics and spread similar ideas in various disciplines.

3 Control design exploiting human/environment dissipativity

The major reason for the success of the passivity formalism in teleoperation is its ability to cope with the largely unknown, nonlinear human arm and environment dynamics, which, however, can assumed to be passive [78]. However, the passivity framework, and therefore all aforementioned works, are known to be conservative resulting in a distorted display of the remote environment properties [74]. As shown in [97] robust stability and transparency of such systems are conflicting design goals. A transparent teleoperation system still remains a challenge and will be addressed in this chapter by introducing knowledge of the human/environment or robot manipulator dynamics or energetic behavior.

A bilateral control system that does not only guarantee stability under unreliable networks, but also shows sufficient performance and a high degree of transparency remained a challenge over the years. In recent work by Buerger and Hogan, the passivity condition for a human limb is shown to be unnecessarily restrictive [14]. Relaxing the passivity conservatism by using knowledge on the human dynamics is addressed in [13] using a natural admittance control (NAC) scheme, a nominal second-order linear model and a maximum deviation for the uncertain human in a human-robot interaction context. However, a nominal model can be difficulty defined for the highly unknown environment side of a teleoperation scenario. Stability analysis is performed with a classical robust control framework, therefore suffers when a nominal model is difficult to determine or when the disturbance from this nominal model does not allow all dynamics to be captured. Besides that, their work is not considering the communication unreliabilities of haptic telepresence. Gillespie in [48] also models the human as a second-order linear time-invariant system. His work goes further to propose an observer for the human model that makes use of real-time data collected by haptic hardware. It is not though reported, how good this method can perform with varying human arm/finger postures. It is assumed that a method that requires only bounds and not exact model of human/environment dynamics can perform more robust. Besides that, stability can be guaranteed only for constant user impedances, which is known to be not the case [168]. Recently input-to-state-stability (ISS) based methods for teleoperation have been developed in [128] that address relatively general classes of human operator and environment models. Although not direct comparison with passivity-based approaches has been seen so far they suffer from the fact that not all possible (passive) environments can provide such bounded external forces as required by the framework, for a discussion refer to [81].

In [108] explicit modeling of human operator dynamics is avoided by establishing the passivity of the haptic display. The results provide some useful insights, such as the role played by the physical damping, i.e. the excess passivity in the haptic device and the sampling rate. Particularly, the designer is able to determine the amount of physical damping required in the device if the class of environments is well characterized (e.g. nee-

dle placement task). The method is based on excess/lack of passivity, which is exploited also in this part of this work. However, only virtual environments are considered and no communication unreliabilities. Similarly, it is shown in [176] that the passivity condition depends on the device friction and on the minimum damping coefficient of the human arm during each sampling time. The achievable maximum stiffness depends also on it. The study is, however, limited to haptic interfaces. Passivity-based control (PBC) is now a well-established technique to design robust controllers for physical systems described by Euler-Lagrange (EL) equations of motions [121]. Recent research has now departed from the EL description of the systems and considers port-controlled Hamiltonian models instead, resulting from the network modeling of energy-conserving lumped-parameter physical systems. Recently the assignment of damping has been recognized as a useful technique to stabilize interconnected systems in [122, 120]. Dissipation has been further used in [19] to prove cyclo-passivity, a necessary (but not sufficient) passivity condition and damping injection has been further used together with a virtual spring coupling to enforce closed-loop passivity under communication unreliabilities, or interconnection of systems with slow or variable rate in [99, 100]. Moreover, the exploitation of the mechanical properties of the environment can also greatly improve the performance of the robotic system, see [32]. Nevertheless, the time-varying nature of human operator dynamics as well as that of the environment have continued to pose a challenge for the design of guaranteed stable but also high-performing and transparent haptic telepresence systems.

In the present chapter the (Q, S, R)-dissipativity theory discussed in Chapter 2 will be used for the human operator, the controlled manipulators and/or the environment to guarantee stability of a telepresence system with haptic feedback system under communication unreliabilities. In fact, it can be shown that only *approximate knowledge* on damping properties of these subsystems can be utilized to the benefit of transparency.

The approach is based on the *generalized* scattering transformation (GST) [77, 106] which applies to (Q, S, R)-dissipative systems, ensuring finite gain $\mathcal{L}_2$-stability with communication unreliabilities satisfying a small gain condition such as arbitrarily large constant time delay and properly handled packet loss do. Apart from the dissipativity framework, which is for first time discussed in the teleoperation context, this chapter innovates also in the fact that, this is the first work where the transparency of a teleoperation system is enhanced by the approximate knowledge of dynamics of any and not a specific subsystem preserving thus the modularity of the approach. Furthermore, the dissipativity framework is for first time discussed in the teleoperation context. A transparency analysis of the proposed scheme with the generalized scattering transformation shows improved performance, in terms of displayed mechanical properties, compared to the standard scattering transformation and passivity formalism.

The remainder of this chapter is organized as follows: In Section 3.1 a dissipativity-based modeling of the constructive modules of a teleoperation system is discussed based on the background knowledge of Chapter 2. The dissipative subsystems are used to render the overall teleoperation architecture as a dissipative system in Section 3.2, two architectures are exemplarily studied. Approximate dynamics knowledge can thus be utilized in the dissipativity of the system. The stability of the overall architecture with the communication unreliabilities is discussed in Section 3.3 and its performance, in terms of transparency is

shown in Section 3.4. It is there shown that the proposed scheme with the generalized scattering transformation shows improved performance, in terms of displayed mechanical properties, compared to the standard scattering transformation. In Section 3.5 and 3.6 a simulative and experimental evaluation is shown, respectively.

3.1 Dissipativity-based modeling of teleoperation systems

A teleoperation system consists of robotic manipulators, namely the human system interface and the teleoperator, a human operator, and the environment. In this section, these different systems are discussed under the dissipativity point of view and it is shown how they can fit to the proposed dissipativity-based framework. Particularly, as discussed in Chapter 2, (Q, S, R)-dissipativity is an input/output property, thus no state or model knowledge is required. On the contrary only the energetic-behavior of the system is of interest; the dissipated (or stored) energy is the difference of the supplied input energy (supply rate) minus the output one.

In the following, two different models of robotic manipulators are exemplarily studied, without however the requirement on their knowledge or the intention to restrict the overall framework to these. Teleoperation architectures made up from (Q, S, R)-dissipative subsystems are discussed in Section 3.2.

3.1.1 Lagrangian dynamics

The Lagrangian dynamics of a rigid and fully actuated n-link manipulator *with dissipation* are first briefly reviewed. The dynamics of such a system is described by the Euler-Lagrange equation [121]

$$B(q)\ddot{q} + C(q, \dot{q})\dot{q} + g(q) + \underbrace{\frac{\partial R}{\partial \dot{q}}(t)}_{\text{dissipation}} = \tau - J^T(q)f \qquad (3.1)$$

where $q \in \Re^n$ is the vector of joint displacements, $\tau \in \Re^n$ are the applied input torques, $B(q) \in \Re^{n \times n}$ the symmetric positive definite manipulator inertia matrix, $C(q, \dot{q}) \in \Re^{n \times n}$ the Coriolis-centrifugal matrix, $g(q) \in \Re^n$ the vector of gravitational torques, J^T is the transposed Jacobian of the manipulator and $f \in \Re^n$ the vector of externally exerted forces. The term $R(\dot{q}) : \Re^{2n} \to \Re$ in mechanical systems is capturing frictional forces in Lagrangian dynamics and is called the *Rayleigh dissipation* function. It satisfies

$$\dot{q}^T \frac{\partial R}{\partial \dot{q}}(\dot{q}) \geq 0, \quad \text{and} \quad \frac{\partial R}{\partial \dot{q}}(0) = 0.$$

Such a system is dissipative with the input/output pair torque τ/angular velocity $\dot{q}$. In order to show that, compensation of gravitational and external forces is assumed and the following positive definite function is selected

$$V(q, \dot{q}) = \frac{1}{2}\dot{q}^T B(q)\dot{q}.$$

Differentiating with respect to time and considering the skew symmetry of $\dot{B} - 2C$ yields

$$\dot{V}(q, \dot{q}) = \dot{q}^T \tau - \dot{q}^T \frac{\partial R}{\partial \dot{q}}(\dot{q}).$$

Considering the superlinearity of the Rayleigh dissipation function, e.g. viscous friction, it holds

$$\dot{V}(q, \dot{q}) \leq \dot{q}^T \tau - \dot{q}^T D_{min} \dot{q} \tag{3.2}$$

where $D_{min} \in \Re^{n \times n}$ a matrix which represents a lower bound of the Rayleigh dissipation function for each degree of freedom. For example, for a fully-damped (also called pervasively damped) system, which satisfies

$$\dot{q}^T \frac{\partial R}{\partial \dot{q}}(\dot{q}) \geq \sum_{i=1}^{n} \alpha_i \dot{q}_i^2 \quad \text{with} \quad \alpha_i > 0 \; \forall \; i \in \{1, ...n\}. \tag{3.3}$$

the minimum damping will be

$$D_{min} = \mathrm{diag}(\alpha_i) \; \forall \; i \in \{1, ...n\}. \tag{3.4}$$

The system (3.1) is, thus, shown to be (Q, S, R)-dissipative with matrix

$$P = \begin{bmatrix} 0 & \frac{1}{2}I \\ \frac{1}{2}I & -D_{min}I \end{bmatrix}. \tag{3.5}$$

Remark 3.1.1 With a more conservative choice of $d_{min} = \min_i(\alpha_i) \; \forall \; i \in \{1, ...n\}$ the system is OFP(d_{min}), whereas for the switched input/output pair, i.e. angular velocity $\dot{q}$ / torque τ, IFP-ness with same d_{min} can be deduced; the proof is omitted for brevity.

3.1.2 Task space impedance controlled manipulator

One of the fundamental requirements for the success of a manipulation task is the capability to handle interaction between manipulator and human/environment. Therefore, often impedance control approaches in task space are used and the corresponding teleoperation architecture is discussed in Section 3.2. In the following, the dissipativity properties of an impedance controlled manipulator will be derived as a second example on dissipative manipulators.

In an impedance control scheme the manipulator is controlled to exhibit a certain impedance in contact with the environment; for details see task space impedance control in [144]. In approximation, the manipulator can be then represented by a mechanical impedance in operational space which models the relationship between the vector of resulting forces and the vector of displacements in operational space (input/output model). Here, we suggest, potentially partially unknown, time-invariant, nonlinear mass-spring-damper systems (as a more general case than a linear mechanical impedance)

$$M\ddot{x}(t) + D(x, \dot{x})\dot{x}(t) + Kx^{2k+1}(t) = f(t), \tag{3.6}$$

with the nonlinear damping term $D(x, \dot{x})\dot{x}$; $k \in \aleph$, and $K \in \Re^{n \times n}$ is the diagonal and positive-definite stiffness matrix, $x \in \Re^n$ is the Cartesian position vector, $f \in \Re^n$ are the external forces, $M \in \Re^{n \times n}$ the diagonal and positive-definite inertia matrix. The components $D_i(x, \dot{x})$ of the damping term $D(x, \dot{x}) = diag\{D_i(x, \dot{x})\}$ are assumed to be continuous and nonlinear functions for which $D(x, \dot{x}) \geq d_{min}\dot{x}$ when $\dot{x} \geq 0$ and $D(x, \dot{x}) \leq d_{min}\dot{x}$ when $\dot{x} < 0$, with $d_{min} \geq 0$ holds componentwise and accounts for viscous damping. The non-linear stiffness term should display also negative forces and therefore only odd powers of the position are allowed.

It will be now shown that with the appropriate choice of the input/output pair the model (3.6) is input-feedforward-output-feedback passive (IF-OFP) system. Consider for example the force f/velocity $\dot{x}$ as input/output pair and the following storage function

$$V = \underbrace{\frac{1}{2}\dot{x}^T M \dot{x}}_{\text{kinetic energy}} + \underbrace{\frac{1}{2k+2}(x^{k+1})^T K x^{k+1}}_{\text{potential energy}}, \tag{3.7}$$

representing the kinetic and potential energy. Taking the derivative of it and integrating it follows

$$V(x(t)) - V(x(0)) = \int_0^t (M\ddot{x} + Kx^{2k+1})^T \dot{x} \, \mathrm{d}\tau =$$

$$= \int_0^t (f - D(x, \dot{x}))^T \dot{x} \, \mathrm{d}\tau \leq \int_0^t f^T \dot{x} - d_{min}\dot{x}^T \dot{x} \, \mathrm{d}\tau$$

The system is, hence, for , $f \mapsto \dot{x}$ shown to be OFP(d_{min}) with $d_{min} = \epsilon \geq 0$. Similarly, the system can be shown to be IFP(δ) with input/output pair the velocity $\dot{x}$/force f, i.e. $\dot{x} \mapsto f$, and storage function (3.7)

$$V(x(t)) - V(x(0)) \leq \int_0^t \dot{x}^T f - d_{min}\dot{x}^T \dot{x} \, \mathrm{d}\tau,$$

$d_{min} = \delta \geq 0$.

Remark 3.1.2 For all subsystems that are represented as such an impedance, i.e. human operator arm, environment, and master/slave manipulators, knowledge of the lower sector bound of the damping force term $D(x, \dot{x})$ of the system (3.6) is sufficient to guarantee IF-OFP properties. Note that in case of a linear damping term, i.e. $D(x, \dot{x}) = diag\{d_i\}$, $i = 1, ..., n$ the dissipativity parameter is $d_{min} = \min_i d_i$. The inertia M and stiffness K components can be unknown as long as it can be shown that the subsystem has a second order structure as (3.6).

Remark 3.1.3 A general (Q, S, R)-dissipative approach allows for a more differentiated consideration of dissipativity than IF-OFP can, in particular the lower bound of the damping can be defined element-wise as in (3.4), i.e. separately for each degree of freedom, if the knowledge exists.

Remark 3.1.4 In case the bound of the damping force term $D(x, \dot{x}, t)$ of the system (3.6) is unknown, the analysis is reduced to the case of simply passive systems as performed in [4] by setting $d_{min} = 0$.

3.1.3 Human dynamics

The human arm dynamics are required at this phase of the control design and should be also modeled under the dissipativity point of view. Actually, it is discussed in Section 2.1.1 that the actual human arm *endpoint* characteristics are close to second-order. For our approach we can, therefore, only assume that the human arm can be represented by a second order structure as (3.6) in task space, *without* knowledge of the specific values of M, $D(\cdot)$, and K though. Taken that, the human arm endpoint characteristics can be easily shown to be $OFP(d_{min})$ or $IFP(d_{min})$ systems depending on their input/output causality. To define the degree of dissipativity, only approximate knowledge of the human arm damping d^h_{min} is required, particularly a lower bound of it. Further knowledge of a bound for each degree of freedom can result in a (Q, S, R) dissipativity matrix as well. In that way, a class of semi-parametric human models is used. Neither a solid second-order model is employed, reducing the robustness of the approach when the model slightly differs from the nominal one, nor are all models characterized as simply passive leading thus to one class of systems that is not distinguishing between two human operators.

Damping lower bound acquisition

As discussed, the presented framework requires only the knowledge of a lower bound d_{min} on the damping each subsystem displays. This is not a restrictive constraint, considering that even unknown lower bound of the damping can be modeled when the lower bound is set to zero $d_{min} = 0$. The dissipativity-based analysis can, in worst case, be reduced to the well-studied case of passive systems.

However, it is known that human arm damping varies depending on neuromuscular activity and other psychophysical factors. In [42] it is shown that the human arm follows a minimum jerk trajectory, and [132] shows that there is a minimum damping on this movement in a human-robot co-operation context, namely 16 Ns/m for a 1-DoF task with a specific grip of the human arm. Although, specific numbers do not apply to the whole range of scenarios, neuromuscular activities and different types of grip, a lower bound can be found by other means, see e.g. the impedance estimation technique in [67]. Speich *et al.* in [151] reported a damping of 3.6 Ns/m by using only a damper-spring model and instructing the human to remain still but maintain a strong grip on the handle and not apply any other tension, i.e. human remained passive to the device's reactions. Kosuge *et al.* in [94] identified the human arm damping to be equal to 17.26 Ns/m in a scenario where the user was allowed to apply intentional force.

In Chapter 5 the problem of estimating this lower bound is further discussed, an approximation of the lower damping bound is there achieved with an estimation based on the human grip force, i.e. tight grasp of the device will imply higher lower bound of the damping. For the rest of the analysis in this chapter a lower bound of the human arm damping d^h_{min} is taken for granted, if not it is set to zero.

3.1.4 Environment dynamics

Similarly to the human arm characteristics, the environment dynamics are also often approximated by that of a linear second-order model that can be straightforwardly applied in the proposed framework. Although it is probably much more difficult to find a lower bound of damping for the environment, as the free space motion is in most of the applications has zero damping thus lower bound $d_{min}^e = 0$, specific applications allow for some improvements. Particularly, in-body operations usually come with some higher environmental damping due to the contact with tissues, not to mention operations were no free space motion at all is employed. Nevertheless, specific environments such as for example the sea water in underwater operations have also significant viscosity factors that further allow for some higher dissipativity, and as will be seen later some corresponding improvement. More indicatively, sea water displays viscosity of $10^{-3} Ns/m^2$, heavy water used in nuclear reactors $1.3 \times 10^{-3} Ns/m^2$ and motor oil $250 \times 10^{-3} Ns/m^2$. A free space environment will have a lower bound $d_{min}^e = 0$ of damping and the dissipativity properties of this subsystem reduce to the case of passive systems.

3.2 Dissipativity properties of teleoperation architectures

In this section two popular delay-free teleoperation architectures are exemplarily investigated under the scope of our dissipativity framework: A task space velocity-force impedance/admittance teleoperation scheme based on the dynamics of the mechanical impedance in Section 3.1.2 and a joint space velocity/coordinated torque control teleoperation architecture based on the Lagrangian dynamics of Section 3.1.1 and assuming two kinematically similar manipulators for the HSI (master) and TO (slave) side.

3.2.1 Task space impedance/admittance control architecture

A velocity-force impedance/admittance teleoperation control scheme in task space is considered where the devices on both sides measure the forces that the user or the environment exert on them and react with motion (acceleration,velocity, position), i.e. admittance-type devices. The desired compliant behavior is achieved by implementing admittances in the form of simple linear mass-spring-damper systems as in (3.6) with linear time-invariant damping and stiffness matrices. The desired admittances are, therefore, also IFP or OFP systems depending on the input/output pair.

In Figure 3.1, the feedback interconnection structure is illustrated for a velocity-force architecture. The communication time delay blocks and the blocks Ξ, Ξ^{-1} should be neglected at the moment, i.e. $\Xi = 1, T_1 = T_2 = 0$, they will be explained in the next section. The admittance controlled manipulators, master and slave, are assumed articulated robots with position control in joint space and Cartesian impedance. The joint controllers are assumed high gain; gravity and external forces are compensated, therefore the internal position loop dynamics can assumed to be negligible and are not shown on the figure; for
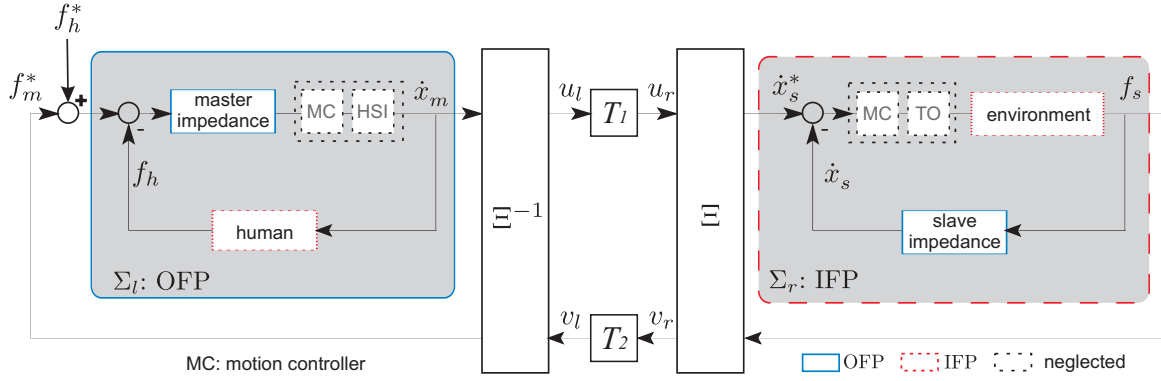
Fig. 3.1: Teleoperation system with time delay and generalized scattering transformation Ξ. The master and slave impedance is given by (3.8) and (3.9), respectively.

more details see [61, 126]. The resulting master and slave dynamics is

$$f_m^* + f_h^* - f_h = M_m \ddot{x}_m + D_m \dot{x}_m, \tag{3.8}$$
$$f_s = M_s \ddot{x}_s + D_s \dot{x}_s + K_s x_s \tag{3.9}$$

where D_i the damping, M_i masses, K_i stiffness, x_i positions, $i = \{m, s\}$ subscripts indicate master and slave, respectively. Therefore, a linear impedance in task space as in (3.6) is rendered for each manipulator. The human and environmental forces are represented by f_h and f_s, respectively, whereas f_m^* is the force-feedback term and f_h^* the voluntarily applied force.

The systems (3.8) and (3.9) are sub-cases of the nonlinear dynamics in (3.6) and the controlled manipulators are, hence, OFP(ϵ_m) and OFP(ϵ_s), respectively, with $\epsilon_m = \lambda_{min}(D_m)$ and $\epsilon_s = \lambda_{min}(D_s)$ being the smallest eigenvalues of the damping matrices.

The human arm and the environment are also modeled as nonlinear mass-spring-damper systems according to (3.6). With the choice of $u = \dot{x}_m$ as input and $y = f_h$ as output the human arm is IFP(δ_h) with $\delta_h = d_{min}^h$. Similarly with input $u = \dot{x}_s^* - \dot{x}_s$ as input and $y = f_s$ as output the environment is also IFP(δ_e) with $\delta_e = d_{min}^e$.

Proposition 3.2.1 The feedback interconnection of the left-hand subsystem in Figure 3.1 with $f_m^* + f_h^*$ as input and $\dot{x}_m$ is OFP(ϵ_l) with $\epsilon_l = \epsilon_m + \delta_h > 0$, and the right-hand subsystem with $\dot{x}_s^*$ as input and f_s as output is IFP(δ_r) with $\delta_r = \delta_e$ and $\delta_e + \epsilon_s > 0$

Proof: Using Lemma 2.3.13 and 2.3.14. ■

From now on the task space impedance/admittance control architecture is considered as the networked interconnection of an OFP(ϵ_l) and an IFP(δ_r) system with $\epsilon_l, \delta_r > 0$ and

$$P_l = \begin{bmatrix} 0 & \frac{1}{2}I \\ \frac{1}{2}I & -\epsilon_l I \end{bmatrix}, \quad P_r = \begin{bmatrix} -\delta_r I & \frac{1}{2}I \\ \frac{1}{2}I & 0 \end{bmatrix}$$

their (Q, S, R)-dissipativity matrices. Stability of this interconnection can be now deduced, see Section 3.2.3. Of course any (Q, S, R)-dissipativity matrix $P_l' \succeq P_l$ and $P_r' \succeq P_r$ applies the same way.

Remark 3.2.2 The modularity of the overall approach allows for similar argumentation with switched causality, i.e. admittance/impedance control architecture with force transmitted in the forward channel and position fed back through the backward one. In this case, the left-hand side system is a IFP(δ_l) system with $\delta_l = \delta_h$ and $\delta_h + \epsilon_m > 0$ and similarly the right-hand side system a OFP(ϵ_r) system with $\epsilon_r = \epsilon_s + \delta_e$.
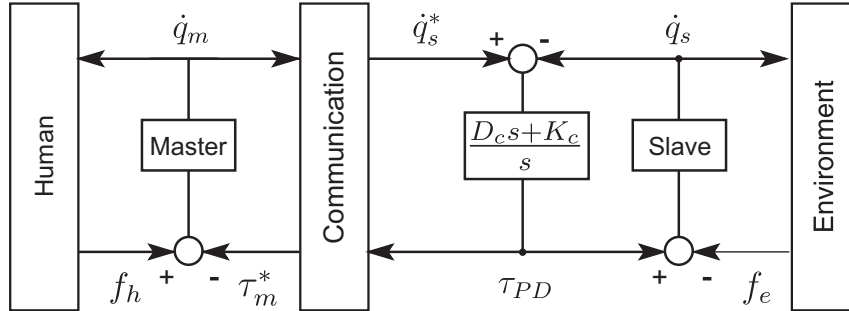
Fig. 3.2: Joint space PD-control architecture: transmission of the joint velocity from HSI to TO and feedback of the coordinating torque.

3.2.2 Joint space PD-control

In the classical PD-control approach of a bilateral teleoperation system a proportional-derivative controller on the slave side is controlling both manipulators. Assuming the manipulators have the Lagrangian dynamics of Section 3.1.1 and are locally compensated for the gravitational forces for both manipulators a simple PD feedback based on the tracking error between master and slave joints is used in joint space

$$
\begin{aligned}
\tau_m &= -g_m(q_m) + \tau_{PD} \\
\tau_s &= -g_s(q_s) + \tau_{PD} \\
\tau_{PD} &= D_c(\dot{q}_m - \dot{q}_s) + K_c(q_m - q_s),
\end{aligned}
\tag{3.10}
$$

where the feedback gains $D_c \in \Re^{n \times n}$ and $K_c \in \Re^{n \times n}$ are constant diagonal positive definite matrices, $\tau_{PD} \in \Re^n$ the computed torque of the PD-controller, and $\tau_m, \tau_s \in \Re^n$ the applied input torques of the Lagrangian master and slave manipulators, see (3.1). With g_m and g_s the gravity compensation of the manipulators is denoted. The control architecture is illustrated in a simplified form in Figure 3.2; the gravity compensation of the manipulators as long as the conversion of the endpoint forces to joint values (using inverse kinematics) are not illustrated. It can be straightforwardly shown that this simple PD controller (3.10) is a dissipative IFP(d_{min}) system with the joint velocity $\dot{q}$ / torque τ_{PD} as input/output pair and $d_{min} = \lambda_{min}(D_c)$; with λ_{min} the smallest eigenvalue is denoted.

The overall teleoperation architecture, seen from the dissipativity point of view, is again an interconnection of dissipative systems as graphically illustrated in Figure 3.3. The end system is a networked interconnection of an OFP($\epsilon_m + \delta_h$) and an IFP(d_{min}^{PD}) system with $d_{min}^{PD} = \min(D_c, D_c + \epsilon_s + \delta_e)$ as Lemma 2.3.13 and Lemma 2.3.14 show.
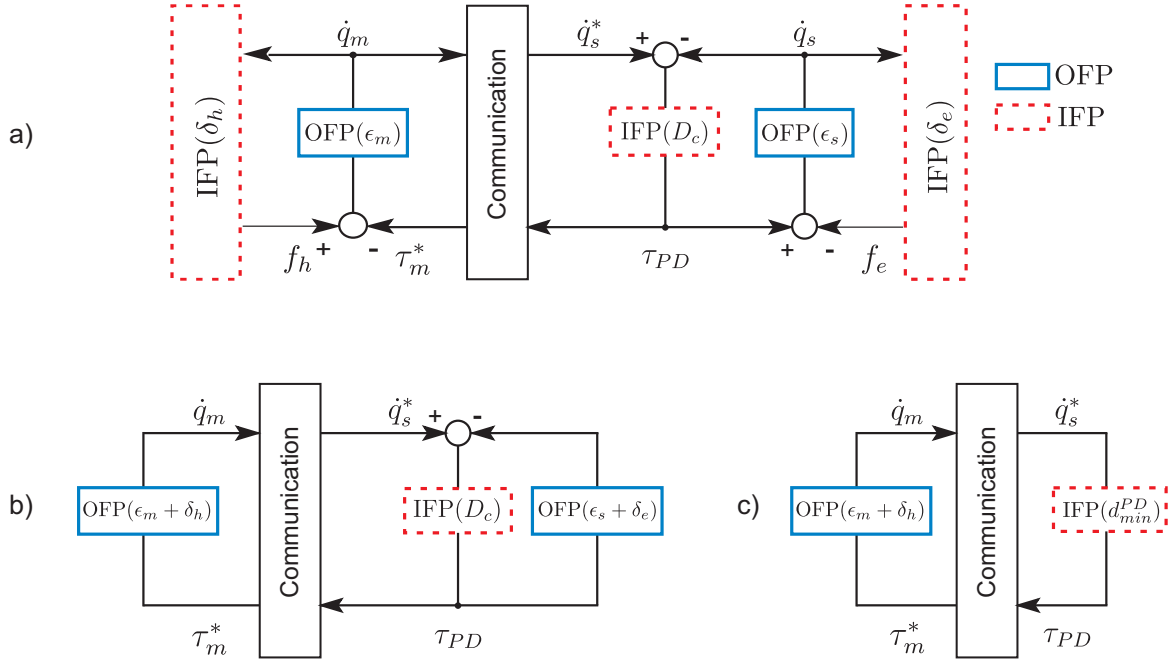
Fig. 3.3: Dissipativity-based analysis of the PD control scheme step by step. a) The overall system composed of IF-OFP subcomponents. b) The feedback interconnections of the human and the master manipulator on the one side, and the environment with the slave manipulator on the other, are merged with the help of Lemma 2.3.13 and Lemma 2.3.14 into two OFP structures respectively. c) The PD-controller in feedback with the OFP systems form an IFP system.

From now on the joint space PD-control architecture is considered as the networked interconnection of an $\text{OFP}(\epsilon_m + \delta_h)$ and an $\text{IFP}(d_{min}^{PD})$ system with $\epsilon_l, \delta_r > 0$ and

$$P_l = \begin{bmatrix} 0 & \frac{1}{2}I \\ \frac{1}{2}I & -(\epsilon_m + \delta_h)I \end{bmatrix}, \; P_r = \begin{bmatrix} -d_{min}^{PD}I & \frac{1}{2}I \\ \frac{1}{2}I & 0 \end{bmatrix}$$

their (Q, S, R)-dissipativity matrices.

3.2.3 Stability without communication unreliabilities

By neglecting any communication network unreliabilities (e.g time delay or packet loss) and by having each subcomponent of the teleoperation architecture modeled as a dissipative system, finite $\mathcal{L}_2$-gain stability of both the task space impedance control of Section 3.2.1 as well as the joint space PD-control of Section 3.2.2 can be deduced from Corollary 2.3.19 or Proposition 2.3.20.

For the task space impedance/admittance control architecture the left- and right-hand side structures have to present some positive dissipative properties as the only sufficient condition. Particularly, $\epsilon_l = \delta_h + \epsilon_m > 0$ should hold for the $\text{OFP}(\epsilon_l)$ left-hand side system ($\delta_l = 0$). The dissipativity properties of the human operator and that of the master manipulator are equally contributing to the overall left-hand side system, see Lemma 2.3.13.

A possible lack of passivity from the human action can thus be compensated just by some

excess of passivity at the master manipulator, and vice versa.

This is a very important fact and consists one of the major novelties of the presented framework as the human is no longer required to be passive, something that, as discussed, was judged on empirical grounds. Similarly, on the right-hand side, a similar sufficient condition holds, i.e. $\epsilon_r = 0$, $\delta_r = \min(\delta_e, \delta_e + \epsilon_s) > 0$ deduced from Lemma 2.3.14. This means that no lack of passivity is allowed for the environment that has to be *at least* passive, however, its excess of passivity can compensate some lack of passivity at the slave manipulator, which is though considered a rare case.

For the switched causality, namely when force is transmitted in the forward channel and velocity in the backward one, similar conditions hold. Particularly, in this case the slave manipulator can compensate for lack of passivity at the environment, and vise versa.

Similarly, in the joint space PD-control architecture, same conditions hold where again ϵ_l and δ_r should be positive. However, in this case the right-hand side allows for lack of passivity to be present in other terms of the structure. Particularly, *the environment can have some lack of passivity* $\delta_e < 0$ as long as the sum $\epsilon_s + \delta_e > 0$, i.e. this is compensated by excess of passivity at the manipulator; see also Figure 3.3b. The feedback gain D_c of the PD-controller is required to be positive.

The above results go one step beyond the passivity setting. Particularly, the fact that not each single parameter is required to be positive for stability, but the sum of the IF-OFP, or (Q, S, R), properties of the system is required instead, allows for some lack of passivity in specific subsystems and hence some reduced conservatism.

3.3 Stability with communication unreliabilities

It is well-known that communication unreliabilities may destabilize an otherwise stable teleoperation system and within the standard passivity-based approach and its extensions, the scattering transformation has been proven a robustly stabilizing control measure. In the following, the problem of communication unreliabilities is considered and it is shown how the *generalized scattering transformation* [105] can be used to stabilize the teleoperation system in this presented dissipativity-based modeling framework. First, the most important results regarding the generalized scattering transformation will be presented and the communication unreliabilities under which the teleoperation system can be stabilized will be discussed thereafter.

3.3.1 Stability with the generalized scattering transformation

The generalized scattering transformation is a linear input/output transformation to guarantee stability in presence of any small gain operator in the communication loop and it is represented by the matrix Ξ in Figure 3.1. Instead of the left-hand output variable $\dot{x}_m$ the variable u_l is transmitted

$$\begin{bmatrix} u_l \\ v_l \end{bmatrix} = \Xi \begin{bmatrix} \dot{x}_m \\ f_m^* \end{bmatrix}. \tag{3.11}$$

Analogously, v_r is transmitted to the HSI instead of the right-hand side output f_s where

$$\begin{bmatrix} u_r \\ v_r \end{bmatrix} = \Xi \begin{bmatrix} \dot{x}_s^* \\ f_s \end{bmatrix}. \tag{3.12}$$

The transformation consists of a rotation R_θ and a positive-definite scaling matrix G[1]

$$\Xi = R_\theta \cdot G = \begin{bmatrix} \cos\theta I & \sin\theta I \\ -\sin\theta I & \cos\theta I \end{bmatrix} \begin{bmatrix} g_{11} I & 0 \\ 0 & g_{22} I \end{bmatrix} \tag{3.13}$$

where I represents the $n \times n$ unity matrix, $\det G \neq 0$ and $\theta \in [-\frac{\pi}{2}, \frac{\pi}{2}]$. The choice of the transformation angle θ is based on the IFP- and OFP-properties of each side, g_{11}, g_{22} represent free tuning scaling parameters. By means of this transformation stability can be achieved for any small gain type network operator as the following proposition states.

Proposition 3.3.1 [77] Assume a system consisting of networked interconnection of an OFP(ϵ_l) and an IFP(δ_r) system with $\epsilon_l, \delta_r > 0$, the bidirectional communication channel with arbitrary large but constant time delay and the input-output transformation (3.13). Delay-independent finite gain $\mathcal{L}_2$-stability is ensured for any small gain operator in the network if and only if for each G the rotation matrix parameter $\theta \in [\theta_l, \theta_r]$. Here θ_l and θ_r are one of the two solutions of

$$\cot 2\theta_i = \frac{\epsilon_{G_i} - \delta_{G_i}}{2\eta_{G_i}}, \ \ i \in \{l, r\} \tag{3.14}$$

which simultaneously satisfy

$$\alpha(\theta_i) = 2\eta_{G_i} \sin\theta_i \cos\theta_i - \delta_{G_i} \cos^2\theta_i - \epsilon_{G_i} \sin^2\theta_i \geq 0, \tag{3.15}$$

$\epsilon_{G_i}, \delta_{G_i}$ and η_{G_i} are given by the matrix P_{G_i}

$$\begin{aligned} P_{G_i} &= \begin{bmatrix} -\delta_{G_i} I & \eta_{G_i} I \\ \eta_{G_i} I & -\epsilon_{G_i} I \end{bmatrix} = G^{-T} P_i G^{-1} = \\ &= \begin{bmatrix} -\delta_i \frac{1}{g_{11}^2} I & \frac{1}{2g_{11}g_{22}} I \\ \frac{1}{2g_{11}g_{22}} I & -\epsilon_i \frac{1}{g_{22}^2} I \end{bmatrix}, \ i \in \{l, r\}. \end{aligned} \tag{3.16}$$

Hence, instead of choosing $\theta = 45°$ and $g_{11} = \sqrt{b}$, $g_{22} = \frac{1}{\sqrt{b}}$, as for standard scattering transformation [4], here θ can be chosen out of an interval. The interval for a choice of θ that will guarantee stability is influenced by the IF-OFP properties of the interconnected systems, the human and the environment side. It is, for $g_{11} = g_{22} = 1$, exemplarily illustrated in Figure 3.4.

---

[1] This transformations consists of a special case of a general class of static transformations presented in [105]. There G should just be an invertible matrix providing thus an additional degree of freedom for performance design aspects.
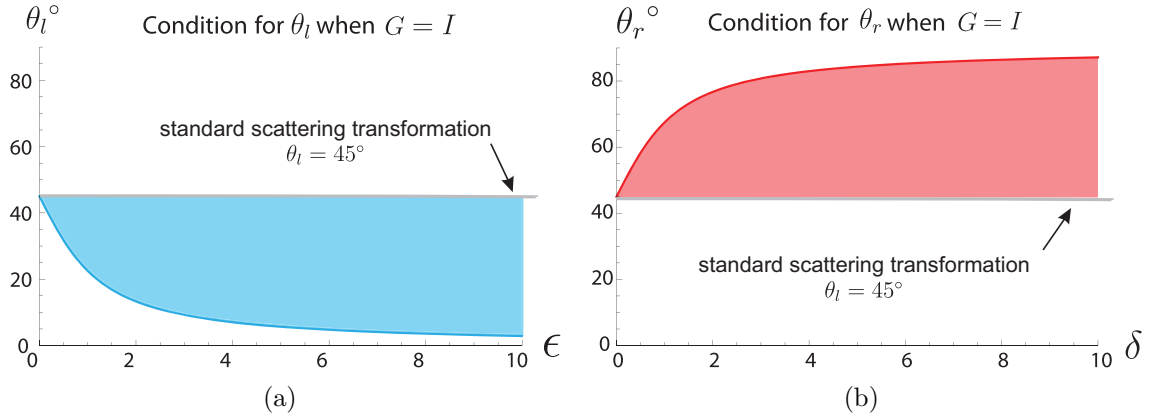
Fig. 3.4: The influence of the IF-OFP-properties of the human and environment subsystems to the stability margins for θ; here for $G = I$. (a) θ_l based on the OFP-ness ϵ. (b) θ_r based on the IFP-ness δ. It is observed that in both cases the more IF-OFP the system is, the larger is the admissible region for the choice of θ.

Remark 3.3.2 It can be shown that for the systems studied here, i.e. either OFP with $\epsilon_l > 0$ and $\delta_l = 0$, or IFP with $\delta_r > 0$ and $\epsilon_r = 0$, and due to our initial assumption on positive-definiteness of G, the rotation matrix parameter $\theta \in \left[0, \frac{\pi}{2}\right]$.

Remark 3.3.3 To gain further insight on the effect that the generalized scattering transformation has on IF-OFP systems one could look at the LTI case, which is, exemplarily here, illustrated on Figure 3.5. A rotation of an OFP or IFP system will cause the characteristic of the Nyquist plot of each system to map to that of a system with finite gain. Note that for a rotation with some specific angle, θ_r or θ_l given by the Proposition 3.3.1, the IF-OFP system will map to a system with small gain $\gamma \leq 1$. For passive systems ($\epsilon = \delta = 0$) this angle is 45°.

Remark 3.3.4 Finite gain $\mathcal{L}_2$-stability is guaranteed for any *small gain operator* in the communication loop. As will be seen in the following this applies not only to arbitrarily large constant time delay, which has a $\mathcal{L}_2$-gain $\gamma_D = 1$, but also for properly handled time-varying delay [22] and packet loss [9, 70].

3.3.2 Small gain communication network operators

In the following the small gain properties of different communication network operators will be discussed.

Time delay

We consider a time delay operator $\mathcal{D} : u(\cdot) \rightarrow y(\cdot)$ with $u, y \in \Re^m$ the input and output respectively, i.e. $y(t) = u(t - T(t))$, where T is the time delay value. In case of constant time delay, i.e. $T(t) = T_0$ it is easy to show that the L_2 gain $\gamma_D = 1$ for arbitrarily large constant time delay.
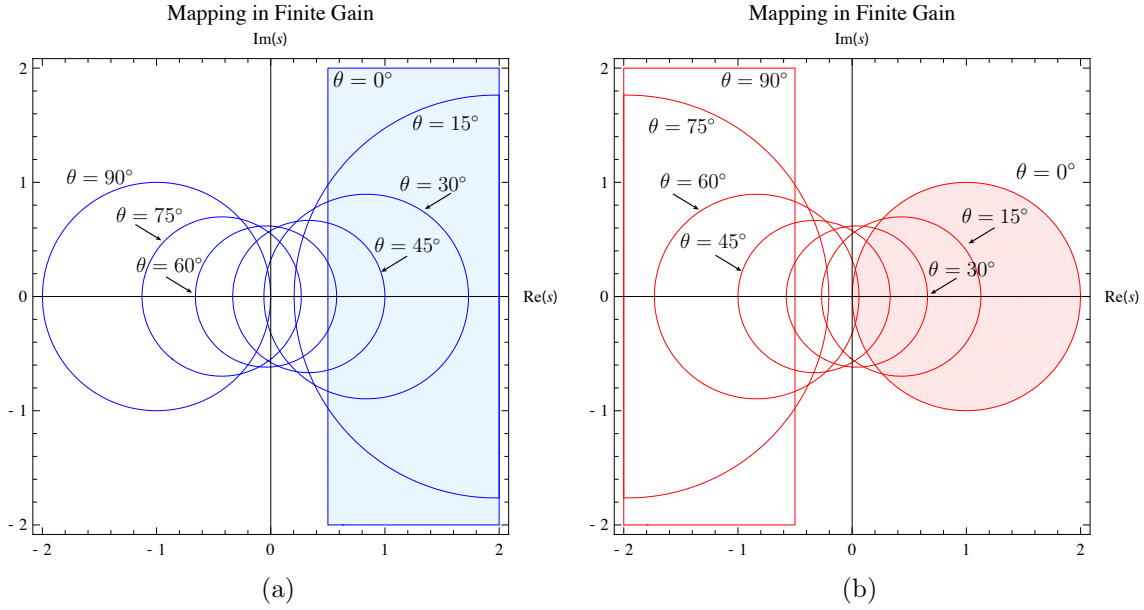
Fig. 3.5: The generalized scattering transformation maps the characteristic of the Nyquist plot of IF-OFP systems into that of finite gain systems. (a) OFP system rotated with various angles. (b) IFP system rotated with various angles.

However, in case of time-varying delay, without further assumptions, the operator becomes unbounded [92]. The time delay operator can be bounded assuming a maximum in the time delay derivative.

Proposition 3.3.5 [92] If the time delay is continuously differentiable and the time delay derivative bounded, i.e.

$$\dot{T} \leq d < 1 \tag{3.17}$$

the $\mathcal{L}_2$ gain of the time-varying delay operator is

$$\gamma_D = \frac{1}{\sqrt{1-d}}. \tag{3.18}$$

We observe from (3.18) that the $\mathcal{L}_2$-gain of the time-varying delay can be larger than one, and therefore violate the small gain condition. It is shown in [107] that the system in Proposition 3.3.1 is globally asymptotically stable if

$$\gamma_{D_1}^2 \gamma_{D_2}^2 < \frac{\beta(\theta)\alpha(\theta) + \Delta}{\beta(\theta)\alpha(\theta) - \Delta} \tag{3.19}$$

where D_1 and D_2 the time delay operators in both channels,

$$\Delta = \min\left[(\epsilon_r + \delta_l)g_{11}^2, (\epsilon_l + \delta_r)g_{22}^2\right] > 0,$$

and

$$\beta(\theta) = \alpha(\theta) + \delta_G + \epsilon_G.$$

From (3.19), we observe that the larger Δ is (the more dissipative the system), the larger

the gain of the time delay operators which do not compromise stability can be, allowing thus larger bounds for the time delay derivatives. Furthermore, many scattering based approaches are addressing time-varying delay [103, 113]: They introduce control actions to keep the $\mathcal{L}_2$ gain of the corresponding input-output operator $\gamma \leq 1$. These approaches are straightforward to combine with the proposed approach.

Packet loss

Packet loss occurs when one or more packets of data traveling across a computer network fail to reach their destination. It can be caused either by network congestion, faulty networking hardware or as a result of time-varying time delay, i.e. packets arriving in permuted order or empty sampling instances at the receiver side due to increasing time delay. In case of a short term signal outage due to packet loss, either due to network congestion or processing, the missing data can be estimated. Packet processing algorithms as presented in [70, 10, 9] can balance the energy and it is straightforward to show that they have an $\mathcal{L}_2$ gain less or equal to one.

The simplest strategy belonging to a largest class of all possible algorithms is the Hold-Last-Sample (HLS), where the last received sample is held for the instance when no packet (sample) is received. However, as it was shown in [70] it is generically not passive and does not satisfy the small gain condition, as the last received sample might have a higher absolute value (energy) than the current one. Stability with the proposed control structure may be compromised.

However, packet processing algorithms as presented in [70, 10, 9] can balance the energy and therefore satisfy passivity and a small gain condition. In fact in [70] three strategies are presented, the strictly passive zeroing strategy where zero packets are considered at packet loss instances, the rate bounding method where bounded change rate is considered to guarantee energy generation does not occur and, finally, low-pass filtering where high frequency components introduced by the hold-last-sample are filtered out. The simple zeroing strategy replaces each missing packet with zero. The network input-output operator can be described as

$$\mathcal{D}_{P,zero} : \begin{cases} u^*(t) = u(t), & \text{when packet received} \\ u^*(t) = 0, & \text{when packet is lost,} \end{cases}$$

where $u(t)$ the transmitted signal and $u^*(t)$ the output of the packet processing algorithm. It can be easily seen that the zeroing strategy is passive and the input-output operator has a $\mathcal{L}_2$-gain $\gamma_{\mathcal{D}_{P,zero}} \leq 1$. Particularly

$$u^*(t)^2 \leq u(t)^2 \ \Rightarrow ||u_t^*||^2 \leq ||u_t||^2$$

where $||u_t^*||^2$, $||u_t||^2$ represent the $\mathcal{L}_2$-norm of the truncated input and output signals respectively. The equality is valid only if no packet is lost. Nevertheless, the zeroing strategy is known to be very conservative.

For the bounded rate strategy, the rate of the transmitted signal is assumed to be bounded $|\dot{u}| \leq |\dot{u}_{max}|$. In application this can be guaranteed by a rate limiter block just before the communication two-port. It is easy to show that this rate limiter does not

generate energy, hence is passive. Considering then data losses on the channel within the time interval $[t_1, t_2]$ with the transmitted signal rate bounded by $|\dot{u}| \leq |\dot{u}_{max}|$ the data recovery algorithm

$$\mathcal{D}_{P,bound} : \begin{cases} u^*(t) & \text{if } \text{sign}\{u(t_1)u^*(t)\} \\ 0 & \text{otherwise} \end{cases} \tag{3.20}$$

where $u^*(t) = u(t_1) - \text{sign}\{u(t_1)\}|\dot{u}_{max}|\Delta t$ with $\Delta_t \in [0, t_2 - t_1]$ is passive. For the proof it is sufficient to show that $u^2(t) \geq u^{*2}$. Given the bounded rate the signal dynamics of the lost data is bounded by

$$|u(t_1 + \Delta t)| \geq |u(t_1)| - |\dot{u}_{max}\Delta t|,$$

hence

$$(u(t_1 + \Delta t))^2 \geq (u(t_1) - \text{sign}\{u(t_1)\}|\dot{u}_{max}|)^2 = u^{*2}(t).$$

Thus, $\gamma_{\mathcal{D}_{P,bound}} \leq 1$.

Remark 3.3.6 The results equally apply to both backward and forward path.

Finally, for architectures or packet processing techniques that do not satisfy a small gain condition the reader can refer to [105], where a *small gain observer* is used, which, by observing the current and past signals, ensures that the output is always satisfying a small gain condition, and if not multiplies it with a gain < 1 so that it does, forcing thus the small gain property of the algorithm.

Haptic data reduction

Haptic data reduction algorithms, as presented in [76, 73] and in [196, 191] by the author, are employed in teleoperation scenarios to avoid network congestion due to the high packet rate of a haptic telepresence system. It can be straightforwardly shown, that those passivity-preserving reduction and reconstruction strategies also comply with the presented work here, namely the small gain condition is satisfied. The data reconstruction techniques will be however further elaborated in Chapter 4.

In summary, the proposed dissipativity-based framework can also guarantee stability for teleoperation systems with communication unreliabilities under the only condition that the corresponding input/output operator of the unreliability has a $\mathcal{L}_2$-gain ≤ 1. Utilizing the dissipativity properties of the subsystems, and as already discussed only approximate model knowledge, the generalized scattering transformation can be applied and a wide range of transformations can be chosen. Later on in this chapter, this wide range of transformations will be investigated for the one that has the best performance.

3.3.3 Passivity-based teleoperation and the scattering transformation

The scattering transformation and the passivity paradigm for teleoperation systems was originally developed by Anderson and Spong [4] and later extended to the concepts of wave variables by Niemeyer and Slotine [118]. Recall Example 2.4 and assume arbitrary large
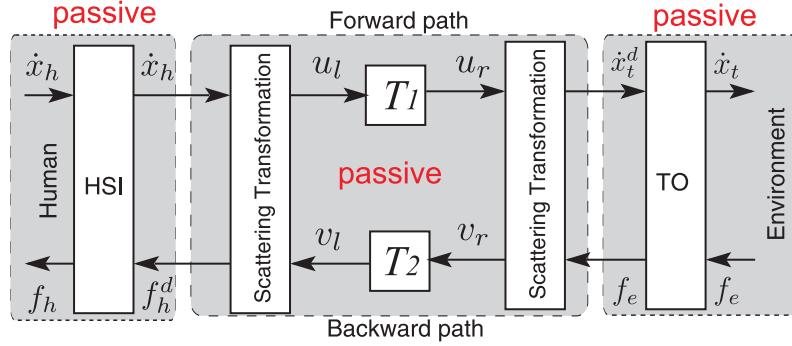
Fig. 3.6: The scattering transformation guarantees stability by making the communication channel passive, and by further assuming passivity of the environment and human together with the fact that a feedback interconnection of passive systems is again passive, hence stable.

constant time-delay is present in the communication channel. The scattering transformation renders the communication 2-port system also passive, thus the systems remains an interconnection of passive systems, thus stable. The scattering transformation consisted the inspiration for the generalized scattering transformation developed in the context of network control systems in [105], and is for this reason presented here. Particularly, the scattering transformation is nothing more than the generalized one, selecting a rotation angle $\theta = 45°$ and scaling $g_{11} = \sqrt{b}$, $g_{22} = \frac{1}{\sqrt{b}}$ in (3.13).

The other way round, if none of the left-/right hand sides in the presented dissipativity-based framework has some dissipativity, but they are considered just passive systems instead ($\epsilon = 0$, and $\delta = 0$), and if G is a positive-definite matrix, Proposition 3.3.1 allows only for one $\theta = 45°$. Selecting the scaling as instructed above one is provided with the scattering transformation

$$\Xi_{scattering} = R_\theta \cdot G = R_{45°} \cdot \begin{bmatrix} \sqrt{b}I & 0 \\ 0 & \frac{1}{\sqrt{b}}I \end{bmatrix}. \tag{3.21}$$

The scattering transformation architecture is illustrated in Figure 3.6. The transmitted scattering (or wave) variables are

$$u_l = \frac{1}{\sqrt{2b}}(f_h^d + b\dot{x}_h), \quad u_r = \frac{1}{\sqrt{2b}}(f_e + b\dot{x}_t^d),$$

$$v_l = \frac{1}{\sqrt{2b}}(f_h^d - b\dot{x}_h), \quad v_r = \frac{1}{\sqrt{2b}}(f_e - b\dot{x}_t^d), \tag{3.22}$$

where $b \geq 0$ defines the characteristic impedance associated with the scattering variables and represents a tuning parameter.

3.4 Transparency evaluation

Performance in a teleoperation system is related to the notion of transparency, which is the ability of the teleoperation system to present the undistorted dynamics of the environment to the human. As a result the human feels like "being" on the remote side and directly interacting with the environment. Modeling the real environment as a mechanical linear time-invariant impedance $Z_e(s)$ and the impedance displayed to the human $Z_h(s)$ transparency is achieved if [97]

$$Z_h(s) = Z_e(s), \tag{3.23}$$

where $s = j\omega$ is a complex variable, representing the Laplace domain; it will be omitted when not needed.

In practice, perfectly transparent teleoperation is difficult to achieve. The interesting question is the degree of transparency that is possible on a teleoperation system. Ignoring the controller dynamics and robot compliance, the case of constant time delay is in this section investigated. The displayed impedance can be computed based on the environment impedance and the generalized scattering transformation according to

$$Z_h = \frac{\xi_{21} - \xi_{11}\Phi e^{-sT}}{-\xi_{22} + \xi_{12}\Phi e^{-sT}}, \quad \Phi = \frac{\xi_{21} + \xi_{22}Z_e}{\xi_{11} + \xi_{12}Z_e}, \tag{3.24}$$

where $T = T_1 + T_2$ the round trip time delay and

$$\Xi = \begin{bmatrix} \xi_{11} & \xi_{12} \\ \xi_{21} & \xi_{22} \end{bmatrix}.$$

In order to analyze and compare different impedances a Padé approximation will be used for the time-delay, which is, however, only valid for low frequencies

$$e^{-sT} \approx \frac{1 - \frac{T}{2}s}{1 + \frac{T}{2}s} \text{ for } \omega < \frac{1}{3T}. \tag{3.25}$$

The teleoperator dynamics are ignored for simplicity. The transformation angle is limited to $\theta \in [0, \frac{\pi}{2}]$, see Remark 3.3.2.

3.4.1 Free space

In case of a free space motion on the environment side ($Z_e = 0$) the eligible range for θ is reduced to $\theta \in [0, 45°]$ as only the left-hand side of the interconnected system is dissipative. The angle θ depends also on (3.14) and (3.15) to give the final eligible range, see Figure 3.4. The displayed impedance is approximated for low frequencies by (3.24) as

$$Z_h^{LF}|_{Z_e=0} = \frac{g_{11}\sin\theta\cos\theta Ts}{g_{22}} \frac{1}{\left(1 + \frac{T}{2}\cos(2\theta)s\right)} \tag{3.26}$$

The above transfer function is stable for all $\theta \in [0, 45°]$. The right-hand term of (3.26) is a low-pass filter with cut-off frequency $\omega_c = \frac{2}{T\cos(2\theta)}$. As $\frac{2}{T} > \frac{1}{3T}$ the term is negligible in the
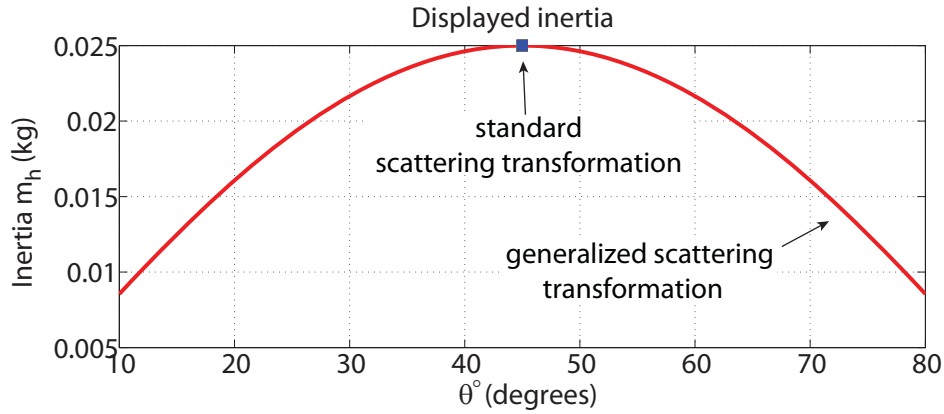
Fig. 3.7: Displayed inertia in free space for various θ values; characteristic impedance and scaling G are set to unity and time delay is set to $T = 50$ ms. The generalized scattering transformation displays lower apparent inertia rendering thus the approach better.

low-frequency range we are focusing on, i.e. $\omega < \frac{1}{3T}$. The remaining displayed impedance indicates an inertia

$$m_h \approx \frac{g_{11}}{g_{22}} \sin \theta \cos \theta T \tag{3.27}$$

linearly increasing with the time delay. For $\theta = 45°$, $g_{11} = \sqrt{b}$ and $g_{22} = \frac{1}{\sqrt{b}}$ this reduces to the known $m_h \approx b\frac{T}{2}$ computed for the conventional scattering transformation, see [71]. Clearly, it can be concluded from (3.27), that the displayed inertia of the generalized scattering transformation outperforms that of the standard scattering approach as the product $\sin \theta \cos \theta$ displays a maximum at $45°$, i.e. the angle of the scattering approach. A numerical example is illustrated in Figure 3.7.

3.4.2 Stiff environment

Analogously, in case of a stiff environment $Z_e = \frac{k_e}{s}$ with a stiffness k_e an eligible range of $\theta \in [0, 45°]$ is allowed depending on the dissipativity of the left-hand system as the right-hand system is simply passive, i.e. the teleoperator dynamics are ignored and the environmental damping is zero. The displayed impedance is approximated for low frequencies by (3.24) as

$$Z_h^{LF}|_{Z_e = \frac{k_e}{s}} = A \frac{\frac{k_e}{s} - \cos(2\theta)\frac{T}{2}k_e + \frac{g_{11}}{g_{22}} sin\theta cos\theta T s}{1 + A\cos(2\theta)\frac{T}{2}s} \tag{3.28}$$

where

$$A = \frac{1}{1 + \frac{g_{22}}{g_{11}} sin\theta cos\theta k_e T} > 0 \text{ for } \theta \in [0, \frac{\pi}{2}].$$

$Z_h^{LF}|_{Z_e}$ is a stable transfer function for $\theta \leq 45°$. As $A < 1$ the displayed stiffness $k_h = Ak_e$ is always smaller than the real environmental one, but A is clearly larger for the generalized scattering transformation. The denominator of (3.28) is a low-pass filter that in the worst case, i.e. $\theta = 0°$, has a cut-off frequency $\frac{2}{T} > \frac{1}{3T}$, therefore, it can be ignored.
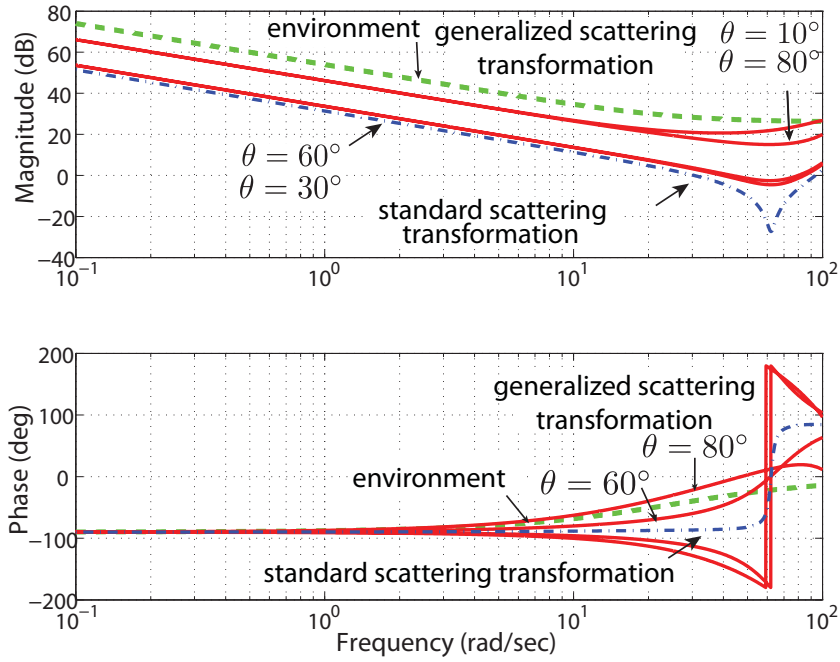
Fig. 3.8: Displayed impedance comparison in contact with the environment. The generalized scattering transformation presents for all θ cases designed an impedance which is closer to the real environmental impedance, thus renders a more realistic (transparent) system.

3.4.3 Stiff-damped environment

The displayed impedance in case of an environment with a spring and a damper $Z_e = \frac{k_e}{s} + b_e$ is approximated for low frequencies by (3.24) as

$$Z_h^{LF}|_{Z_e} = \frac{\gamma\frac{k_e}{s} + b_h + m_h s}{1 + \gamma(\frac{T}{2}\left(\cos(2\theta) + \frac{g_{22}}{g_{11}}Tb_e sin\theta cos\theta\right)s} \tag{3.29}$$

with $\gamma = \frac{1}{1+\frac{g_{22}}{g_{11}}Tk_e sin\theta cos\theta}$, $b_h = \gamma(b_e - \frac{T}{2}k_e\cos(2\theta))$, $m_h = \gamma(\frac{g_{11}}{g_{22}}Tsin\theta cos\theta - \frac{T}{2}b_e\cos(2\theta))$.

The requirement on stable transfer functions in the approximation gives $\frac{g_{22}}{g_{11}} < \frac{\cos(2\theta)}{2b_e sin\theta cos\theta}$. The denominator of (3.29) can be shown to be a low pass filter that can be ignored in the lower frequencies. The resulting displayed impedance is then

$$Z_h^{LF}|_{Z_e=\frac{k_e}{s}+b_e} = \gamma\frac{k_e}{s} + b_h + m_h s \tag{3.30}$$

Remark 3.4.1 We observe that the above displayed impedance in (3.30) can for some values of $\theta \in [0, 90°]$ result in a negative displayed damping part. In order to avoid that and to preserve a non minimum-phase structure of the displayed impedance θ should be chosen such that

$$\cos(2\theta) < \frac{2b_e}{Tk_e}. \tag{3.31}$$
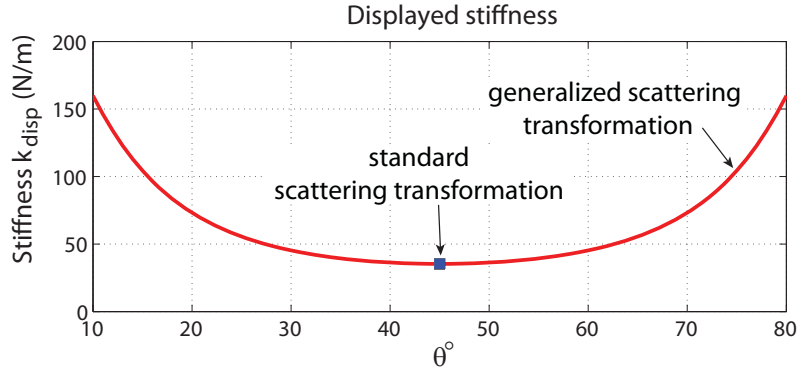
Fig. 3.9: Displayed stiffness for various θ values, environment stiffness is 300 N/m, characteristic impedance is $b = 1$. The generalized scattering transformation displays an increased stiffness. For fair comparison the scaling G of the generalized scattering transformation is tuned such that the free space performance of both methods is the same.

Example 3.1 (Numerical comparison with standard scattering transformation)
In order to exemplarily compare the standard scattering transformation with the generalized scattering transformation we choose the scaling components of the generalized scattering transformation such that the displayed inertia in free space (3.27) is the same as for the standard scattering transformation, namely $\frac{g_{11}}{g_{22}} = \frac{b}{2\sin\theta\cos\theta}$. The approximated displayed stiffness k_h is then compared for the two methods, see Figure 3.9, and it is seen that the stiffness of the generalized scattering transformation outperforms the one displayed by the conventional scattering transformation approach, i.e. for $\theta = 45°$ and the choice $b = 1$. The bigger the deviation from the $45°$ the larger the improvement in terms of displayed stiffness, however, the damping properties are slightly distorted, see (3.30) and the remark below.

Remark 3.4.2 In Figure 3.9 a symmetry around $45°$ is observed in terms of displayed stiffness. This symmetry holds for the displayed stiffness only as the displayed damping will not be the same for $\theta < 45°$ and $\theta > 45°$ making thus one choice of the angle preferable than the other. If the eligible range for θ allows a dubious choice, the angle that will satisfy (3.31) should be preferred. Note that an angle $\theta > 45°$ always satisfies the requirement, pointing out that an IFP-dissipative environment will not face this problem.

3.4.4 Scaling

By (3.28), (3.30) and (3.27) it can be derived that the scaling matrix alters the performance of the system in a similar way the characteristic impedance adjusts the performance of the scattering transformation architecture, cf. [71]. Considering the low frequency approximation, a small factor $\frac{g_{11}}{g_{22}}$ will avoid large inertia in free space movement whereas a large one is required to display high stiffness. Moreover, it can be seen in (3.14), (3.15) and (3.16) that the choice of the scaling components influences the region $[\theta_l, \theta_r]$ that finite gain $\mathcal{L}_2$-stability can be guaranteed. An increasing factor $\frac{g_{11}}{g_{22}}$ will allow for lower θ_l whereas if $\frac{g_{11}}{g_{22}}$ is decreased, the interval $[\theta_l, \theta_r]$ is increasing from the right-hand side, i.e. higher θ_r.

Furthermore, it should be noted that for simplicity in our approach a positive-definite scaling matrix is chosen in (3.13), consequently constraining the eligible range of θ. However, this is just a special case of a range of static transformations as presented in [105]. Theoretically, in case of SISO systems only invertibility of G is required, whereas for MIMO systems the scaling matrix is restricted to the form

$$G = \left[\begin{array}{cc} g_{11}I & g_{12}I \\ g_{12}I & g_{22}I \end{array} \right],$$

with arbitrary $g_{11}, g_{12}, g_{12}, g_{22} \in \Re$, however, under the requirement of invertibility of G. Such a scaling matrix can provide a further degree-of-freedom for performance design aspects and affects the eligible range for angles θ.

3.5 Evaluation

The proposed approach is analyzed in simulation for a velocity - force admittance control scheme consisting of a linear time-invariant spring-damper environment $Z_e = \frac{500}{s} + 20$ and negligible slave dynamics, i.e. $\delta_r = \delta_e = 20$. The left hand-side subsystem is assumed to be OFP(ϵ_l) with $\epsilon_l = 10$ resulting from either the human or master dynamics' minimum damping. For comparison reasons a characteristic impedance $b = 1$ is chosen for the standard scattering transformation and the generalized scattering transformation is tuned with scaling components, $g_{11} = \sqrt{b} = 1$ and $g_{22} = \frac{2g_{11} \sin\theta \cos\theta}{b}$ such that in free space motion both methods display same inertia, i.e. have the same free space performance. The resulting system is delay-independently stable for all $\theta \in [3°, 85°]$. The time delay is set to $T_1 = T_2 = 50$ ms. The Bode plots of the environment impedance and the displayed impedance are depicted in Figure 3.8 for the stiff environment. The system is tuned such that the free space motion is the same for both methods, and the comparison is thus fair. It is observed that the displayed impedance in Figure 3.8 is closer to the environment impedance for the generalized scattering transformation. Particularly for the case $\theta = 30°$, $\theta = 60°$ a stiffness of 48.2 N/m is displayed, whereas for $\theta = 80°$, $10°$ a stiffness of 204 N/m is displayed. This is by far closer to the real environment stiffness than with the use of the standard scattering transformation, where a stiffness of 36.9 N/m is displayed, see Figure 3.8.

3.6 Experimental evaluation

Experiments are performed to demonstrate the benefits of the proposed control approach in contrast to the standard scattering-based approach. The experimental testbed consists of a real teleoperation system with two 3-DoF manipulators. All three DoF were active and were used during the non-contact phase, however, contact and haptic interaction occurred only in the Z-direction to simplify the comparison and its demonstration. A 6-DoF force/torque-sensors (JR3) is mounted at the tip of each manipulator to measure interaction forces with the human operator and the environment, only the three forces measurements were used. The sampling rate of the haptic signals and the local control loops

Tab. 3.1: Controller parameters

Master manipulator	
P-gain	diag(1400,1400,1400)
D-gain	diag(44,44,44)
Inertia[Kg]	diag(12,12,12)
Damping[Ns/m]	diag(30,30,30)

Slave manipulator	
P-gain	diag(1400,1400,1400)
D-gain	diag(44,44,44)
Inertia[Kg]	diag(40,40,40)
Damping[Ns/m]	diag(1000,1000,1000)
Stiffness[N/m]	diag(5000,5000,5000)

human+HSI   communication subsystem   teleoperator+environment
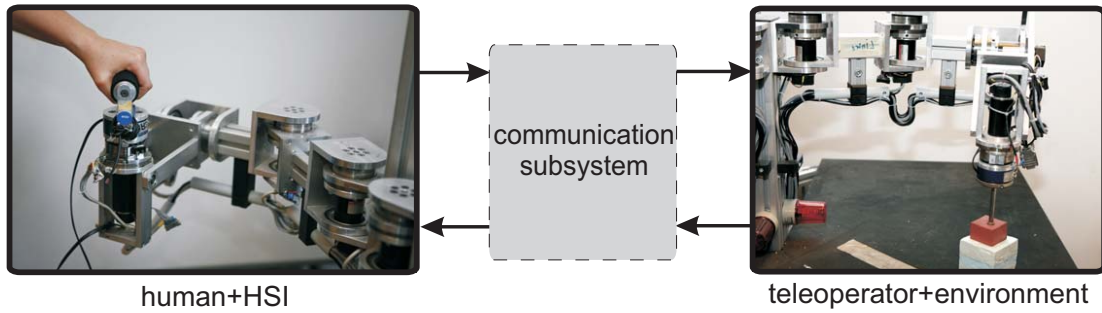
Fig. 3.10: Experimental setup consisting of two networked 3-DoF manipulators equipped with force sensing.

is 1 kHz. A position-based admittance control scheme is considered with the slave rendering a virtual tool. A proportional-derivative joint controller is used as motion controller; gravity and external forces are compensated. All controller parameters are summarized on Table 3.1.

The empirical values identified in [94], namely 17.6 Ns/m were used for the human damping resulting (together with a master damping of approximately 20 Ns/m) in an overall master-side damping of 37 Ns/m in all three degrees-of-freedom; we set the lower bound hence at a conservative value of $\epsilon_m = 30$. On the slave side the virtual tool has 1000 Ns/m damping thus $\epsilon_s = 1000$. A silicon cube is used as environment, having a damping 10 Ns/m, however, free space motion is also employed in the experiment, thus, we choose $\delta_e = 0$. The human arm damping is considered unknown, i.e we just assume passive behavior of the human arm as typically done in the literature, $\delta_h = 0$. The scaling parameters are chosen such that the free-space motion displayed dynamics are similar for both methods, $b = 800$, $g_{11} = \sqrt{b}$, $g_{22} = \frac{2g_{11}\sin\theta\cos\theta}{b}$ and result in $\theta_l = 0.1°$ and $\theta_r = 45°$. The time delay is 50 ms in both channels. The system is stable throughout the experiment. During the experiment the silicon cube, which has a stiffness 1400 N/m, is haptically explored. The proposed scheme is tested with $\theta = 11°$, see Fig. 3.11 and
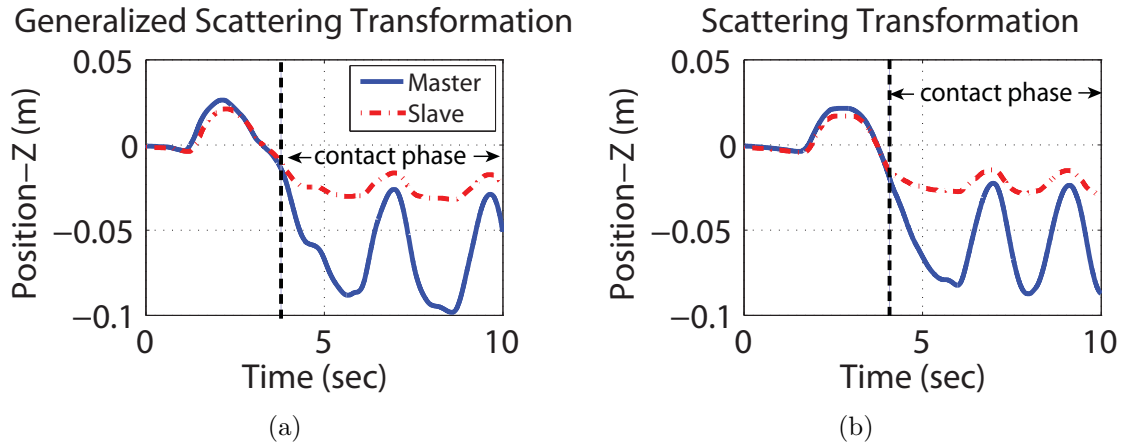
Fig. 3.11: Position tracking for (a) the generalized scattering transformation and (b) the standard scattering transformation. Together with the Figure 3.12 it is observed that for the same position displacements in both experiments, higher force is displayed in the generalized scattering transformation architecture.

Fig. 3.12 for a position and force tracking illustration, respectively. For almost the same displacement of the manipulators, a much larger in amplitude force is displayed for the generalized scattering transformation architecture. The displayed impedance is identified by a least-squares method and shown in Table 3.2. The same experiment is repeated, with a higher delay, i.e. 150 ms in each channel. Both approaches were stable and the identified displayed impedance results are also shown in Table 3.2. As expected, derived also from the transparency analysis, the environment feels "softer" in both methods, with the generalized scattering transformation still superior in terms of displayed impedance. This generally results in more realistic contact, particularly in the first experiment a 34% increase of displayed stiffness is observed, whereas in the second a 65 %, both above the stiffness discrimination threshold reported in [89].

Overestimating the dissipativity of the right-hand side can result in instability, e.g. choosing or estimating the right-hand side as $\delta_r = 50$ whereas in reality the damping is less, and choosing $b = 100$ results in a wider range of eligible $\theta \in [0, 59°]$ for the transformation. Selecting the angle $\theta = 55°$, which should be a safe choice if everything was done correctly, resulted in a unstable system, as illustrated by the positions in Figure 3.13.

3.7 Discussion

Networked haptic teleoperation systems are facing the challenge of stability. Even a small amount of time delay can destabilize an otherwise stable closed-loop system. To mitigate this, the stability is studied under various communication unreliabilities of packet-switched networks. Previous researchers successfully used the passivity paradigm, however, to avoid the over-conservatism, only partially acquired knowledge about the unknown human and environment dynamical systems is, here, desired to be used.

Consequently, in this chapter, the stability of teleoperation architectures is studied under a dissipativity theory point-of-view. It is shown that all the subsystems of the overall
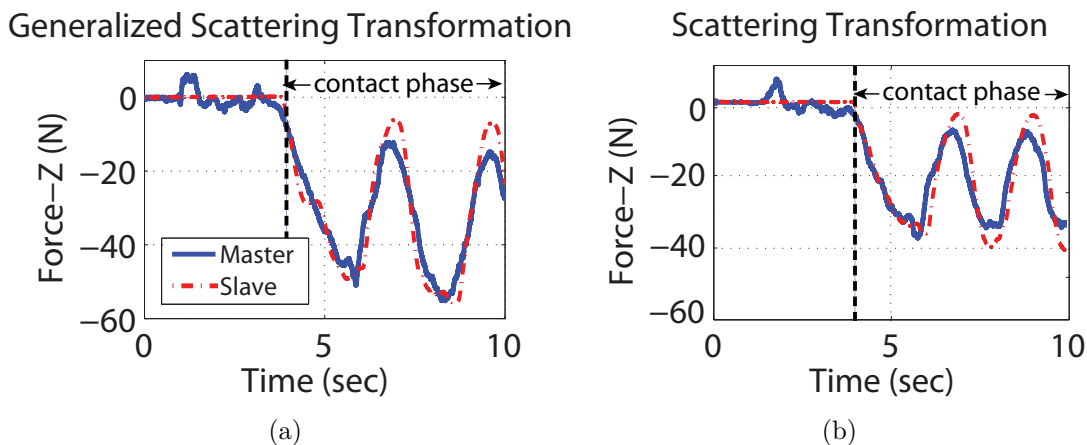
Fig. 3.12: Force tracking for (a) the generalized scattering transformation and (b) the standard scattering transformation. Higher in amplitude forces are observed in the case of the generalized scattering transformation.

teleoperation architecture can be modeled as IF-OFP dissipative systems, a subclass of (Q, S, R)-dissipative systems. Only approximate knowledge of their energetic behavior is required for that, and the overall approach avoids exact modeling of the internal states by preserving the input/output properties of energy-based approaches. A lower bound of the dissipation each systems has is in most cases enough for the framework to apply. In that way, a human-centered approach is achieved, as the knowledge about the human arm dynamics is used in the control design and it is shown to help for performance improvements of the controller. Moreover, a semi-parametric class of systems is in that way used for the human dynamics. On the one hand, a constant second-order human arm model is not required as it would reduce the robustness of the approach in case the real model slightly differs from the nominal one. On the other hand, most passivity-based approaches seen so far characterized the human as simply passive, failing to distinguish between two human operators. With the proposed framework this is avoided. Furthermore, the approach, allows for *non-passivity of certain components to be compensated by the excess passivity of others.* This is a very important finding, considering the conservatism of the control design implied so far by requiring passivity of each subsystem. For the first time, for example, a human taking some non-passive action can be used in an energy-based teleoperation approach as his lack of passivity is expected to be compensated by some excess of passivity at another subsystem.

Besides that, a more general class of transformations, i.e. the generalized scattering transformation, helps to guarantee delay-independent finite gain $\mathcal{L}_2$-stability. The results can be extended to accommodate with other communication unreliabilities present in the channel, e.g. packet loss or missing samples due to data reduction (variable-rate updates). This practically allows every operator that satisfies some small gain property to be introduced in the communication channel.

A transparency analysis demonstrates the superior performance of the proposed approach. Particularly, the generalized scattering transformation outperformed the standard scattering approach in all cases in terms of displayed impedance. An experiment using
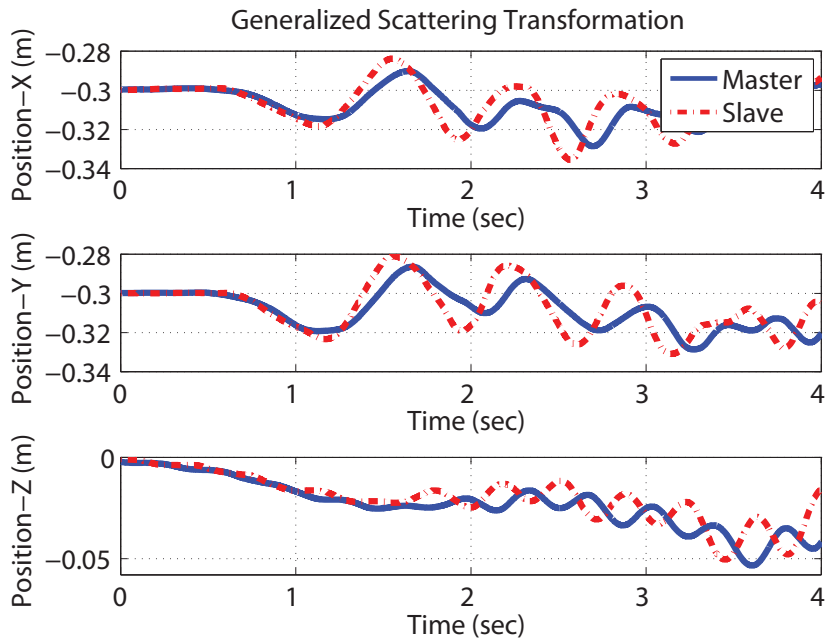
Fig. 3.13: Position tracking for $\theta = 55°$, having overestimated the dissipativity of the right-hand side. The system is unstable.

a 3-DoF telerobotic system validated the effectiveness of our novel approach in terms of displayed impedance.

Further research of the presented methodology should look at the extension to dynamical transformations. The ability to change the transformation online, using sensor data that will notify significant changes of either the human or the environment is expected to overcome the conservatism that comes with the fact of a priori designing a static controller. Moreover, the online acquisition of model knowledge of the highly nonlinear human and environment systems still poses a significant challenge and remains an open problem. In Chapter 5, some ideas about the human arm dynamics knowledge are sketched.

Tab. 3.2: Displayed impedance results for the experimental comparison.

Time delay $T_1 = T_2 = 50$ ms

	Disp. Stiffness	Disp. Damping
ST	367 N/m	68 Ns/m
$GST_{\theta=11°}$	492 N/m	12 Ns/m
Environment (ideal)	1400 N/m	10 Ns/m

Time delay $T_1 = T_2 = 150$ ms

	Disp. Stiffness	Disp. Damping
ST	201 N/m	49 Ns/m
$GST_{\theta=11°}$	332 N/m	4 Ns/m
Environment (ideal)	1400 N/m	10 Ns/m

4 Perceptual haptic data reduction

In teleoperation systems haptic information needs to be sent bidirectionally between the human and the teleoperator, and a global control loop is closed over the communication system. For real-time processing and communication of haptic data in TPTA systems, very strict delay constraints are imposed by the involved control loops. Already milliseconds of time delay may destabilize the overall system. Besides that, the transmission resources for typical communication networks used in teleoperation scenarios are sometimes limited. Severe communication constraints are imposed by communication technology and infrastructure in space [170] and underwater telepresence applications [2] where the available bandwidth is generally limited and high packet rates are simply not feasible. Generally, in mobile (wireless) applications, higher network traffic is also directly related to higher power consumption. High network traffic may also lead to network congestion, in packet-switched networks as for example the Internet [104], and hence, to large transmission time delays and packet loss that can destabilize the control system or degrade the performance of a force-reflecting teleoperator [39, 169]. *Efficient* use of the communication channel and its resources is therefore of high interest. It has been significantly investigated by researchers in the previous decades and successfully employed standards for video (MPEG-4) and audio (MP3) are nowadays widely used. Here, *data reduction methods*, as well as transmission protocols, are investigated for the haptic modality. We envision, thus, efficient, resource-friendly haptic telepresence systems over communication networks.

Data compression for efficient storage and/or transmission has been investigated extensively by the information theory and source coding communities. For the compression of multimedia signals, lossy compression algorithms are most suitable, as they explicitly detect and remove irrelevant information, which either is not perceivable by the human or cannot be displayed due to hardware limitations. If compression is done without affecting the perceptual quality and without disturbing system performance, the applied signal processing methods are said to be transparent. Lossy compression schemes achieve high compression rates and are therefore of great interest for the compression of haptic signals. Data reduction for haptic signals is, however, fundamentally different from the compression of audio and video due to the haptic closed loop that a bilateral haptic communication requires. As a result of the strict delay and stability requirements, approaches that compress haptic signals without algorithmic delay are required.

In this chapter, data reduction schemes for haptic data are given. Focus is given, as in video and audio compression, on the perception of possibly introduced artifacts, thus the *human psychophysics* are strongly considered. First, the human perceptual abilities of motion and force are studied, and only then human-centered haptic data reduction approaches are discussed. For the evaluation of the proposed data reduction schemes, human factors are considered leading thus to a holistic human-centered data reduction algorithms design.

4.1 State-of-the-art and current challenges

Early approaches for haptic data compression can be found in [11, 64, 119], where different sampling and quantization techniques for haptic data are introduced. Applying differential pulse-code modulation (DPCM) and adaptive DPCM with Huffman coding on haptic signals has been treated in [148]. The concept of perceptual lossy compression for haptic data is there introduced and the authors propose to adjust the quantization coarseness such that the introduced quantization noise stays below absolute human haptic perception thresholds. None of the aforementioned approaches, however, addresses the reduction of the high packet rates which is the main challenge for real-time haptic interaction across packet-switched networks. The first proposal that targets packet rate reduction for networked control systems can be found in [123]. If the difference between the most recently sent update and the current input value exceeds a fixed threshold, signal updates are triggered. The receiver reacts to a missing sample by holding the value of the most recently received sample. Kuschel et. al developed a class of lossy data reduction methods for haptic telepresence systems that guaranteed stability in [96]. However, their approach adds additional time delay and estimation errors that do not allow for a subjective evaluation performance of the algorithms. Therefore, there is no guaranty provided that the data reduction algorithms will not impair the human perception. On the other hand, they benefit from the fact, that a specified upper-bound of the required bandwidth can be defined.

Haptic data reduction algorithms considered in this work should comply with three basic requirements

- high data *reduction rate*,

- *transparency*, i.e. the loss of information should be perceptually imperceiveable, and

- *stability* of the control loop should not be impaired by the loss of information.

Actually, the first two requirements are common in data reduction/compression algorithms and are met in MP3 and JPEG standards. The combined approach from a communication, control-theoretic as well as psychophysics point of view resulted in the deadband-based haptic data reduction in [76, 68]. It is shown, that the deadband-based data reduction can lead to high reduction rates. Psychophysical studies indicate that the loss of information induced by the algorithm can be considered imperceiveable. Stability of the global control loop is challenging as long as some information is removed from it. Therefore, all aforementioned approaches consider it and guarantee stability of the system with proper reconstruction strategies on the receiver side.

Aiming at an efficient communication resources usage in a haptic telepresence system, there are still significant challenges to be addressed. Teleoperation systems, nowadays, employ a lot of degrees-of-freedom. A human-like arm will need at least 7-DoF, whereas a cyber-hand haptic system is using more than 18 sensors [84, 27]. The future trend towards multi-DoF in robotic applications is illustrated also by the active artificial skin system presented in [160], showing the tendency of future applications that will of course require proper fusion and usage of large amount of data. Unfortunately, all presented approaches fail to address data-reduction of a multi-DoF system, at least in an efficient way. Having

the human user always in mind, and avoiding a transparency degradation by considering human perceptual limits, we propose, here, a data-reduction scheme appropriate for multi-DoF systems. The psychophysical background of the scheme is discussed whereas the conditions for stability are given.

Time delayed communication channels are also considered in this context. Although, the problem of data-reduction in time-delayed systems has been already studied in [73], human haptic perception still poses a challenge as it was not considered in the time-delayed setting. Particularly, all current approaches fail to satisfy all three criteria mentioned above when time delay is present, namely reduction, transparency and stability. Therefore, we propose a modified control scheme that uses the perceptual deadband-based data reduction technique on a time-delayed system, as long as the time delay is measurable. It is then managed to achieve, not only stability and high data reduction rates but also transparency as the underlying algorithm used is based on psychophysical findings.

To conclude, in this chapter, deadband-based data reduction is considered as a means of an efficient use of communication resources, especially in packet-switched networks. The main contribution of the chapter is the design of algorithms that satisfy first of all the three aforementioned criteria, namely data reduction, transparency, and stability. In parallel, they allow for realistic implementation in multi-DoF systems and over delayed communication channels too. The remainder of this chapter is organized as follows: The human perceptual characteristics are discussed in Section 4.2 and after briefly mentioning the deadband-based data reduction, see Section 4.3, a new approach for adaptive deadband is examined in Section 4.4. The chapter continues with the scheme for perceptual data reduction in time-delayed teleoperation in Section 4.5 and an algorithm for stable and transparent multi-DoF deadband in Section 4.6. Finally, a discussion concludes the chapter in Section 4.7.

4.2 Human perceptual characteristics

It is well known that the human may not discriminate arbitrarily small differences in a physical quantity. In order to investigate whether a human can detect a stimulus, differentiate between two stimuli, and quantify the magnitude or nature of this difference, its psychophysics are studied and psychophysical experiments are performed. In this context, typically two different types of thresholds are of interest. Absolute (sometimes called detection) thresholds refer to the smallest stimulus amplitude that can be perceived by a subject. Difference thresholds refer to the smallest difference in stimulus magnitude that can be perceived.

In 1834, the experimental physiologist Ernst Weber was among the first to propose a mathematical relationship between the physical intensity of a stimulus and its phenomenologically perceived intensity [172, 47]. Specifically, he proposed the size of the difference threshold (or just noticeable difference, JND) to be a linear function of stimulus intensity. This has become known as Weber's Law of the JND. It can be described by the following equation

$$\frac{\Delta I}{I} = \kappa = constant \tag{4.1}$$

Haptic property	JND [%]
Force	7 %
Velocity	8 %
Torque	12,7 %
Angular velocity	12,5 %
Stiffness	23 %

Tab. 4.1: Examples of JND values for haptic entities reported in the literature [89] and [86].

where I is the stimulus intensity, ΔI is the so-called Difference Threshold or the Just Noticeable Difference (abbreviated as JND) and κ is a constant called the Weber fraction. It describes the smallest amount of change of stimulus intensity I which can be detected just as often as it cannot be detected. In this context, the constant κ describes the linear relationship between the JND and the initial stimulus intensity I. According to Weber's Law, the psychophysical perception of a signal change is therefore proportional to the stimulus intensity itself.

Weber's Law of the JND was found to apply to almost every sense modality, including haptic perception, and over a wide stimulus range [47, 162, 15, 52, 3]. It allows for the construction of a simple, yet efficient psychophysical model of human haptic perception. Discrimination thresholds for mechanical parameters such as stiffness [89, 88], inertia [139], and viscosity [90] and for quantities, such as position, velocity and force can be found in literature, see e.g. [87, 153]. A summary of the the most important haptic entities for this work are listed in Table 4.1. These values correspond to the perception for hand and arm.

Remark 4.2.1 The JND values also depend on the experiment conditions. They represent statistically determined empirical values and have in some cases wide variations.

Consequently, they can be applied to perceptual coding schemes, enabling the detection of perceived differences caused by coding artifacts in order to keep them continuously within imperceptible ranges. Interestingly enough, JNDs are most of the times identified in one-dimensional settings, this problem will be discussed in Section 4.6.

4.3 Deadband-based data reduction for haptic signals

The deadband approach is a lossy perceptual coding approach for haptic signals that exploits human haptic perception limits using Weber's law of JND. It enables the detection of *imperceptible* changes in the signal that do not need to be signaled and can therefore be dropped at the encoder leading to packet rate reduction.

4.3.1 Deadband approach

With the deadband approach data are sent over the communication channel only if the difference between the most recently sent sample $x(t')$ and the current value $x(t)$, where $t > t'$, exceeds a perception threshold $\Delta_{x(t')}$ then a signal update event is triggered and
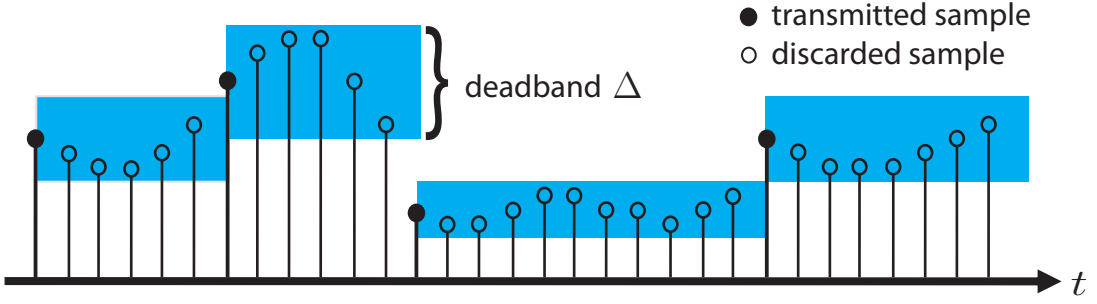
Fig. 4.1: Principle of the Weber-inspired deadband approach. Haptic samples that lie in the deadzone Δ are not transmitted. The deadband changes analogously to the amplitude of the signal.

the packet is transmitted

$$\begin{aligned} \text{If:} \quad & |x(t') - x(t)| \leq \Delta_{x(t')} \quad \text{Do not transmit} \\ \text{Else:} \quad & \qquad\qquad\qquad\qquad\quad \text{Transmit new value.} \end{aligned}$$

The current deadband is redefined based on the update sample's intensity value. Using the insights of Weber's law this threshold is chosen to grow proportionally with the magnitude of the signal $x(t')$

$$\Delta_{x(t')} = k \cdot |x(t')| > 0, \tag{4.2}$$

where $k \in [0, 1)$ is a factor that influences the size of the deadband. We intentionally use different notation for the deadband parameter as for the JND, i.e. κ, as the proposed compression scheme is inspired by Weber's law but is not destined to identify JNDs. Therefore, a meaningful choice, from the transparency point of view, would be $k \leq \kappa$. The time instant t or t' will be in the following omitted for brevity; the most recently sent value $x(t')$ will be referred also as x'. The Weber-inspired deadband is proposed in [68] and has also been called relative deadband, as it grows relatively with the amplitude of the haptic signal.

The principle of the Weber-inspired deadband approach is also illustrated in Figure 4.1. Only samples that exceed the deadband Δ are transmitted and are indicated as black circles of this discrete signal output. Samples with blank circles fall within the currently defined deadband and can be dropped as the change is considered to be too small to be perceptible. Note that the deadband increases with the signal amplitude. As only the samples which violate the deadband are considered to contain perceptible information, the deadband-based data reduction scheme allows for signal-adaptive downsampling and therefore reduces the amount of samples within the haptic data streams. If the signal $x(t)$ is close to the origin the deadband becomes infinitely small. For practical reasons, e.g. in the case of noisy sensors, a minimum absolute deadband size exceeding the current noise level should be defined and the deadband is lower bounded

$$\Delta \geq \Delta_{min},$$

such that when the signal has a low amplitude no new packets are transmitted.
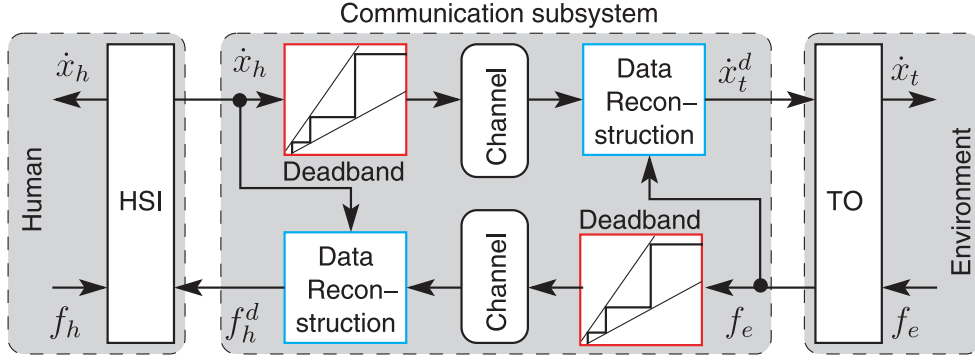
Fig. 4.2: Haptic telepresence system with deadband-based data reduction.

Remark 4.3.1 [75] The signs of the haptic signals define the direction of the power flow in the communication subsystem. As soon as the input $x(t)$ changes sign it must be transmitted. Therefore when the haptic signal $x(t)$ is close to the origin $|x(t)| < \Delta_{min}$ the deadband is unequally spaced such that

$$|x(t)| \in [0, x(t') + \Delta_{min}] \quad \text{if } |x(t')| < \Delta_{min} \tag{4.3}$$

$$|x(t)| \in \left[|x(t')| \pm \Delta_{x(t')} \right] \quad \text{if } |x(t')| \geq \Delta_{min}. \tag{4.4}$$

With this definition of the deadband the sign consistency between transmitted values and current values at the sender is guaranteed

$$x(t)x(t') \geq 0. \tag{4.5}$$

4.3.2 Stability with deadband control

In order to guarantee the stability of the haptic telepresence system within the considered passivity approach the passivity of the subsystems has to be verified. Although this has been discussed for the human/HSI and the teleoperator/environment subsystem by assumption in Section 3.3.3, the passivity of the communication channel has to be studied again as now some artifacts due to the data reduction scheme are expected that can eventually lead to active behavior (energy generation). This can be examined by computing the energy balance of the bilateral communication line which for passivity must satisfy

$$\int_0^t \left(\dot{x}_h f_h^d - \dot{x}_t^d f_e \right) d\tau \geq 0 \quad \forall t > 0. \tag{4.6}$$

Without the deadband control the equality holds as $\dot{x}_t^d = \dot{x}_h$ and $f_h^d = f_e$ for all times t; the communication subsystem is passive (lossless).

The use of deadband results in empty sampling instances at the receiver side. The missing values need to be estimated to reconstruct the (quasi-)continuous signal at the corresponding receiver side; it is indicated as data reconstruction block in Figure 4.2. The data reconstruction block must not generate energy in order to preserve the passivity of the communication channel.
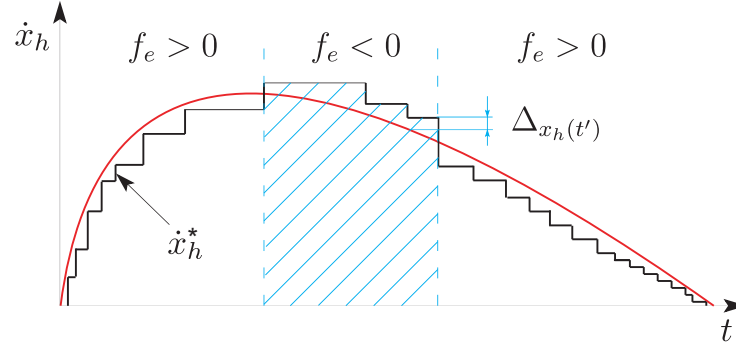
Fig. 4.3: Effect of modified deadband approach on signal, here for OP side. With red the original haptic signal is indicated, whereas the black line denotes the reconstructed values.

The most common strategy used is the Hold-Last-Sample (abbreviated as HLS) algorithm. It uses the information of previous signal behavior and can be interpreted as zero-order hold, i.e. zero-order Taylor expansion. However, it is shown in [23, 70] that this algorithm may inject energy and, consequently, violate passivity.

Remark 4.3.2 Note that the non-passivity of the HLS algorithm does not necessarily lead to unstable behavior of the haptic telepresence system. In fact, there exist configurations of signal behavior where the HLS acts as a dissipative element. Still, stability cannot be guaranteed.

Therefore, it is here shown how a *modified HLS* strategy can reconstruct the empty sample instances of the transmitted signal without injecting energy in the communication channel, and hence, preserve passivity. It is expressed by

$$\dot{x}_h^*(t) = \dot{x}_h(t') - \text{sign}\{f_e(t)\}\Delta_{\dot{x}_h}, \tag{4.7}$$

at the OP side and

$$f_e^*(t) = f_e(t') + \text{sign}\{\dot{x}_h^d(t)\}\Delta_{f_e}.$$

at the TO side where $\dot{x}_h^*$ denotes the modified velocity at the OP side which equals the desired teleoperator velocity $\dot{x}_t^d$ in Figure 4.2 and f_e^* is the modified environment force value which equals the desired human force f_h^d. $\Delta_{\dot{x}_h}$ and Δ_{f_e} denote the currently applied deadbands and $t' < t$ the time instant of the most recent signal update, and the sign function

$$\text{sign} = \begin{cases} -1 & \text{if } x < 0 \\ 1 & \text{otherwise.} \end{cases}$$

Depending on the sign of the environmental force, the value is modified to upper or lower end of the deadband interval in order to dissipate energy. This is illustrated in Figure 4.3 for the OP side. By keeping the value within the deadband the change in signal is still considered as imperceivable.

Proposition 4.3.3 Assuming passivity of the human/HSI and TO/environment systems as described in Section 3.3.3, the modified HLS algorithm passifies the communication channel.

Proof: [75] We want to show that (4.6) is satisfied. The output of the data reconstruction $x_h^*(t)$ and $f_e^*(t)$ is fed to the TO and HSI, respectively, i.e. $\dot{x}_h^*(t) = \dot{x}_t^d$ and $f_e^*(t) = f_h^d(t)$ as shown in Figure 4.2. Due to the passivity of the human/HSI and TO/environment subsystems

$$\dot{x}_h(t) f_e^*(t) \geq 0$$

and

$$\dot{x}_h^*(t) f_e(t) \geq 0.$$

It is, therefore, sufficient to show that

$$|\dot{x}_h(t)||f_e^*(t)| > |\dot{x}_h^*(t)||f_e(t)|.$$

From the deadband control in (4.3) we know that

$$|\dot{x}_h(t)| \geq |\dot{x}_h(t')| - \Delta_{x_h(t')}.$$

From the passivity condition on the subsystem human/HSI follows that

$$\text{sign}\{f_e^*(t)\} = \text{sign}\{\dot{x}_h(t)\}$$

which by the sign consistency in (4.5) gives

$$\text{sign}\{f_e^*(t)\} = \text{sign}\{f_e(t')\}.$$

Hence from (4.7) the reconstructed value can be rewritten as

$$|f_e^*(t)| = |f_e(t') + \Delta_{f_e(t')}|.$$

In consequence

$$|\dot{x}_h(t)||f_e^*(t)| > (|\dot{x}_h(t')| - \Delta_{x_h(t')})|f_e(t') + \Delta_{f_e(t')}|.$$

Similarly

$$|\dot{x}_h^*(t)||f_e(t)| \leq (|\dot{x}_h(t')| - \Delta_{x_h(t')})|f_e(t') + \Delta_{f_e(t')}|.$$

Hence, it is true that

$$|\dot{x}_h(t)||f_e^*(t)| > |\dot{x}_h^*(t)||f_e(t)|,$$

and the reconstruction strategy (4.7) renders the communication block passive. ∎

4.4 Velocity-adaptive perceptual thresholds

4.4.1 Human perception in relative movement

Weber's law infers perceptual limits of the human haptic modality as seen in Section 4.2; however, very few of the empirical studies which investigate these limits consider the effects of dynamic movements and attentional requirements, both of which are important aspects of real-life task performance. Based on this rationale, it is here proposed to extend the previously discussed Weber-inspired deadband-based data reduction principle by incorporating an additional perceptual dimension, namely the velocity of the operator's hand movement.

Whilst several studies suggest that haptic perceptive abilities are superior with active as opposed to passive movements [62, 158], attentional theories suggest that the opposite occurs when attention is divided between several goals or directed towards a specific task; see [38] for an overview. For example, in a realistic TPTA-based scenario, an operator would be required to plan, control and execute certain movements. These movements usually need to be executed with some degree of precision, in terms of position as well as force, in order to achieve a task objective. In this case, one would speculate that less cognitive resources are available to devote attention to the perception and interpretation of the force feedback received, in particular, if these force signals, or a distortion thereof, are not strictly task-relevant. Thus, it would seem likely that task-directed movement reduces the operator's ability to perceive changes in displayed force-feedback, thus increasing JNDs between stimuli.

Although literature on this topic is scarce, empirical evidence seems to support this assumption. Several studies suggest that attention may have a direct effect on human haptic perceptive ability by triggering a remodulation of neuronal activity in the primary sensory cortex [83, 12]. Other studies found direct support for increased JNDs in the presence of multiple attentional demands. For example, [177] found in a study on change blindness, that the log of the Weber parameter is proportional to the log of the number of targets given. Moreover, [178] found that force discrimination thresholds were greater during hand movements than they were reported by studies in which no hand movement occurred. This effect was independent of the speed of movement. The influence of hand movements on absolute force perception thresholds (AFT) in the context of haptic data reduction is analyzed in [182]. They found AFTs to increase when the operator's hand is in motion. However, neither difference detection thresholds nor performance and/or efficiency of corresponding data reduction architectures were investigated in their work. Based on these findings, and by using the acquired knowledge for human perception in relative movement, we investigate, here, the use of adaptive deadbands at the benefit of an efficient data transmission for haptic applications.

4.4.2 Velocity-adaptive deadband

Aiming to adjust the deadband data reduction approach to the demands of real-life TPTA-applications, we propose to modify the deadband approach with respect to the operator's hand velocity, thus exploiting the potentially increased JNDs during task-directed hand

movement for the purpose of increased, yet still imperceptible, data reduction. This part of our work appeared first in [188]. The deadband-based reduction scheme constitutes a very useful tool for this study. Its simple mathematical model on the one hand side, and the guarantee of stability on the other, allow its direct use in TPTA-systems. Therefore, here, only the adaptive part of it will be investigated and its performance will be shown by psychophysical experiments. In the following only the force-discrimination when using a velocity-adaptive deadband is examined, therefore we will refer only to force deadband.

Specifically, we extend the deadband model, and the deadband parameter is now defined as a function of velocity

$$\phi = k + \alpha \cdot |\dot{x}| \tag{4.8}$$

where the velocity-adaptive deadband parameter ϕ is determined by the sum of the constant component k and a velocity-proportional component characterized by the factor $\alpha \geq 0$. The parameter k represents a velocity-independent component of the JND as it was seen in Section 4.3.1. Adjusting α allows us to control the influence of the velocity on the resulting modified deadband parameter ϕ. For $\alpha = 0$ the velocity independent relationship in (4.2) is obtained.

Accordingly, the size of the applied deadband bounds becomes

$$\Delta_f = \phi \cdot |f(t)| = (k + \alpha \cdot |\dot{x}(t)|) \cdot |f(t')| \tag{4.9}$$

where the last violation of the deadband occurred at time $t' > t$.

Example 4.1 An example of the applied adaptive deadband parameter ϕ is visually illustrated in Figure 4.4. The random velocity signal $\dot{x}$ referring to the operator's hand movements is illustrated in Figure 4.4(a). It is used to define the velocity-adaptive deadband parameter ϕ, shown in Figure 4.4(c); $\alpha = 0.3$ whereas the constant deadband parameter $k = 10\%$. The original, as well as the after-deadband, force signal is illustrated in Figure 4.4(b). A simulated packet rate comparison of both method is illustrated in Figure 4.4(d) for this example. A clear benefit of the adaptive deadband approach is observed.

4.4.3 System architecture

The architecture of our proposed velocity-adaptive deadband-based data reduction scheme is illustrated in Figure 4.5, where $\dot{x}_h$ and f_h denote the velocity and the force-feedback signal on the human operator side, respectively; $\dot{x}_t$ denotes the velocity of the teleoperator and f_e represents the environment force. The HSI measures the human operator's hand movements and corresponding motion commands are sent across the network at high rate in order to control the teleoperator.

Remark 4.4.1 In this part of the work, the focus is on the evaluation of our proposed velocity-adaptive deadband scheme and, therefore, the latter is applied only on the force
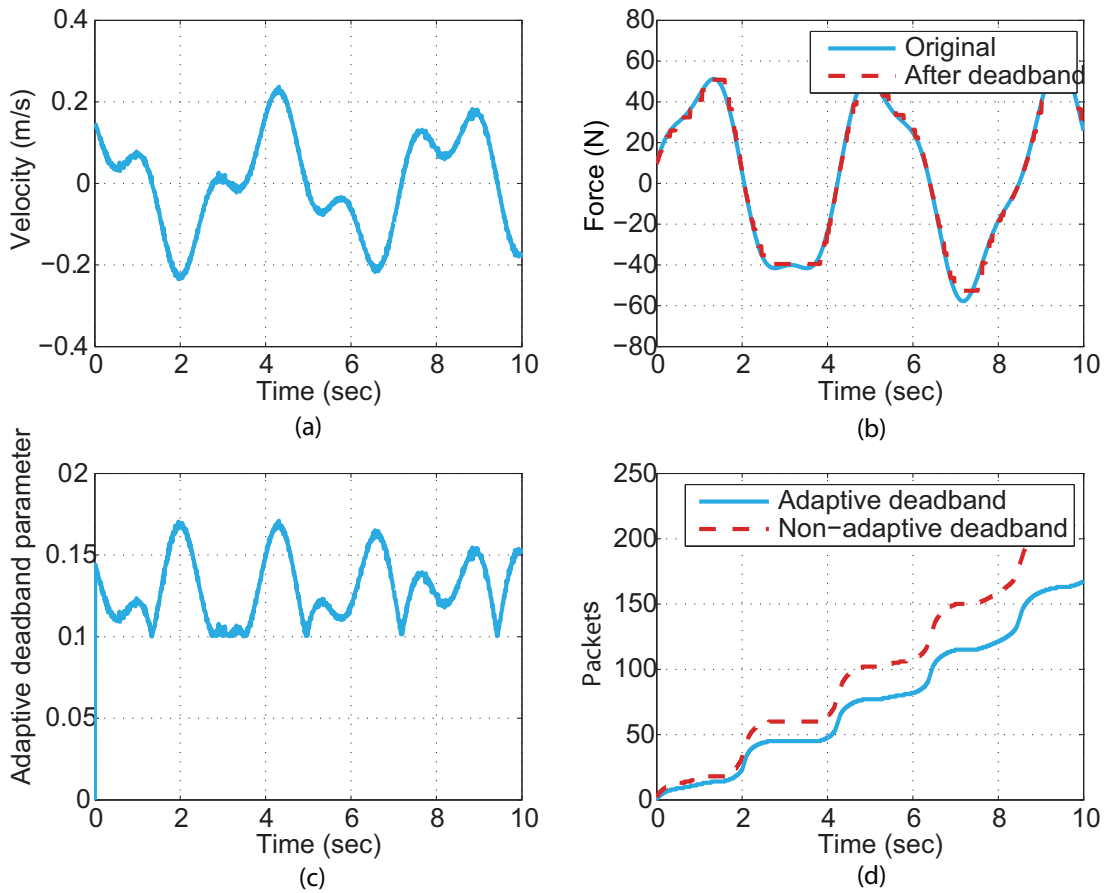
Fig. 4.4: Overview of the adaptive deadband algorithm. (a) An example of the velocity signal. (b) The corresponding force signal with and without deadband. (c) The adaptive deadband parameter ϕ. (d) The number of transmitted packets with adaptive and standard deadband approach.

channel; no data reduction is applied on the velocity channel. However, previously developed schemes can be applied on the velocity transmitting forward channel in order to achieve bilateral haptic data reduction in the system [68].

At the teleoperator, the received velocity information enters the novel adaptive deadband block modifying the current deadband size according to (4.9). Compared to the data reduction principle of Section 4.3.1, larger deadbands can be applied during movements of the operator's hand. A change in the force-feedback signal is only transmitted in case the applied perception threshold is violated. Thereby, an additional reduction in packet rate on the communication channel can be achieved.

4.4.4 Performance evaluation

To evaluate whether the velocity-dependent deadband coding scheme constitutes an improvement to the traditional Weber-inspired approach in terms of transparent, i.e. imperceptible, data reduction, an experimental study has been conducted. Firstly, it was aimed to determine the respective disturbance detection thresholds of the coding parameters, e.g.,
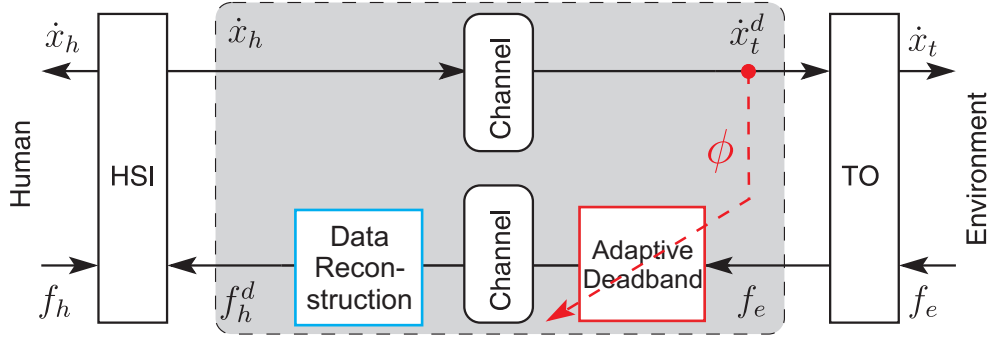
Fig. 4.5: Architecture of the adaptive deadband data reduction principle. The size of the applied deadband adapts to the velocity signal $\dot{x}$.

the constant component k, basis of the traditional Weber-inspired deadband approach, as well as the velocity adaptation parameter α from (4.9), which forms the basis of the proposed velocity-adaptive deadband extension. Secondly, it was to be tested whether either factor changed significantly with the speed of the movement performed by participants. Finally, it was to be investigated whether incorporating the velocity adaptation parameter α into the Weber-inspired deadband data reduction approach would lead to a significant packet rate reduction without adversely affecting the accuracy of teleoperator control.

Participants

18 male and 3 female students participated in the experiment (mean age = 27 years, std. deviation = 2.5 years), all of whom were right-handed and naive to the purpose of the experiment and the experimental setup. One person's data set had to be excluded from further analysis due to measurement irregularities.

Apparatus

The experimental testbed consisted of a linear haptic device operated in force control mode as more extensively discussed in Appendix A. The remaining dynamics of the devices, i.e. 0.35 kg inertia and 3.01 Ns/m damping, were considered negligible for the purpose of the experiment. The human holding the linear haptic device interacted with a virtual environment. A virtual spring was chosen, supported by the fact that the mechanical spring represents a generic and simple design of many environments on haptic tasks. It acted as an admittance, namely it received velocity information from and provided force feedback to the device. A second PC, also running a real-time Linux kernel, received the position information from the haptic device in order to visualize the virtual teleoperator within a virtual telepresence environment. The connection between the two PCs was UDP/IP-based and time delay was on average less than 1 ms and was considered to be negligible. Two potentiometers enabled participants to control the parameters k and α online and allowed for adjustments of k and α to maximum settings of 0.40 and 1.20, respectively, with a resolution of 0.01. For an illustration of the experimental testbed see Figure 4.6.

(a) Tubular linear motor, Thrusttube 2510   (b) Simulated visual feedback
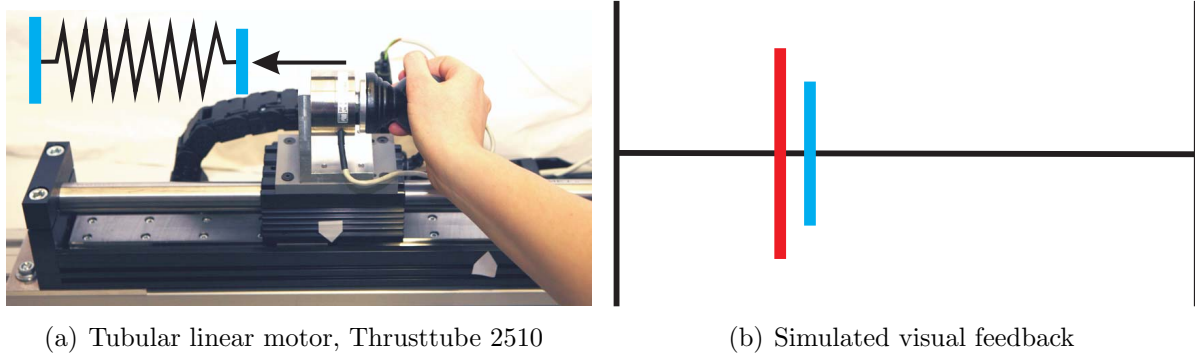
Fig. 4.6: Illustration of the experimental testbed. The left Figure 4.6(a) shows the deployed HSI device where subjects experience force-feedback from a virtual spring. The right Figure 4.6(b) shows a virtual teleoperator environment; users were instructed to follow the red cursor.

Experimental design

The study made use of a 2 (deadband type) x 3 (motion speed) within-subjects design. In order to introduce a measure of task performance accuracy and to ensure that participants move the master device with similar motion speeds, participants were given a task. Task objective was to control the movement of the virtual teleoperator so as to follow a moving cursor as closely as possible whilst participants experienced force-feedback originating from a virtual spring which covered the entire motion range on both directions. The spring constant was set to 100 N/m during all experiments. Assuming the users followed the cursor perfectly a maximum displacement of 15 cm was measured resulting in 15 N of maximum intended force. A screenshot of the visual feedback is illustrated in Figure 4.6(b). The motion speed with which the cursor moved from one side of the computer screen to the other was manipulated in a sinusoidal manner using three different frequencies: low, medium and high (2, 3 and 4 rad/s). The maximum for each motion speed level was 0.12 m/s, 0.18 m/s and 0.24 m/s. During the experiment, preferable configuration settings for the force component k, and for the velocity adaptation parameter α were measured for each speed. Also measured for each speed of movement were the resulting mean squared error (mse) of the distance between computer cursor and teleoperator positions including the data packet rates with use of the two deadband schemes.

Procedure

Participants were first demonstrated the effects of the component k as well as the velocity adaptation parameter α on the quality of the displayed force feedback signal; and they were given the opportunity to familiarize themselves with the task, the potentiometers and their effects on the control of the teleoperator. A carefully designed training phase ensured that all participants were approximately at the same level of training, as far as the detection of possible signal disturbances is concerned. They were then asked to continuously perform the task of following the moving cursor as closely as possible using the haptic device and the cursor coupled to it. In our experiment, an adapted method of adjustment was used

for detecting and measuring absolute thresholds that allowed us to test a wide range of parameter values, see e.g. [47]. Whilst performing the task, participants were to adjust the parameters k and α, using the potentiometers, until they found the maximum setting with which no disturbance was felt. This disturbance would manifest itself in the form of increasingly abrupt dislocations of the force feedback device, which in turn required greater physical effort to precisely control the position of the teleoperator. All participants were instructed to use the same strategy for finding this setting, that is, to alternate between settings that lie below and above the perceived threshold. Specifically, they were asked to approach the target setting from both directions, i.e., initially starting to slowly increase from the minimum parameter value, followed by slowly decreasing from a maximum value, until they were confident that they had found the highest setting at which they felt no disturbance in the control of the teleoperator.

In a first step, participants focused on finding an optimum configuration for k starting with its lowest setting ($k = 0$) while the velocity adaptation parameter α was set to zero. When they were confident that they had found the target setting, performance was measured for 10 seconds using the setting that participants had adjusted to. During these 10 seconds, participants only focused on their task performance. This procedure was repeated to find an optimum velocity adaptation parameter α with k still set to the participants' preferred configuration. Afterwards, both steps were repeated with two other speeds of movement.

The order of the three speed conditions, which determined the speed of the computer cursor, and consequently participants' hand movements, was systematically randomized for each participant. Participants were also given headphones which prevented them from hearing sounds that might distract or influence them in any way. In addition, all participants were instructed to use the same type of grip, i.e., a heavy wrap grip as classified by [29], on the master device.

4.4.5 Results

Data were inspected for outliers, as well as for normality and homogeneity of variance. Data with z-scores of $z > \pm 3.29$ were excluded from further analysis. Where a violation of the assumptions of parametric data was suspected, necessary corrections have been made, as specified below.

Disturbance detection thresholds for k and α

The mean settings and standard deviations for parameters k and α that participants adjusted to for each movement speed without feeling any introduced coding artifacts are displayed in Table 4.2.

The presented results indicate that the mean preferred setting for the constant component k lies at around 0.06. The mean preferred value for the velocity adaptation parameter α has been detected to be approximately 0.15.

Guided speed	Parameter $\boldsymbol{k}$		Parameter $\boldsymbol{\alpha}$	
	mean	std. deviation	mean	std. deviation
low	0.053	0.053	0.15	0.11
medium	0.064	0.056	0.15	0.10
high	0.059	0.027	0.16	0.13

Tab. 4.2: Preferred configuration for the parameters k and α of the adaptive deadband coding scheme with respect to different speed levels. Maximum settings possible were 0.40 and 1.20 for k and α, respectively.

Velocity dependency of parameters k and α

In order to determine the influence of the velocity of the operator's hand on the respective deadband detection thresholds for the Weber-inspired and velocity-adaptive deadband types, as indicated by k and α, two within-subjects univariate analyses of variance (ANOVA) were conducted with hand movement speed as independent variable and adjusted k and α settings as dependent variables, respectively. Since Mauchley's test of sphericity was significant ($\chi^2(2) = 9.74, p < 0.05$), F-values for factor k were adjusted using Greenhouse-Geisser corrections ($\epsilon = 0.71$). The ANOVA showed that neither k ($F(1.41, 26.80) = 0.58, p = 0.57$) nor α ($F(2, 38) = 0.08, p = 0.93$) varied significantly with motion speed. This suggests that *the effects of each component are velocity independent.* That is, participants adjusted to very similar values for k and α, regardless of the speed at which they performed their movement. While the number of participants in this study would not suffice to detect small effects of speed on k and α values, the results provide an indication that the design and the deployed psychophysical function consisting of a constant component k and a velocity-proportional component characterized by α is a valid assumption.

Effects of parameters k and α on operator task performance and data reduction performance

In order to determine whether or not the use of velocity-adaptive deadbands achieves greater data reduction compared to the Weber-inspired approach without deteriorating performance accuracy, two further repeated-measures ANOVA were conducted with movement speed (low, medium, high) and deadband type (non-adaptive vs. adaptive) as independent variables, and task performance accuracy (mean squared position error) as well as data reduction performance (signal updates per second) as dependent variables, respectively.

With regard to data reduction performance, F-values for speed effects were adjusted using Greenhouse-Geisser corrections ($\epsilon = 0.68$) as Mauchley's test of sphericity was significant ($\chi^2(2) = 11.83, p < 0.05$). Despite a trend of increasing signal updates with increasing motion speed as indicated by the mean values, the ANOVA did not find a significant main effect of speed on data reduction performance ($F(1.35, 25.65) = 0.57, p = 0.51$). However, it did reveal a significant main effect of deadband type ($F(1, 19) = 18.43, p < 0.001$, part. $\eta^2 = 0.49$). The interaction between motion speed and deadband type was not significant
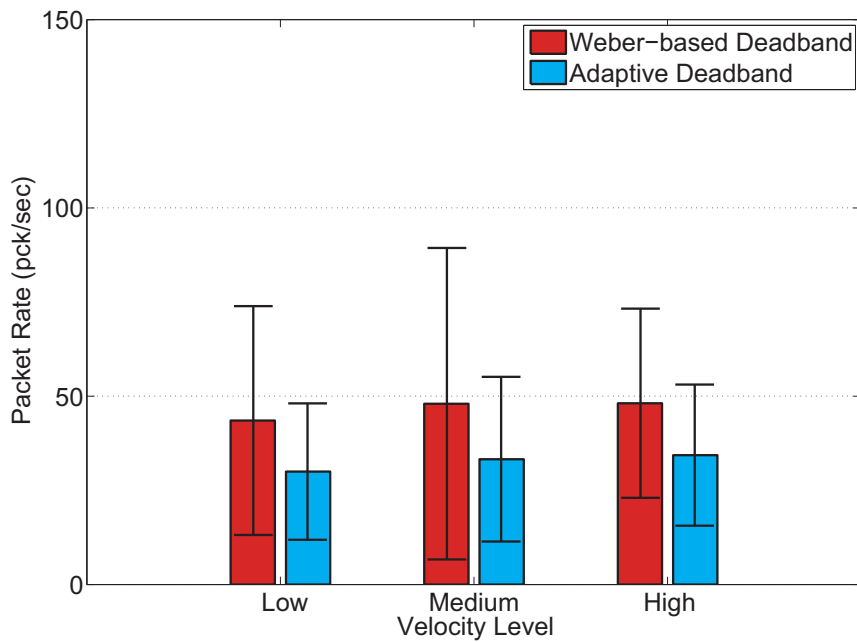
Fig. 4.7: Mean values and standard deviations of packet rates with respect to velocity level and deadband type. Compared to Weber-inspired deadbands, an additional mean packet rate reduction of 30.1% without effects on task performance accuracy as observed on Figure 4.8 is achieved when using velocity-dependent deadbands.
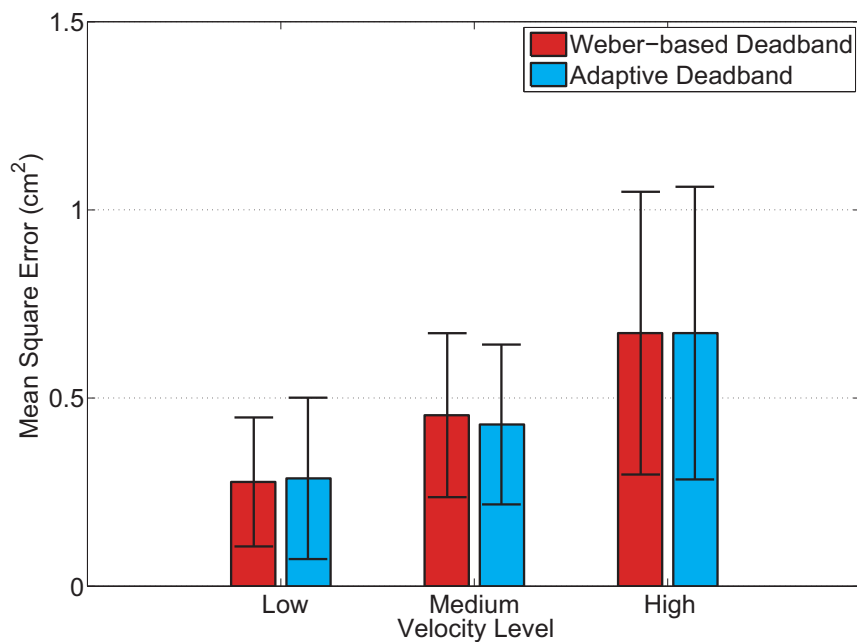
Fig. 4.8: Task performance accuracy with respect to velocity level and deadband type. It is observed that the adaptive deadband does not significantly influence the task performance compared to the case where the Weber-based deadband is applied.

($F(2, 38) = 0.03$, $p = 0.98$). Looking at the mean values, the results indicate that *the use of adaptive deadbands* significantly *reduced the number of signal updates performed per second, see Figure 4.7, regardless of the speed at which participants moved their hands.*

For the ANOVA of task performance data, F-values for speed effects were adjusted using Greenhouse-Geisser corrections ($\epsilon = 0.62$) as Mauchley's test of sphericity was significant ($\chi^2(2) = 16.60, p < 0.05$). The ANOVA revealed a significant main effect of speed on mean squared position error ($F(1.25, 23.71) = 32.59$, $p < 0.001$, part. $\eta^2 = 0.63$). Not surprisingly, Bonferroni-adjusted post-hoc comparisons indicated that the mean squared position error increased significantly with higher levels of velocity (low vs. medium $F(1, 19) = 32.32$, $p < 0.001$, part. $\eta^2 = 0.63$; medium vs. high $F(1, 19) = 13.34$, $p < 0.01$, part. $\eta^2 = 0.41$), as indicated by the mean values illustrated in Figure 4.8. However, there was no significant main effect of deadband type on position error ($F(1, 19) = 0.04$, $p = 0.85$), suggesting that *task performance accuracy did not significantly deteriorate with the use of velocity-adaptive deadbands* compared to the use of nonadaptive deadbands.

The mean values of the respective packet rates for each velocity showed that the adaptive deadband approach led to significantly greater data reduction compared to the Weber-inspired deadband coding scheme, as shown in Figure 4.7.

4.4.6 Summary

The main contribution of this part of the work is a novel data reduction approach for haptic signals with deadbands that dynamically change in order to exploit human haptic perception and discrimination limitations during task-directed hand movements. It is inspired by Weber's Law of the JND and assumes the deadband size to be a linear function of the velocity of the human operator's hand movement.

Psychophysical experiments were conducted aiming to assess whether or not the proposed perceptual coding scheme can be considered superior to the traditional deadband approach in terms of transparent data reduction.

The results indicate an optimum configuration of approximately $k = 0.06$ and $\alpha = 0.15$, regardless of the speed at which participants operated the master device. These settings indicate the average deadband detection threshold, defined as the maximum setting at which no disturbance is felt by the participants. It should be kept in mind that, since participants were motivated to find settings that lie below the disturbance threshold, these settings are likely to reflect a conservative response tendency. Thus, there remains a possibility that even greater data reduction may be used without a noticeable deterioration in performance accuracy or signal quality. On the other hand, one must also consider that the present study was only designed to test for large effects. Using a substantially larger participant pool might find small deteriorative effects. Nevertheless, considering the fine resolution of the potentiometers combined with the fact that participants' optimum settings confine themselves to a fairly narrow range of the entire spectrum possible, see Table 4.2, the results presented in this study appear to represent a fairly accurate approximation to participants' subjective experiences.

Overall, the results suggest that the velocity-adaptive deadband approach constitutes a significant improvement to the traditional Weber-inspired deadband approach in terms of data reduction performance. In our experiment, adding the velocity-proportional com-

ponent controlled by α to the constant component k led to further significant reduction in sent data packets, thus allowing for an additional data reduction of up to 30% compared to the Weber-inspired deadband approach (total data reduction of 96%), without perceptibly impairing the quality of the force-feedback signal or significantly affecting task performance accuracy. Since this effect was observed for all three motion speeds tested, the concept of the velocity-dependent data reduction approach seems to be valid.

It should be pointed out that, whilst the adaptive deadband approach is certainly inspired by traditional psychophysical models and draws on findings of cognitive and neuropsychological studies, the present study was neither designed nor destined to make any substantiated claims regarding the role of directed attention in force perception. As such, it provides further impetus for future studies to examine the role of cognition in human haptic perception.

4.5 Perceptual data reduction in time-delayed teleoperation

In the previous sections we discussed how perceptual coding can be applied to haptic communication channels, and we provided the reconstruction strategies that will guarantee a stable haptic control loop based on the assumption of ineligible time delay. In most applications there exists a propagation as well as transmission delay depending on the protocol, network congestion etc. Guaranteeing stability can require transformation such the ones used in Chapter 3. In its simplest form, i.e. scattering transformation, the linear transformation of the power conjugated signals is transmitted over the communication challens instead of the power conjugated signals, i.e. force and velocity. Perceptual coding as discussed previously is, therefore, not directly applicable. Only the modified variables are transmitted over the communication network. Taken that, a modification of the deadband approach and the presented scattering transformation control architecture is discussed here, to further allow for *perceptual* coding on time delayed teleoperation.

4.5.1 Local computation of wave variables

In the following, we present a modification of the wave variable (or scattering transformation) control architecture which allows for directly sending perceptually encoded haptic signals over the communication channel while ensuring wave variable based teleoperation for TPTA systems with known constant communication latency. Expanding the wave variables equation (3.22), the desired force at the HSI can alternatively be written as
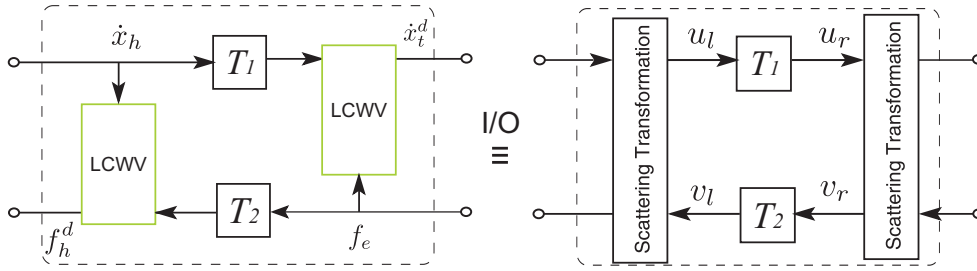
Fig. 4.9: The LCWV approach has an equal input/ouput behavior with the scattering transformation.

$$
\begin{aligned}
f_h^d(t) &= b\dot{x}_h(t) - \sqrt{2b}v_l(t) = b\dot{x}_h(t) - \sqrt{2b}v_r(t - T_2) \\
&= b\dot{x}_h(t) - \sqrt{2b}[\frac{b}{\sqrt{2b}}\dot{x}_e(t - T_2) - \frac{1}{\sqrt{2b}}f_e(t - T_2)] \\
&= b\dot{x}_h(t) - [b(\sqrt{\frac{2}{b}}u_r(t - T_2) - \frac{1}{b}f_e(t - T_2)) - f_e(t - T_2)] \\
&= b\dot{x}_h(t) - [\sqrt{2b}u_l(t - T_1 - T_2) - f_e(t - T_2) - f_e(t - T_2)] \\
&= 2f_e(t - T_2) + \underbrace{b\dot{x}_h(t) - b\dot{x}_h(t - T_1 - T_2) - f_h(t - T_1 - T_2))}_{\text{all variables locally known at the OP}}.
\end{aligned} \tag{4.10}
$$

The displayed force is, therefore, depending on the HSI velocity and the delayed HSI velocity/force which are all locally accessible assuming some storage element that stores these signals for the round-trip time delay, and the environment force which is transmitted over the backward time-delayed communication channel. Therefore, no real transmission of the wave variable v_r is needed, the environmental force f_e is transmitted instead. This technique is called Local Computation of Wave Variables (LCWV) and is presented for first time in [196].

Similarly, it holds for the desired velocity of the teleoperator

$$
x_t^d(t) = 2\dot{x}_h(t - T_1) + \underbrace{x_t(t - T_1 - T_2) - f_e(t - T_1 - T_2) - \frac{1}{b}f_e(t)}_{\text{all variables locally known at the TO}}, \tag{4.11}
$$

where now the HSI velocity is communicated via the forward communication channel.

The transmission block of the presented approach with locally computed wave variables (LCWV) has an equivalent input/output behavior as the standard wave variable architecture, see Figure 4.9, hence the passivity property is preserved and the stability is guaranteed. Observe that now haptic signals instead of wave variables are transmitted over the communication channel. This enables the use of perceptual coding schemes. In order to perform the computation, however, the local signals partially have to be stored for the round-trip time delay $T_1 + T_2$: $\dot{x}_h$, f_h at the OP side and $\dot{x}_t$, f_e at the TO side. Hence, the round-trip time delay needs to be known, which poses a limitation compared to the original wave variable approach where the exact knowledge is not required.
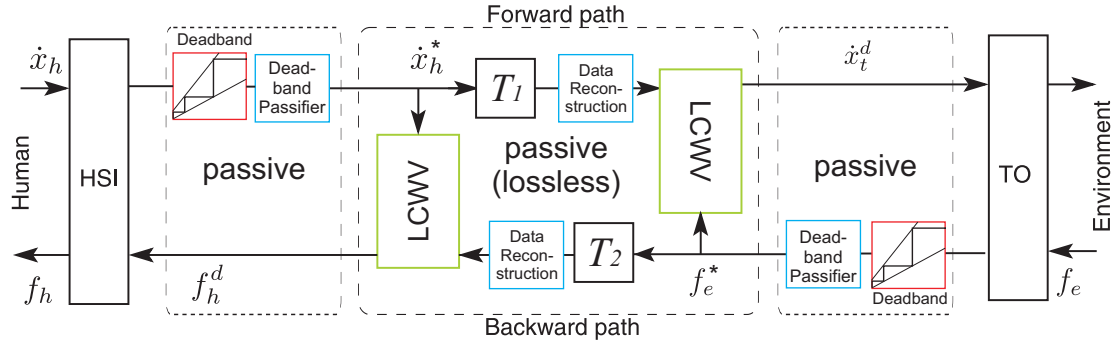
Fig. 4.10: The LCWV architecture combined with a perceptual coding scheme and deadband passifier blocks to guarantee stability.

Remark 4.5.1 The approach above, can be straightforwardly extended to other linear transformations as well, in particular, here the generalized scattering transformation is of interest. Unfortunately, measurable constant time delay is a prerequisite coming against most of the advantages GST comes with, such as the inclusion of any operator satisfying a small gain property in the network loop. This extension is thus not presented here and we limit ourselves to the standard scattering transformation approach.

4.5.2 System architecture

The proposed coding scheme, using the LCWV architecture to make the communication channel passive, is seen in Figure 4.10 as a cascade of two-port systems. A deadband block is now applied immediately on the haptic signals, i.e. the velocity of the human $\dot{x}_h$ and the force of the environment f_e. On the receiver side a data reconstruction block takes place. However, in order to guarantee the passivity of the channel, an extra deadband passifier block is introduced which is nothing more than the implementation of the modified HLS reconstruction strategy in Section 4.3.2. The cascade connection of those three 2-port systems, each of them dissipating energy, with the passive human/HSI and passive TO/environments leads then to a stable overall system.

4.5.3 Evaluation

To evaluate the proposed LCWV control scheme and the modified deadband scheme within a TPTA system, the packet rate reduction ability and system's transparency is investigated. Our performance evaluation of the proposed control and coding architecture distinguishes two cases. We analyze the packet rate when both systems show a similar degree of transparency and also compare the transparency when both systems indicate similar packet rates. In lines with the transparency criterion from [97] we analyze the displayed mechanical impedance Z_h in comparison to the environment impedance Z_e. The mechanical impedance is given as the mapping between velocity $\dot{x}$ and force f, if a valid linear approximation exist it can be represented in the Laplace domain as $Z(s) = \frac{F(s)}{sX(s)}$. If the displayed impedance Z_h at the OP side is equal to the environment impedance Z_e at the TO side $Z_e = Z_h$ then the TPTA system is transparent [97]. In order to make the transparency

of two approaches comparable we will use the degree of similarity of two impedances as presented in Section 2.1.2 and in (2.4). Particularly, we consider two impedances $Z_{h_{1,2}}$ as similar if

$$J(Z_{h_1}, Z_{h_2}) = \int_{\omega_{min}}^{\omega_{max}} \frac{1}{|Z_{h_1}|} |Z_{h_1}(j\omega) - Z_{h_2}(j\omega)| d\omega < \rho$$

with $\rho > 0$ some threshold value. The deadband algorithm changes the dynamics of the system and no analytical representation or linear model for the displayed impedance $Z_h(s)$ can be derived. We assume, however, that a linearization of the displayed impedance around some working point exist and use identification methods to estimate its frequency response.

For the simulations we consider a haptic TPTA system where the dynamics of HSI and TO are assumed to be negligible, only the environment and the coding/transmission blocks are considered. The system is excited with sinusoidal velocity inputs within a frequency window $[\omega_{min}, \quad \omega_{max}] = [10^{-2} \quad 10^3]$ rad/s and unity amplitude. The gain and phase relation between the velocity signal and the resulting force feedback, i.e. the frequency response of the displayed impedance, is computed using a standard cross-correlation method [85]. The results for two prototypical cases: contact with a spring environment with a spring constant of 200N/m and free space motion are studied. The simulated time delay is $T_1 = T_2 = 30$ms which is considered to be a realistic assumption for teleoperation scenarios on earth using modern packet-switched networks. The sampling rate of the local control loops at HSI and teleoperator is 1 kHz. Accordingly, 1000 pks/s represents the standard packet rate without any data compression.

Results

Initially, the LCWV approach with modified deadband is applied with threshold parameter of $k = 10\%$ which is an empirically preferable value for transparent data reduction of haptic signals within TPTA systems, as presented in [68]. Additionally, the same Weber-inspired deadband scheme is applied on wave variables as proposed in [73], also configured with $k = 10\%$. The mean packet rates measured for both methods during the simulation are:

WV - Weber-inspired deadband:	↑ 262 pks/s, ↓ 262 pks/s
LCWV - Weber-inspired deadband:	↑ 265 pks/s, ↓ 245 pks/s,

where the average of the packet rate is taken over time and over all exciting frequencies, ↑ stands for the forward and ↓ for the backward channel. Both approaches show approximately the same packet rates which are substantially reduced compared to the original 1000 pks/s. However, the proposed LCWV based coding scheme achieves greater transparency according to displayed stiffness indicated by the amplitude and phase impedance characteristics, i.e.

$$J(Z_e, Z_{h_{LCWV}}) < J(Z_e, Z_{h_{WV}}),$$

as shown in Figure 4.11. It can be observed that the spring characteristics is lost for the WV architecture as no integrator behavior is apparent in its frequency response. This observation complies with the results of [73] where a relative (Weber-inspired) deadband is applied in the wave variable domain directly. Interestingly, there, a constant,
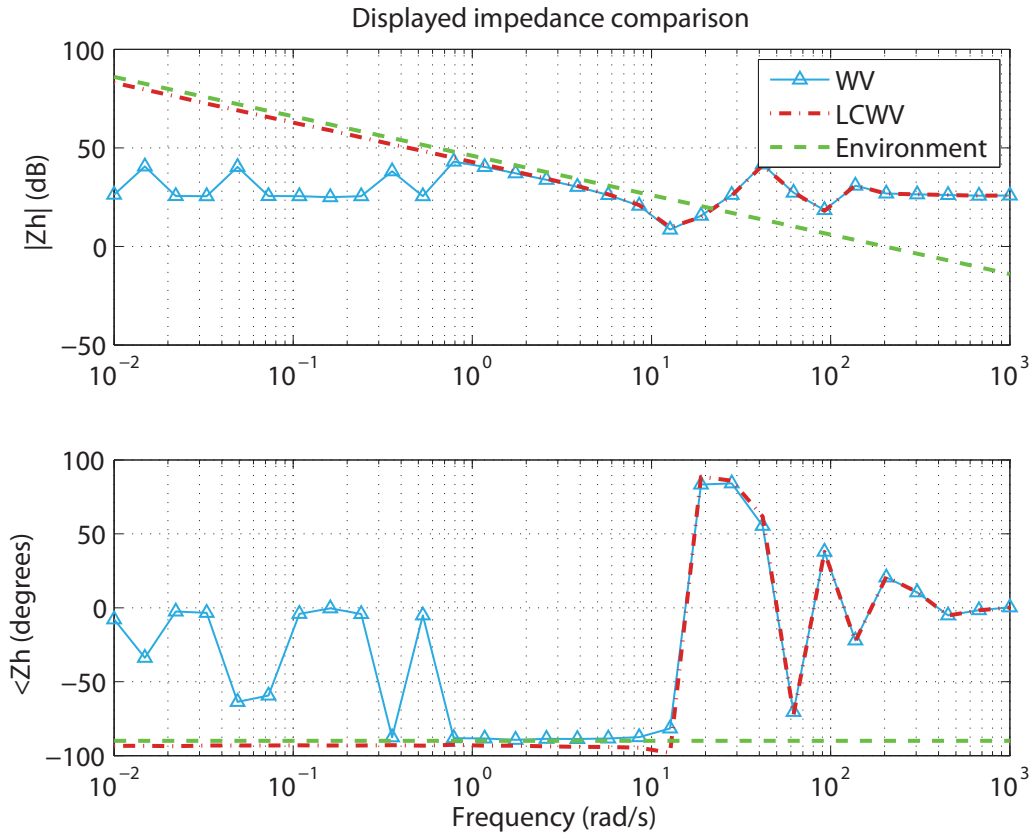
Fig. 4.11: Bode plot of displayed impedance for spring environment: LCWV with Weber-inspired deadband with $k = 10\%$; WV with Weber-inspired deadband with $k = 10\%$.

magnitude-independent deadband turns out to provide better results with respect to transparency/compression ratio than a relative one. Therefore, in the following we will compare our approach with the constant deadband approach for wave variables in [73].

A similar degree of transparency for the LCWV approach with $k = 10\%$ and the wave variable (WV) approach with constant deadband, i.e. similar displayed impedances $J(Z_{h_{LCWV}}, Z_{h_{WV}}) = 0.0015$, is achieved if the constant deadband value is chosen to be $0.02\sqrt{W}$ as identified in a line search. The corresponding Bode plots are shown in Figure 4.12. It should be noted here that part of the deviation of the displayed impedance in both approaches from the environment impedance is also a result of the original wave variable approach even without data compression as consequence of dynamics of the bilateral controller and the time delay. This deviation usually results in stiff environment being displayed softer. The mean packet rates are strongly - by further 38% - reduced within the LCWV approach.

$$\begin{aligned} \text{WV - constant deadband:} \quad &\uparrow 544 \text{ pks/s}, \downarrow 525 \text{ pks/s} \\ \text{LCWV - Weber-inspired deadband:} \quad &\uparrow 324 \text{ pks/s}, \downarrow 332 \text{ pks/s} \end{aligned}$$

Finally, free space motion is simulated using the same deadband configuration as in the previous simulation, see Figure 4.13 for the corresponding impedance plots. For both architectures a deviation from the ideal displayed impedance, $Z_h(s) \to -\infty$, is observed
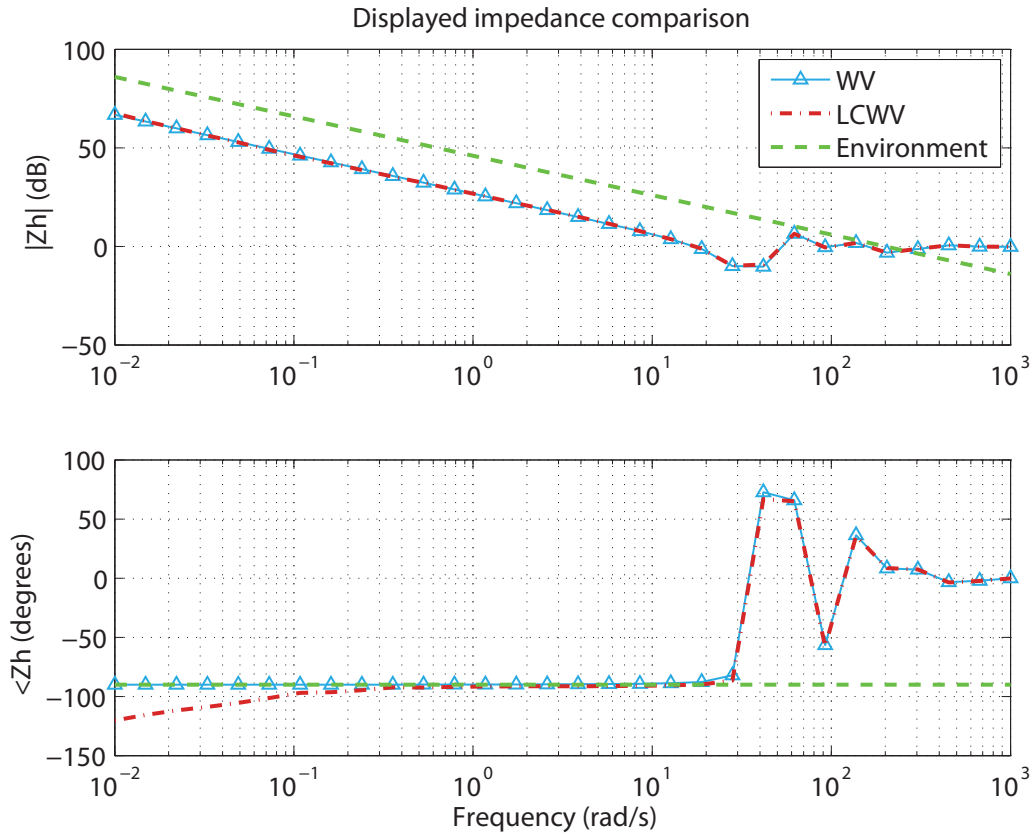
Fig. 4.12: Bode plot of displayed impedance for spring environment: LCWV with Weber-inspired deadband with $k = 10\%$; WV with constant deadband of $0.02\sqrt{W}$.

as the bilateral control dynamics and the time delay degrade the degree of transparency. The mean packet rate for the LCWV architecture is reduced by further 61% compared to the WV architecture, overall only 13% of the original data are transmitted:

$$\begin{array}{rl} \text{WV - constant deadband:} & \uparrow 352 \text{ pks/s}, \downarrow 334 \text{ pks/s} \\ \text{LCWV - Weber-inspired deadband:} & \uparrow 265 \text{ pks/s}, \downarrow \mathbf{0} \text{ pks/s} \end{array}$$

Qualitatively similar results are obtained for different deadband thresholds k, i.e. different compression rates, and different environments.

4.6 Systems with multiple degrees-of-freedom

The challenging and complex human perception of haptic signals in a multidimensional space restrains the deadband-based data reduction scheme to be as efficient as possible. In particular, the presented up to now schemes do not provide the ability of a compression scheme to fuse two different modalities, e.g. force and torques, or two dimensions, e.g. is a force with small magnitude in the y Cartesian direction perceivable if a force with a high magnitude in the x Cartesian direction dominates? Consequently, the reduction techniques in realistic multi-DoF scenarios are conservative and the reduction rates achieved can be
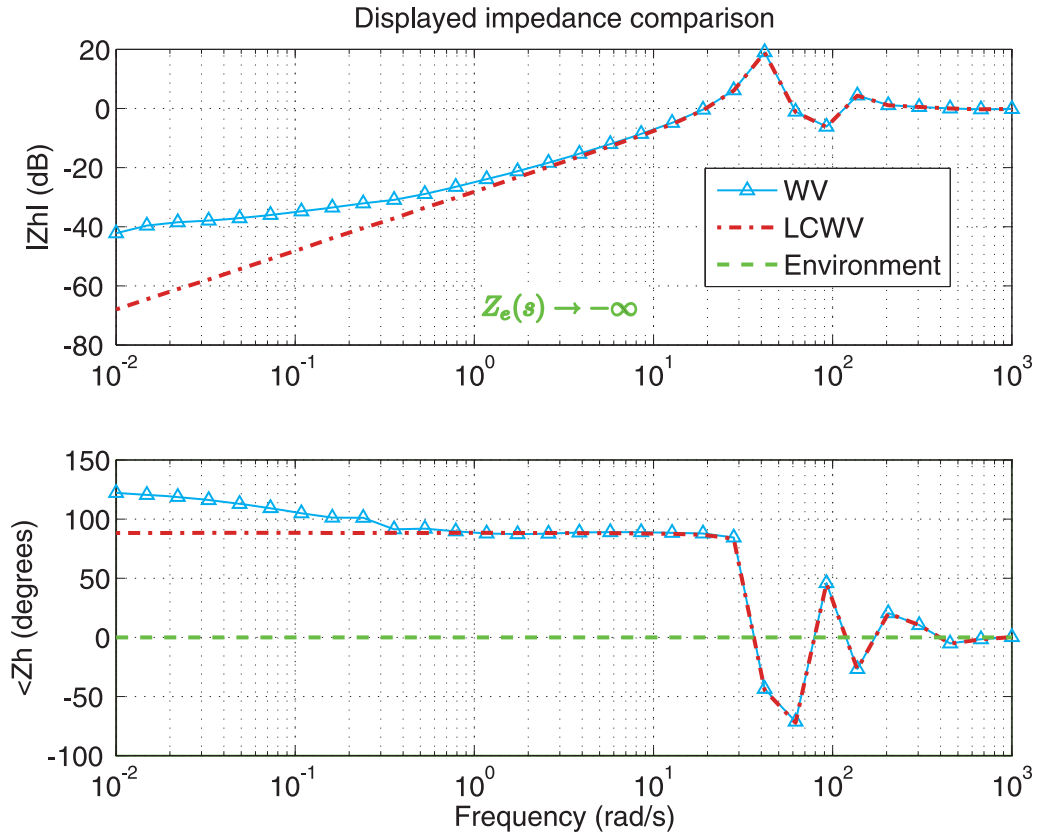
Fig. 4.13: Bode plot of displayed impedance in free space motion: LCWV with Weber-inspired deadband with $k = 10\%$; WV with constant deadband of $0.02\sqrt{W}$.

low. In this section, a simple, generic, easily-adaptable to many scenarios deadband-based reduction scheme for multi-DoF systems, first presented by the authors in [191], is proposed considering all different and complex perceptual limits of the human. A fit-for-all deadband form is given and by solving an optimization problem stability is guaranteed when using the proposed reconstruction strategy.

4.6.1 Human perception aspects

If a stimulus has more than one dimension, e.g. a force in the 3-dimensional space, or if stimuli of different nature are influencing the perception, e.g. 6-dimensional wrench in robotics, the multidimensional perception of the human has to be considered. Literature is scarce on this topic and the author could argue that the perception of multidimensional haptic stimuli is a rather poorly discovered field. Considering stimuli of different nature fused together, e.g. forces and torques, makes the problem even more complicated.

In [35] a two-dimensional Weber law is realized by determining the stimulus coordinates for all just noticeably different stimuli in all directions. The unidimensional Weber law provides a heuristic for the formulation of a law for two or more dimensions, assuming that Weber's constants are equal along the dimensions x and y. Therefore, a JND zone can be formed, that has in general a hyperspherical form. It is considered that stimuli that lie in
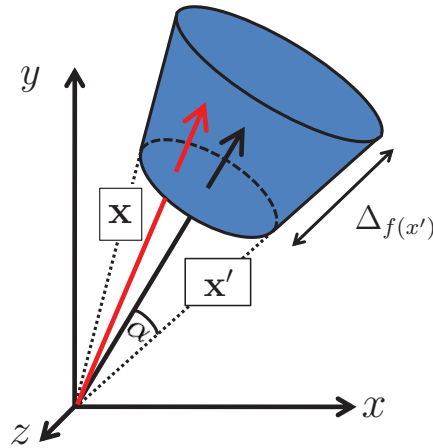
Fig. 4.14: Direction-dependent perception thresholds adopted from [91]. The black vector indicated the last transmitted vector. All new vectors that will lie in the blue region are considered as imperceivable.

it, are imperceivable when the human is displayed with the initial stimulus I.

Approaches with more complicated geometry are also discussed in [35], e.g. Helmholtz's approach. However, the complexity of such forms makes them difficult to parametrize and to use. Besides that, Helmholtz's approach has been criticized on empirical grounds.

Going one step further, there are unfortunately very few psychophysical studies investigating the dependency of the proportionality factor on the direction of haptic quantities. Pongrac *et al.* in [129] studied the discrimination of perturbating force depending on its direction. The results show a complex relation between the JND and the direction also depending on the reference value. Kammerl et. al propose in [91] to apply direction dependent perception thresholds for multi-DoF telepresence scenarios and revealed that the perception of artifacts arising from deadband-based data reduction is influenced by the direction of force feedback, and therefore, the multi-DoF equivalent of the 1-DoF deadzone is not isotropic for the force discrimination; see Figure 4.14 for an illustration.

The following work is psychophysically inspired and based on all these principles. As literature on this topic is still at an immature level, careful attention is given in the proposed framework to allow for most of the proposed perceptual models that face the problem of multidimensionality and multimodality in perception to be easily enclosed in our generic data reduction scheme.

4.6.2 Deadband for multi-DoF systems

In teleoperation systems with multi degrees-of-freedom a vector $\mathbf{x} \in \Re^n$ is transmitted instead of a signal. Applying the 1-DoF deadband approach to every single component of the representation is a straightforward extension, which however, turns out to be very inefficient with respect to the data transmission rate; in the following this approach will be called *component-wise* deadband. If random movements with identically distributed directions and magnitudes of forces and velocities are examined, the component with the lowest magnitude and therefore the smallest deadband is mostly responsible for packet generation, see e.g. [68]. Moreover, the probability of having a component with low mag-

(a) The component-wise deadband.

(b) The vectorial deadband.
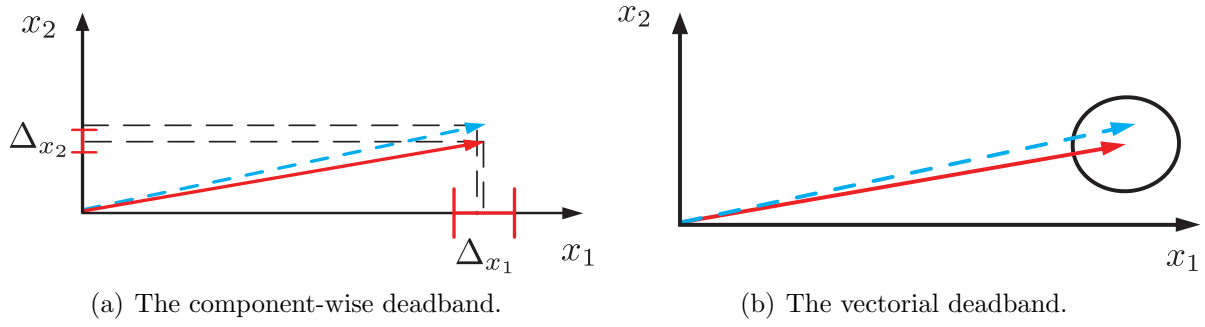
Fig. 4.15: Multi-DoF deadband approaches. With the continuous line the signal received at time t' is denoted, whereas the new signal is illustrated by the dashed blue line. It is observed that the new haptic signal (blue dashed line) does not trigger a new packet in the case of the vectorial deadband as it still lies in the deadzone. This is not the case for the component-wise deadband where the new haptic signal will indicate a new packet transmission despite the small, maybe imperceivable, change.

nitude increases with the number of components, i.e. degrees-of-freedom, used. This effect is illustrated in Figure 4.15(a) where it is shown that a small change on the x_2 direction will violate the deadband although the change at the tip of the vector can be considered "small". A new multi-DoF deadband is proposed here and aims to overcome this limitation. Let $\mathbf{x} \in \Re^n$ and $\mathbf{x}' \in \Re^n$ be the current and the last sent signal vectors respectively. Analog to the 1-D case, if the norm of the difference is smaller than the deadzone, then no signal is sent, otherwise the new value is transmitted and the deadzone is reset. This idea is illustrated for a 2-dimensional signal in Figure 4.15(b) and the algorithm is named *vectorial deadband*. The deadband control algorithm can be defined

$$\text{If:} \quad d(\mathbf{x}, \mathbf{x}') \leq \Delta_{\mathbf{x}'} \quad \text{Do not transmit}$$
$$\text{Else:} \qquad\qquad\qquad \text{Transmit new value,}$$

where $d(\mathbf{x}, \mathbf{x}')$ is the difference between the two stimuli $\mathbf{x}$ and $\mathbf{x}'$ and $\Delta_{\mathbf{x}'}$ defines the deadband zone.

In this work we consider a control architecture where velocities (linear and angular) and forces/torques are transmitted between HSI and teleoperator. As a result all transmitted variables can be assumed to be from finite dimensional vector spaces. Therefore, the general case of norm, the p-norm, can be used as the distance metric between the two vectors. For a given $\mathbf{x} \in \Re^n$, it is defined

$$||\mathbf{x}||_p = (\sum_{i=1}^{n} |x_i|^p)^{1/p}.$$

Remark 4.6.1 The use of a p-norm is not meaningful when orientations have another representation, e.g. quaternions or Euler angles.

In psychophysics, a special case, the Eucledian norm, i.e. $p = 2$, is often used [47] and thus will be adopted here

$$d(\mathbf{x}, \mathbf{x}') = ||\mathbf{x} - \mathbf{x}'||,$$

(a)   (b)
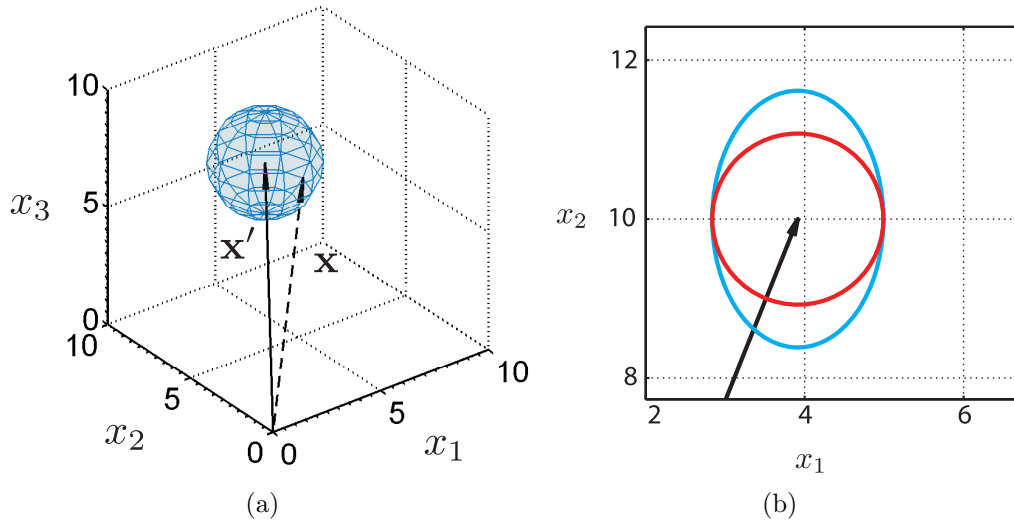
Fig. 4.16: Multi-DoF deadbands. (a) Spherical 3D deadzone with $k = 20\%$. The vector with the continuous line indicates the last received vector $\mathbf{x}'$, whereas the dashed-lined vector indicates the value $\mathbf{x}$ at the current time instance. (b) 2D elliptical (blue) and spherical (red) deadband zones for $\mathbf{x} = [4\ 10]$, $k_{x_1} = 10\%$, $k_{x_2} = 15\%$. and $k_{\mathbf{x}} = k_{x_1} = 10\%$ respectively.

where $||.||$ is used instead of $||.||_2$ to simplify the notation. In the simplest case, the deadband $\Delta_{\mathbf{x}'}$ can be defined analog to the 1-D case

$$\Delta_{\mathbf{x}'} = k \cdot ||\mathbf{x}'||.$$

The multi-DoF deadband control algorithm can thus be described as follows

$$\text{If:} \quad ||\mathbf{x}' - \mathbf{x}|| \leq k \cdot ||\mathbf{x}'|| \quad \text{Do not transmit}$$
$$\text{Else:} \qquad\qquad\qquad \text{Transmit new value.} \qquad (4.12)$$

In this case the deadband zone has a hyper-*spherical* form; see Figure 4.16(a) for an illustrative example. A signal with a small amplitude in one direction will no longer trigger redundant transmissions, the norm of the signal is used in the deadband instead.

However, the complex structure of the perceptual thresholds of a human, as discussed in the previous section, is not always isotropic but depends on the direction. Hence, nothing can guarantee that the perceptual space of the human or the spatial distribution of the JND is spherical. Therefore (4.12) might not be the best choice for a multidimensional signal. The presented framework should allow for the parameter k not to be equal for all spatial directions, i.e. non-istotropical perceptual spaces should be included. The data reduction scheme in (4.12) can still be considered valid although it is conservative. There, the smallest JND is still responsible for the choice of k, i.e. the smallest allowable radius for a sphere will be chosen. As a result the efficiency of the data reduction mechanism may be low for the degrees of freedom which would allow for a higher k. Hence, it is here proposed, to apply independent values for each corresponding dimension based on
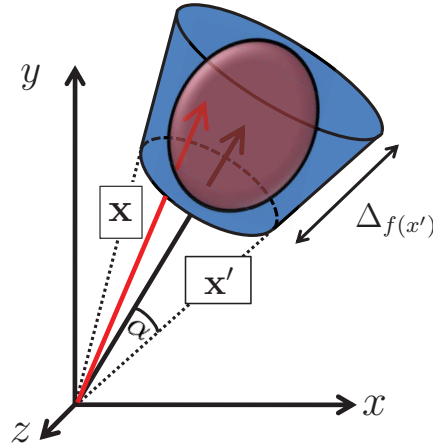
Fig. 4.17: The vectorial deadband (red) applied in the direction-dependent JND of Kammerl *et al.* in [91] (blue).

psychophysical findings instead of using the same deadband factor for all the vector components. This generalization of the case discussed above has the advantage of defining a larger deadband zone, that can therefore lead to further data reduction without impairing the human perception. The proposed data reduction algorithm is now described as

$$||\Omega_x(\mathbf{x}' - \mathbf{x})|| \leq ||\mathbf{x}'|| \tag{4.13}$$

with

$$\Omega_{\mathbf{x}} = \begin{pmatrix} \frac{1}{k_1} & 0 & \cdots & 0 \\ 0 & \frac{1}{k_2} & \cdots & 0 \\ \vdots & \vdots & \ddots & \vdots \\ 0 & 0 & \cdots & \frac{1}{k_n} \end{pmatrix} \tag{4.14}$$

a diagonal positive-definite matrix. The deadband zone is in this case an axis-aligned *ellipsoid*.

Remark 4.6.2 If $\Omega_{\mathbf{x}}$ is a non-diagonal positive-definite matrix the deadband zone is a rotated ellipsoid. The cross-terms in $\Omega_{\mathbf{x}}$ refer then to the masking effects between the different components of the vector considered. However, as the purpose of this work is neither to study masking effects nor are there available psychophysical studies to support it with proper values, they are set to 0.

Note that the positive-definiteness property of $\Omega_{\mathbf{x}}$ is, here, a necessary condition. Since the set of changes that are unperceivable to human is bounded, the deadband zone must also form a bounded set, which is guaranteed here by $\Omega_{\mathbf{x}}$ being positive-definite. An example of an elliptical deadzone compared to the spherical is illustrated for 2-dimensions in Figure 4.16(b). In Figure 4.17 it can also be seen, how the presented framework can be applied on different perceptual zones.
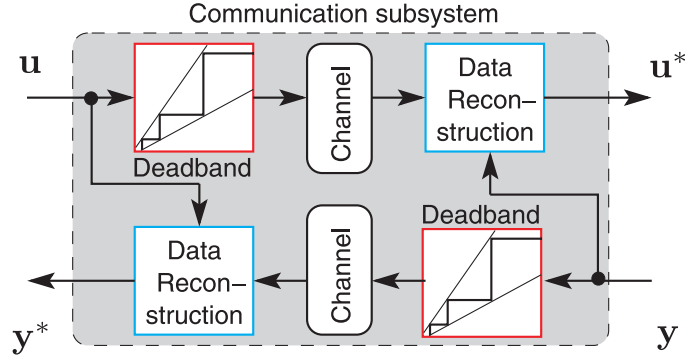
Fig. 4.18: A 2-port model of the network with deadband control.

4.6.3 Stability issues

Similarly to Section 4.3.2 a reconstruction strategy has to preserve the passivity of the communication channel, which is now using a multi-DoF deadband. As high sampling rates of the local control loops at the HSI and the teleoperator are assumed, the effects of discretization will be neglected in the following analysis: The locally controlled systems are approximated by continuous time systems.

We will refer to flow $\mathbf{u}$ and effort $\mathbf{y}$ variables, instead of the velocity and force signals of the 1-DoF case. For the 2-port network model shown in Figure 4.18 the passivity condition can be formulated recalling (2.15) as follows

$$\int_0^t \left(\underbrace{\mathbf{u}^T \cdot \mathbf{y}^*}_{P_M} - \underbrace{\mathbf{y}^T \cdot \mathbf{u}^*}_{P_S} \right) \, d\tau \geq 0 \quad \forall \, t > 0, \tag{4.15}$$

where the $*$ indicates reconstructed values, P_M represents the power on the master side, and P_S the power on the slave side. Unfortunately, the term P_M is not known on the slave side, and the term P_S is not known on the master side. A direct comparison between those two terms is thus not possible for passivity check. It is therefore here proposed, to maximize $\mathbf{u}^T \cdot \mathbf{y}^*$ and minimize $\mathbf{u}^{*T} \cdot \mathbf{y}$ to guarantee there exist no vector $\mathbf{y}$ that generates more energy than the $\mathbf{y}^*$ we are using for reconstruction, and no vector $\mathbf{u}$ that generates less energy than $\mathbf{u}^*$. This is a conservative reconstruction strategy which guarantees passivity, recall Section 2.3.1 and Proposition 4.3.3.

Reconstruction of flow signal

The reconstruction vector $\mathbf{u}^*$ should at each time instance minimize the power under the constraints that

1. it lies in the deadband zone, and

2. that the power in (4.15) is positive, namely energy is dissipated by the communication channel and power is flowing from master to slave.

The first constraint ensures the transparency of the reconstruction algorithm, and the second is defined to guarantee that the reconstruction algorithm will not change the power

flow direction. However, by assumption the environment and the human dynamical systems are considered passive. Therefore it is true that

$$\int_0^t \mathbf{u_h}^T \mathbf{y_h}^* = \int_0^t \mathbf{u}^T \mathbf{y}^* \geq 0, \tag{4.16}$$

due to the passivity of the human, where $\mathbf{u_h}$ and $\mathbf{y_h}$ the human effort and flow variables, respectively. Similarly,

$$\int_0^t \mathbf{y_e}^T \mathbf{u_e}^* = \int_0^t \mathbf{y}^T \mathbf{u}^* \geq 0, \tag{4.17}$$

due to the passivity of the environment, where $\mathbf{u_e}$ and $\mathbf{y_e}$ the environmental effort and flow variables, respectively. Hence, the second condition is, here, always satisfied.

A constrained minimization problem of the energy P_S is then formulated as

$$\begin{aligned} \text{Minimize} \quad & p(\mathbf{u}^*) \quad = \mathbf{u}^* \cdot \mathbf{y} \\ \text{with} \quad & c_1(\mathbf{u}^*) \quad = ||\Omega_{\mathbf{u}^*}(\mathbf{u}' - \mathbf{u}^*)|| \leq ||\mathbf{u}'||, \end{aligned}$$

$$\tag{4.18}$$

and can be solved using the Karush-Kuhn-Tucker method [109] by solving the following conditions

$$\begin{aligned} \mathbf{u}^* \mathcal{L}_{\mathbf{u}^*} \quad &= \quad 0 \\ \lambda_1 \mathcal{L}_{\lambda_1} \quad &= \quad 0 \\ \lambda_1 \geq 0 \quad &\text{and} \quad c_1(\mathbf{u}^*) \leq ||\mathbf{u}'||, \end{aligned} \tag{4.19}$$

where

$$\mathcal{L}(\mathbf{u}^*, \lambda_1) = p(\mathbf{u}^*) + \lambda_1(c_1(\mathbf{u}^*) - ||\mathbf{u}'||),$$

and $\mathcal{L}_{\mathbf{u}^*}$, $\mathcal{L}_{\lambda_1}$, the partial derivative of $\mathcal{L}(\mathbf{u}^*, \lambda_1)$ with respect to $\mathbf{u}^*$, and λ_1, respectively. A solution exists when $p(\mathbf{u}^*)$ and $c_1(\mathbf{u}^*)$ are real-valued differentiable functions.

Solving the optimization problem yields

$$\mathbf{u}^* = \mathbf{u}' - \frac{\Omega_{\mathbf{u}}^{-1} \Omega_{\mathbf{u}}^{-T} \mathbf{y}}{||\Omega_{\mathbf{u}}^{-T} \mathbf{y}||} ||\mathbf{u}'||. \tag{4.20}$$

Proposition 4.6.3 The reconstruction strategy (4.20) solves the optimization problem (4.18).

Proof: The partial derivatives of $\mathcal{L}$ in respect to λ_1 and $\mathbf{u}^*$ have to be calculated

$$\mathcal{L}_{\mathbf{u}^*} = \frac{\partial p}{\partial \mathbf{u}^*} + \lambda_1 \underbrace{\frac{\partial(c_1 - ||\mathbf{u}'||)}{\partial \mathbf{u}^*}}_{C}.$$

The term C can be developed as follows

$$
\begin{aligned}
\frac{\partial(c_1)}{\partial \mathbf{u}^*} &= \frac{\partial\left(\left((\mathbf{u}^* - \mathbf{u}')^T \, \Omega_{\mathbf{u}}^T \Omega_{\mathbf{u}} \, (\mathbf{u}^* - \mathbf{u}')\right)^{\frac{1}{2}}\right)}{\partial \mathbf{u}^*} \\
&= \frac{\left(\Omega_{\mathbf{u}}^T \Omega_{\mathbf{u}} + \Omega_{\mathbf{u}} \Omega_{\mathbf{u}}^T\right)(\mathbf{u}^* - \mathbf{u}')}{2\left((\mathbf{u}^* - \mathbf{u}')^T \, \Omega_{\mathbf{u}}^T \Omega_{\mathbf{u}} \, (\mathbf{u}^* - \mathbf{u}')\right)^{\frac{1}{2}}} \\
&= \frac{\left(\Omega_{\mathbf{u}}^T \Omega_{\mathbf{u}} + \Omega_{\mathbf{u}} \Omega_{\mathbf{u}}^T\right)(\mathbf{u}^* - \mathbf{u}')}{2c_1(\mathbf{u}^*)}.
\end{aligned}
$$

Without loss of generality, Ω is assumed to be symmetric. This way

$$
\left(\Omega_{\mathbf{u}}^T \Omega_{\mathbf{u}} + \Omega_{\mathbf{u}} \Omega_{\mathbf{u}}^T\right) = 2\Omega_{\mathbf{u}}^T \Omega_{\mathbf{u}}
$$

Based on these results, $\mathcal{L}_{\mathbf{u}^*}$ can be expressed as

$$
\mathcal{L}_{\mathbf{u}^*} = \mathbf{y} + \lambda_1 \frac{\Omega_{\mathbf{u}}^T \Omega_{\mathbf{u}} (\mathbf{u}^* - \mathbf{u}')}{c_1(\mathbf{u}^*)}, \tag{4.21}
$$

$$
\mathcal{L}_{\lambda_1} = c_1(\mathbf{u}^*) - ||\mathbf{u}'||, \tag{4.22}
$$

where

$$
\mathcal{L}_{\mathbf{u}^*} = \left(\frac{\partial \mathcal{L}}{\partial u_1^*} \quad \frac{\partial \mathcal{L}}{\partial u_2^*} \quad \frac{\partial \mathcal{L}}{\partial u_3^*}\right)^T,
$$

$$
\mathcal{L}_{\lambda_1} = \frac{\partial \mathcal{L}}{\partial \lambda_1}.
$$

The Karush-Kuhn-Tucker conditions for (4.18) are the following

$$
\mathbf{u}^* \mathcal{L}_{\mathbf{u}^*} = 0, \tag{4.23}
$$

$$
\lambda_1 \mathcal{L}_{\lambda_1} = 0, \tag{4.24}
$$

$$
\lambda_1 \geq 0 \quad \text{and} \quad c_1(\mathbf{u}^*) \leq ||\mathbf{u}'||,
$$

Since $\mathbf{u}^* \neq \mathbf{0}$, it follows from (4.23)

$$
\mathcal{L}_{\mathbf{u}^*} = \mathbf{0}.
$$

Considering the Karush-Kuhn-Tucker conditions there are two possible combinations of λ_1.

Case1: $\lambda_1 = 0$: Setting $\lambda_1 = 0$ in (4.22) would lead to $\mathbf{y} = \mathbf{0}$ which is not an admissible solution.

Case2: $\lambda_1 > 0$: Since $\lambda_1 > 0$, solving (4.24) leads to $(c_1(\mathbf{u}^*) - ||\mathbf{u}'||) = 0$ which means

$$c_1(\mathbf{u}^*) = ||\mathbf{u}'|| \Leftrightarrow ||\Omega_{\mathbf{u}}(\mathbf{u}^* - \mathbf{u}_\ell)|| = ||\mathbf{u}'||. \tag{4.25}$$

By replacing (4.25) in (4.22) and solving for $\mathbf{u}^*$, the following expression for $\mathbf{u}^*$ can be derived

$$\Omega_{\mathbf{u}}^T \Omega_{\mathbf{u}} (\mathbf{u}^* - \mathbf{u}') = \frac{-\mathbf{y}\,||\mathbf{u}'||}{\lambda} \tag{4.26}$$

$$\Rightarrow \mathbf{u}^* = -\Omega_{\mathbf{u}}^{-1}\Omega_{\mathbf{u}}^{-T}\frac{\mathbf{y}\,||\mathbf{u}'||}{\lambda} + \mathbf{u}'. \tag{4.27}$$

Note that since $\Omega_{\mathbf{u}}$ is positive definite, it is always invertible and its inverse is also positive definite. Using the form (4.27) in (4.25) results in

$$\left\|\Omega_{\mathbf{u}}\left(-\Omega_{\mathbf{u}}^{-1}\Omega_{\mathbf{u}}^{-T}\frac{\mathbf{y}\,||\mathbf{u}'||}{\lambda} + \mathbf{u}' - \mathbf{u}'\right)\right\| = \left\|\Omega_{\mathbf{u}}^{-T}\frac{\mathbf{y}\,||\mathbf{u}'||}{\lambda}\right\| = ||\mathbf{u}'||$$

$$\Rightarrow \frac{||\mathbf{u}'||}{\lambda}\left\|\Omega_{\mathbf{u}}^{-T}\mathbf{y}\right\| = ||\mathbf{u}'||. \tag{4.28}$$

By solving for λ we get

$$\lambda = \left\|\Omega_{\mathbf{u}}^{-T}\mathbf{y}\right\|.$$

By replacing λ in (4.27) the solution of the minimization problem (4.18) can be found as

$$\mathbf{u}^* = \mathbf{u}_\ell - \frac{\Omega_{\mathbf{u}}^{-1}\Omega_{\mathbf{u}}^{-T}\mathbf{y}}{||\Omega_{\mathbf{u}}^{-T}\mathbf{y}||}\,||\mathbf{u}'||. \tag{4.29}$$

This completes the proof. ∎

Remark 4.6.4 In the case of spherical deadband, i.e. when $\Omega_{\mathbf{u}} = \frac{1}{k_{\mathbf{u}}}I$, where k a positive constant and I the unity matrix, (4.20) can be simplified to

$$\mathbf{u}^* = \mathbf{u}' - \frac{\mathbf{y}}{||\mathbf{y}||}k_{\mathbf{u}}\,||\mathbf{u}'||.$$

Remark 4.6.5 The above results comply in the 1-DoF case with the result in [76, 73] where it is shown that

$$\mathbf{u}^* = \mathbf{u}' - \text{sign}\{\mathbf{y}\}k_{\mathbf{u}}\,||\mathbf{u}'||. \tag{4.30}$$

Reconstruction of effort signal

Similarly to the expression for $\mathbf{u}^*$ in (4.20), a maximization problem can be solved for $P_M = \mathbf{u}^T\mathbf{y}^*$, such that the reconstruction of the effort signal $\mathbf{y}^*$ will maximize the power flow P_M. This is equivalent with a minimization problem of $-\mathbf{u}^T\mathbf{y}^*$. Using the same

constrained optimization method the problem is formulated as as

$$\text{Maximize} \qquad \mathbf{u^T} \cdot \mathbf{y}^*$$
$$\text{with} \quad ||\Omega_\mathbf{y}(\mathbf{y}' - \mathbf{y}^*)|| \leq ||\mathbf{y}'||, \tag{4.31}$$

which is equivalent to

$$\text{Minimize} \qquad -\mathbf{u^T} \cdot \mathbf{y}^*$$
$$\text{with} \quad ||\Omega_\mathbf{y}(\mathbf{y}' - \mathbf{y}^*)|| \leq ||\mathbf{y}'||. \tag{4.32}$$
$$\tag{4.33}$$

Solving the optimization problem (4.33) yields

$$\mathbf{y}^* = \mathbf{y}' + \frac{\Omega_\mathbf{y}^{-1}\Omega_\mathbf{y}^{-T}\mathbf{u}}{||\Omega_\mathbf{y}^{-T}\mathbf{u}||} \, ||\mathbf{y}'|| \,. \tag{4.34}$$

Proposition 4.6.6 The reconstruction strategy (4.34) solves the optimization problem (4.33).

Sketch of Proof: The solution follows the same steps as with the minimization problem solved above for the reconstruction vector $\mathbf{u}^*$. ∎

Remark 4.6.7 For the spherical deadband (4.34) can be simplified to

$$\mathbf{y}^* = \mathbf{y}' + \frac{\mathbf{u}}{||\mathbf{u}||}k_\mathbf{y} \, ||\mathbf{y}'|| \,.$$

4.6.4 Pose drift correction for multi-DoF systems

It can been shown that any disturbance, such as some missing samples due to data reduction, on a velocity-based architecture will induce a velocity error that consequently causes the human system interface and the teleoperator to drift from each other. Velocity-based architectures, e.g. suffer from this position and orientation drifts due to the integration error of the controllers. Such a position drift does not only deteriorate the transparency, but may also drive the system to inoperability if either the HSI or the TO reach their workspace limits. In [22] a time-delayed velocity/force architecture is extended by a position feedforward. It is designed with a saturated position controller at the teleoperator such that the passivity condition is not violated. However, a system with only one degree-of-freedom is considered. Similarly, in a multi-DoF system a pose update in Cartesian space can be transmitted to compensate for the pose drift.

Here, a pose (position and orientation) update strategy within a closed-loop kinematic control as in [18] is used instead. A clever strategy will guarantee that this will not sacrifice for the efficiency in the transmissions of the communication channel. Particularly, a pose update is always transmitted *together* with the velocity data packets to improve the position tracking. This does not create any considerable load on the network, since haptic

telepresence systems are characterized more by increased packet rate rather than by high payload utilization. On the other hand, when a new position update packet is required, as will be seen later, the velocity information is also included in the same packet, avoiding thus an extra transmission when the deadzone will be violated.

Example 4.2 (Augmenting the payload data with position updates)
Assume a haptic telepresence system with 6 degrees-of-freedom. Its orientation is expressed in quaternion space, the translation in Cartesian space; therefore 7 double end effector values have to be transmitted. Needing 8 bytes per each double value will require a relatively small 56 bytes data packet payload. The available payload of a UDP datagram which is carried in a single IP packet is 65.507 bytes for IPv4 and 65.527 bytes for IPv6. Therefore, the packet utilization that the haptic telepresence does is only 0.08% of the available packet payload. With the addition of a pose update strategy, i.e. another 7 double values, this will double up to 0.16%, which is however still extremely low. It is therefore obvious, that unless there is no large increase in the degrees-of-freedom, the transmission of additional signals is not problematic as long as now new packets are transmitted which could lead to network congestion.

From the control point of view, the orientation and position errors introduced by the deadband control are considered as kinematic disturbances. The updated pose values are used in the closed kinematic controller in the sample time when they are received. For the rest of the time the kinematic control loop is considered open until a new update arrives. The closed-loop kinematic equation has the following form

$$\dot{\boldsymbol{q}} = J^{-1} \begin{bmatrix} \mathbf{v}^* + \mathbf{K}_t e_t \\ \boldsymbol{\omega}^* + \mathbf{K}_o e_o \end{bmatrix} \tag{4.35}$$

where $\mathbf{v}^*$ and $\boldsymbol{\omega}^*$ the reconstructed linear and angular target velocities, q the joint angles, J the Jacobian matrix of the robot, $\mathbf{K}_t$ and $\mathbf{K}_o$ positive-definite matrices of the kinematic controller gains, and e_t, e_o the translational and orientational error, see Figure 4.19 for an illustration. For the orientation error and the closed kinematic loop see Appendix B.2. Asymptotic stability of this kinematic control, with the use of quaternions for orientation representation, is proven in [18].

Nonetheless, if no deadband updates are transmitted for a long time, e.g. when velocity remains constant, there might still be some significant position and orientation drift. In some telerobotic scenarios, a maximum position drift $\tilde{x}_{max}$ is allowed. There exists, therefore, a maximal period of time T_{max} that can elapse without new packets being sent, and it is depending on the maximum velocity of the system. By knowledge of the maximum allowable error, based on the last velocity value sent, and on the deadband parameter $k_{max} = \frac{1}{\lambda_{min}(\Omega_{\mathbf{x}})}$, where $\Omega_{\mathbf{x}}$ is defined in (4.14), we can compute the maximum period T_{max} so that the upper bound of the position drift is not violated as follows.

Let $\mathbf{x}$ and $\mathbf{x}^*$ be the position of the master and slave respectively, corresponding to the
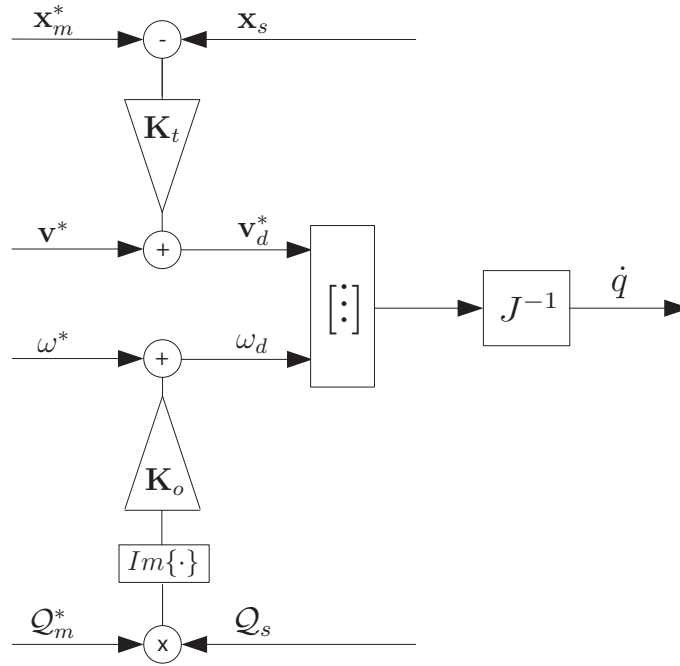
Fig. 4.19: The closed kinematic control used for the pose updates.

velocities $\mathbf{v}$ and $\mathbf{v}^*$ respectively, with $\mathbf{x}(0) = \mathbf{x}^*(0)$. The following relations hold

$$
\|\mathbf{x} - \mathbf{x}^*\| \le \tilde{x}_{max}
$$

$$
\Rightarrow \left\| \int_0^t \mathbf{v}\, d\tau - \int_0^t \mathbf{v}^*\, d\tau \right\| \le \tilde{x}_{max}
$$

$$
\Rightarrow \left\| \int_0^t (\mathbf{v} - \mathbf{v}^*)\, d\tau \right\| \le \tilde{x}_{max}. \tag{4.36}
$$

Using the Cauchy-Schwarz inequality

$$
\left\| \int_0^t (\mathbf{v} - \mathbf{v}^*)\, d\tau \right\| \le \int_0^t \|\mathbf{v} - \mathbf{v}^*\|\, d\tau.
$$

This means that

$$
\underbrace{\int_0^t \|\mathbf{v} - \mathbf{v}^*\|\, d\tau \le \tilde{x}_{max}}_{C} \Rightarrow \left\| \int_0^t (\mathbf{v} - \mathbf{v}^*)\, d\tau \right\| \le \tilde{x}_{max}. \tag{4.37}
$$

So the condition C in (4.37) must hold in order to keep the position error below the its maximum allowed value. Since $\mathbf{v}$ and $\mathbf{v}^*$ are bounded by the deadband ellipsoid, the maximum distance between the points presented by these vectors is

$$
\max\left(\|\mathbf{v} - \mathbf{v}^*\|\right) = 2k_{max}\|\mathbf{v}'\|.
$$

In the case of an axis-aligned ellipsoid $k_{max} = \frac{1}{\lambda_{min}(\Omega_{\mathbf{x}})}$. If the ellipsoid is rotated, it can

be first transformed into an axis-aligned ellipsoid using the principal component analysis, and then k_{max} can be calculated as described above.

In the period of time where no packets are sent, $k_{max} \, ||\mathbf{v}'||$ is constant since $\mathbf{v}'$ is constant. This leads to

$$\int_0^t \max\left(||\mathbf{v} - \mathbf{v}^*||\right) d\tau = 2k_{max} \, ||\mathbf{v}'|| \cdot t.$$

This way, the maximal period of time T_{max} can be determined, so that the upper bound of the position drift is not violated

$$
\begin{aligned}
2k_{max} \, ||\mathbf{v}'|| \, T_{max} &= \tilde{x}_{max} \\
\Rightarrow T_{max} &= \frac{\tilde{x}_{max}}{2k_{max} \, ||\mathbf{v}'||}.
\end{aligned}
\tag{4.38}
$$

Concluding, an *augmented* pose update strategy is proposed here to compensate for position and orientation drifts in velocity-based architectures. Pose updates are *always* transmitted together with the velocity updates as in the classical position update strategies, without having any significant influence on the efficiency of the system as it is shown in Example 4.2. If, however, the maximum allowable time T_{max} is exceeded between two consecutive transmission, an extra pose update packet is triggered to avoid exceeding the maximum allowable drift.

$$
\begin{aligned}
\text{If:} \quad & t - t' > T_{max} \quad \text{Transmit pose update} \\
\text{Else:} \quad & \qquad\qquad\qquad \text{Do nothing.}
\end{aligned}
$$

4.6.5 Experiments

The goal of the experiments here is to evaluate the proposed multi-DoF deadband scheme in terms of packet rate reduction, stability and position as well as stiffness error. As the main focus of this work, is rather the extension of previous results for systems with multiple degrees-of-freedom and the corresponding reconstruction criteria, these experiments are not destined to identify JNDs or argue about the perceptual performance of the proposed approach.

Experimental setup

The multi-DoF haptic teleoperation consists of a master 7-DoF manipulator, i.e. VIsHaRD 7, and a human-scaled 7-DoF robotic arm for the teleoperator; for further technical details see Appendix A. Both robots are admittance-type devices and are thus controlled using a position-based admittance control scheme. Gravity and external forces are compensated. The rotation is represented in both robots in the quaternion space, however, the multi-DoF deadband approach applies to finite dimensional vector spaces. Therefore, the quaternions were converted to angular velocities, only for the transmission, and then converted back to quaternions. For the teleoperation experiment a velocity/force architecture was used. Hence, a 6-dimensional vector consisting of the master device Cartesian velocity as well
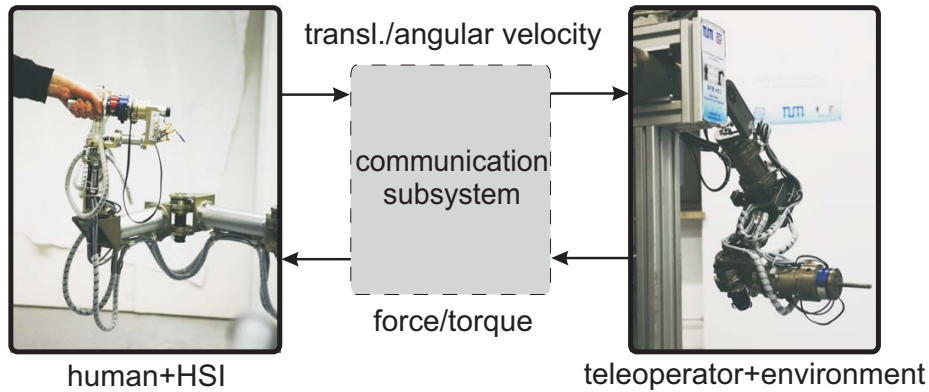
Fig. 4.20: The 7-DoF teleoperation setup used for the experiment. The communication subsystem is visualized in Figure 4.18. More technical details on the HSI and the teleoperator in Appendix A.

as the angular velocity, i.e. twist, were transmitted. On the slave side, the corresponding quaternion had to be computed and fed into the lower position-based controller of the robot. The 6-DoF force/torque, i.e. wrench, sensor of the slave device, measures the interaction forces/torques with the environment and transmitted it as a force-feedback to the HSI device. The teleoperation architecture is illustrated on Figure 4.20. The network channel consists of simple LAN with 100 MB/s bandwidth. Time delay is therefore considered negligible. Packet losses are ignored.

Experiment design

Deadband was applied on both channels and the reconstruction strategy given in (4.20) and (4.34) was applied at each receiver side. A multi-DoF deadband was defined independently for the linear and angular velocity, as well as for the forces and torques, totally four deadbands were used. The reason for this design, as explained previously, is that a psychophysical scaling quantity has to be defined between e.g. a force and a torque, otherwise they have different scales and the one deadband would mask the influence of the other quantity.

The experiment consisted of a free space motion and a contact phase where a silicon cube with stiffness 1400 N/m is haptically explored. The contact occured in a constant angle near 45°, so both the x- and z-components of the force were triggered. During the interaction the deadband algorithm switched between the multi-DoF deadband approach and the straightforward extension of the 1-DoF deadband, i.e. component-wise deadband. The same k is used in each dimension for simplicity. The displayed stiffness to the human is then estimated offline using least-squares identification.

Results

Pose update strategy The position and orientation updates contributed to a better position tracking of the system. A comparison of the translational position error in all three directions, x, y, and z with and without position update is illustrated in Figure 4.21.

Parameter	Value
Kinematic controller gain $\mathbf{K}_t$	1000
Kinematic controller gain $\mathbf{K}_o$	500
$\Delta_{f_{min}} [N]$	1
$\Delta_{\tau_{min}} [Nm]$	0.01
$\Delta_{\omega_{min}} \left[\frac{rad}{s}\right]$	0.1
$\Delta_{\mathbf{v}_{min}} \left[\frac{m}{s}\right]$	0.05

Tab. 4.3: Deadband control parameters
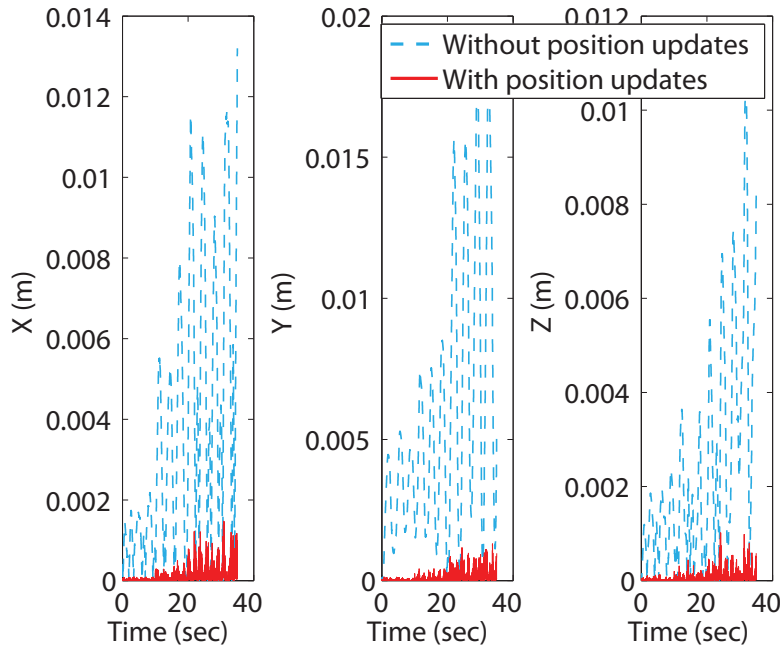
Fig. 4.21: Position tracking with and without position update. An overall error of less than 2mm is observed when position updates are transmitted, whereas significant position drift is observed when not.

It is observed that after 35 sec of interaction with the system the position drift has increased significantly. With the proposed position update strategy the position drift is much smaller, less than 2 mm in this experiment, and considered negligible. In parallel, the whole approach does not significantly increase the packet rate. As observed in Figure 4.22 the packets transmitted with the position update strategy are not significantly increased compare to the packets transmitted without using this technique. The maximal period without update T_{max} was heuristically set to $50ms$, hence position updates were transmitted *at least* every $50ms$.

Stiffness error   Results are illustrated in Figure 4.24. It is observed that the multi-DoF deadband can lead to high data reduction without significant error on the stiffness; for 90% of packets reduced the stiffness error was measured to be below 5%. Psychophysical studies indicate a stiffness error up to 8% to be imperceivable for pinch/finger movements [161]
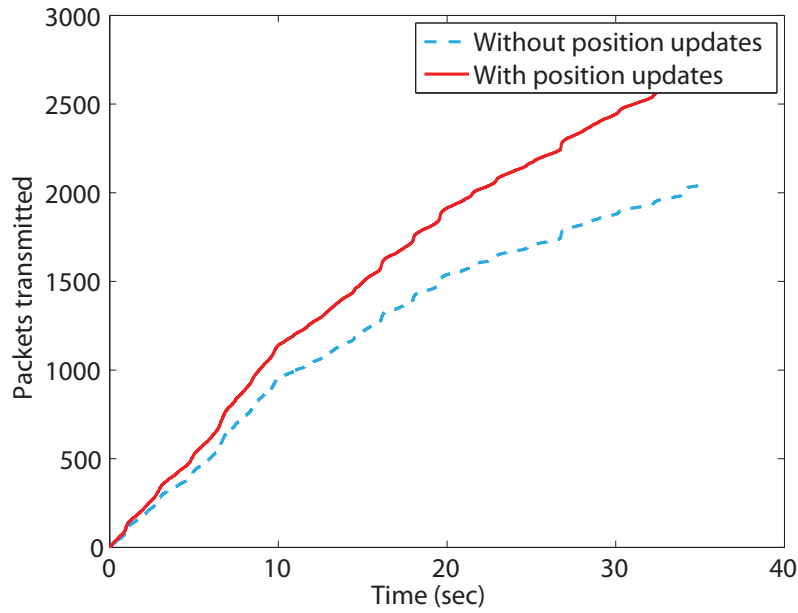
Fig. 4.22: The packets transmitted with the use of the position update strategy and without it. It is observed that the position updates do not significantly increase the packet rate. The packets that would be transmitted without the use of deadband-based data reduction algorithm would be in that case $35 \times 1000 = 35000$ packets.

whereas the stiffness error perception threshold is increased up to 23% for the arm/forearm as shown in [89, 88]. Moreover, the fact that the curve for the multi-DoF deadband lies always below the component-wise deadband in both figures indicates the increased performance of the proposed approach. For the same amount of transmitted packets less stiffness error is induced.

4.6.6 Summary

To summarize, the novel multi-DoF haptic data reduction framework proposed here is considered to aid the development of algorithms for data reduction in multidimensional or multimodal settings. The ability to use hyper-ellipses in a multidimensional space and configuring them individually to the perceptual characteristics, that are of course in many cases yet to define by the psychophysics society, is a very important property, as it poses a generic tool to the field of haptic data reduction. Besides that, stability of the presented approaches is not endangered as the presented frameworks complies with the passivity (or dissipativity) setting. Experimental results validate our findings, indicating first, no significant packet rate increase when position updates are transmitted, and second, illustrating a clear benefit for the multi-DoF deadband scheme in terms of displayed stiffness error, compared to the classic component-wise deadband approach.
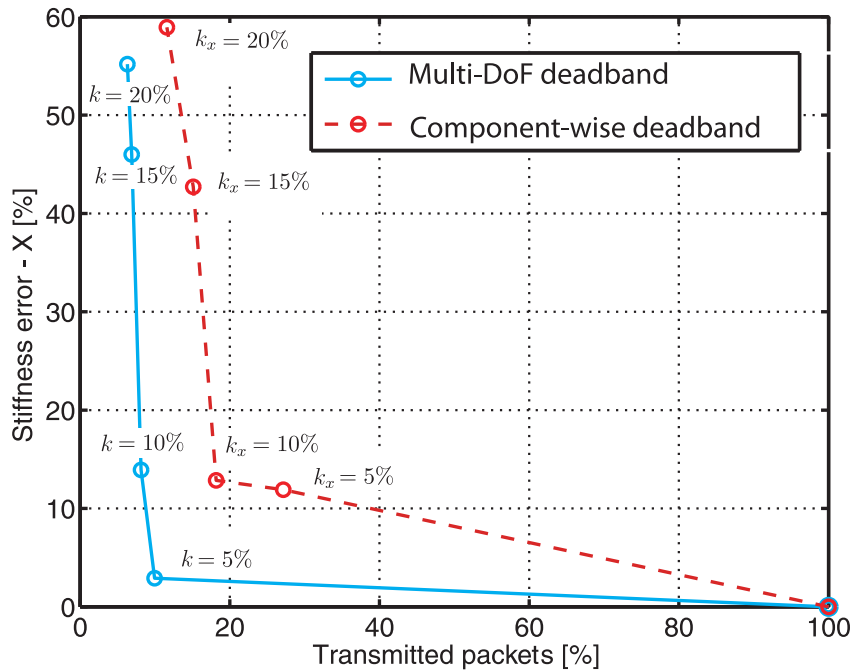
Fig. 4.23: Stiffness error: x-component. The proposed Multi-DoF deadband outnumbers the component-wise approach as it transmits less amount of packets for the same stiffness error and vice versa.

4.7 Discussion

Modern haptic telepresence systems employ a lot of degrees-of-freedom. Consequently, the amount of data exchanged between the two principal components of a teleoperation system over the communication network is significant. Besides that, high packet rates are required for the haptic information, that are hard to maintain on long distances in current packet-switched communication networks. This can lead to network congestion and transmission delay. Especially, in wireless or underwater scenarios the high packet rates are far from realizable. Strategies to reduce the network traffic in haptic telepresence systems are reviewed in this chapter and extended to allow for further applicability in various scenarios. Core aspect of all approaches is the human perception, meaning that the artifacts introduced by the algorithms have to be imperceivable. The deadband control is thus chosen as underlying approach and deadband-based haptic data reduction schemes are employed.

First of all, the importance of the dynamics of the movement of the human arm in a teleoperation scenario is for first time, here, exploited to adapt accordingly the data reduction scheme. Higher data reduction rates are therefore achievable by just increasing the deadband when the human operator is moving with high velocity, and thus becomes less attentive to the forces applied on him/her, and vice versa. The method is evaluated experimentally and the results suggest that the velocity-adaptive deadband approach constitutes a solid improvement to the traditional Weber-inspired deadband approach. In the conducted experiments, adding the velocity-proportional component led to a additional
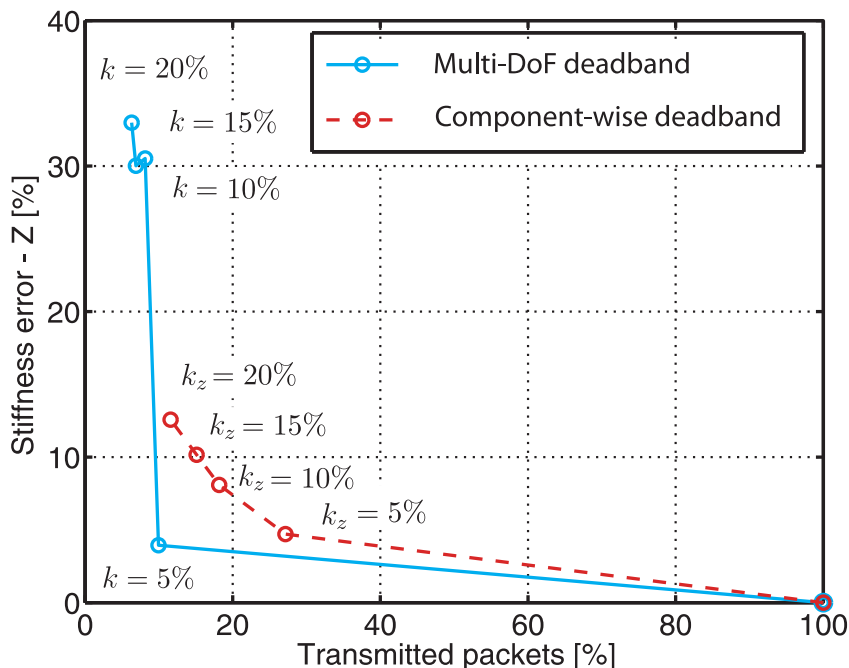
Fig. 4.24: Stiffness error: z-component. The proposed Multi-DoF deadband outnumbers the component-wise approach in this component as well. The fact that the Multi-DoF deadband curve lies below the component-wise one indicates its superior performance as it transmits less amount of packets for the same stiffness error and vice versa.

data reduction of up to 30% compared to the original Weber-inspired deadband, without significantly affecting the task performance accuracy. Furthermore, the effect was proved to be speed-invariant.

Besides that, the need for a perceptual scheme that will reduce the haptic data in a time-delayed teleoperation scenario without impairing the overall system stability is mentioned. An algorithm that uses the successful scattering transformation (or wave variables) approach to treat with the problem of stability on the other hand, but applies the perceptual deadband algorithm on haptic signals, and not on their transformed variables, is here proposed. It is shown how this technique can lead to higher data reduction rates.

Finally, the overall deadband-based data reduction scheme is generalized for multi-degree-of-freedom haptic telepresence systems. This aims to satisfy the requirement of efficient reduction in multidimensional spaces, which none of the approaches presented in the literature has touched upon. Moreover, the presented multi-DoF framework complies with the passivity-based architectures widely used in haptic teleoperation.

In summary, this chapter exploits the interaction, and especially the perceptual characteristics of the human to enable an *efficient* way of transmitting haptic data over a communication channel, usually packet-based. It builds upon well employed standards of the haptic data reduction literature, such as the Weber law and the deadband control, to enable for its realistic use in various teleoperation scenarios by integrating more of the acquired knowledge about the human in the design of the algorithms. Future studies should further

concentrate on acquiring human perception knowledge, e.g. in multi-dimensional/modal spaces, to further drive the field of haptic data reduction forward. Built on solid findings, the establishment of a haptic data protocol could also be considered.

5 The grip force employed for human-centered teleoperation

Obtaining knowledge of the human in a form of perceptual discrimination thresholds, i.e JNDs, is just one way of designing the system in favor of transparency and efficiency in terms of communication resources. The human operator is far more complicated than that. Revolutionary ideas, as discussed in Chapter 3, incorporate human knowledge to the benefit of both stability and transparency. As the human is coupled with the telerobotic system and exchanges mechanical energy with it, this is done based on the energetic behavior or the apparent minimum damping the human arm displays. The inclusion of the human-knowledge in the design process still poses significant challenges. The work in Chapter 3 sets the stage by implying knowledge of the human operator to be acquired offline. In this chapter, we investigate the human dynamics and envision their *online* use in a human-centered control design, to the benefit of stability and transparency of the human-robot interaction and consequently of the overall haptic teleoperation system.

Amongst many human identification techniques, an extra degree-of-freedom, poorly exploited so far, is here investigated to acquire the knowledge of some human arm dynamics: the *grip force of the human*. It is believed, that by easily measuring how tight a human operator grasps the human system interface it is possible to adapt the haptic system accordingly and increase the interaction realism and the control performance. Particularly, it is found that the human grip force correlates with the mechanical impedance of his/her arm, or better specific parameters thereof. As a consequence, an approximation of the human arm mechanical impedance can be employed online by the controller and all this coming from a single, fast and reliable measurement. Along with this study, it is found, that the energetic behavior of the human arm, in terms of the dissipativity-based framework discussed in previous chapters, also correlates with the grip force offering thus great potential for energy-based approaches using this measurement and without requiring the measurement of the energy or the solution of process consuming linear matrix inequalities to estimate the (Q, S, R) properties. In parallel, through the experiments conducted in this chapter the theory on dissipativity of the human arm discussed in Chapter 3 is further validated.

The innovation in this chapter lies thus in the inclusion of the human grip force, poorly exploited in human-robot interaction applications so far, in a teleoperation system design to improve transparency. Considering the fact that the damping is the most important parameter to stabilize an unstable system, either in a remote teleoperation setting, or in interactions with a virtual environment, we aim to utilize this relationship to improve the control performance. Moreover, visionary ideas are discussed combining the results of the previous chapters. The open problems highlighted in this chapter are expected to direct future research in this direction.

The remainder of this chapter is organized as follows: In Section 5.1 the state-of-the-

art in estimating the impedance of the human operator arm is presented. The idea of utilizing the grip force for an impedance estimation is sketched in Section 5.2 where a pilot experiment and its results are also illustrated. The benefit of the possible correlation of the grip force intensity with the human arm impedance is discussed in Section 5.3 and the chapter concludes with Section 5.4 discussing open problems and ideas for future work.

5.1 State-of-the-art

5.1.1 Modeling: Accuracy vs. robustness

As discussed in Section 2.1.1, human arm models can be distinguished to structured and unstructured ones. Structured models, such as e.g. the linear mass-spring-damper model are widely used for the human arm and are

- easier to identify,

- more useful in a control scheme, and

- can offer parametric stability conditions.

Such models are identified in [114, 43, 167, 34, 151] and used in various control schemes in [45, 163] and in teleoperation [94]. Nevertheless, they are criticized on their robustness as even small deviations from the nominal model may cause instabilities which is a significant disadvantage in approaches with high inter-subject variability. An online identification and an adaptive control scheme would definitely contribute to their wider use.

Non-parametric models, on the other hand, can allow for more nonlinearities. Moreover, the passivity paradigm also allows for an unknown structure appropriate to model the unknown changing human behavior/dynamics leading thus to greater robustness of the control approaches based on this principle; see [114, 78] and the discussion in Section 2.1.1. Nevertheless, non-parametric models difficultly distinguish between models. E.g. if two models are treated as passive, the same control strategy applies to both and, consequently, with the same results. They are therefore unsuitable for parameter adaptation.

Bridging the gap between those two cases, the dissipativity framework in Chapter 3 uses *semi-parametric* models by characterizing the human arm as dissipative and utilizing only approximate knowledge on its lower damping, in general its energetic behavior. This still allows for a partially nonlinear and unknown structure, but on the other hand two systems can be distinguished from each other and can differ on their degree of dissipativity facilitating the use of adaptive techniques without the disadvantages of model-based approaches. To the best of the author's knowledge, no approach exist for the online identification of such semi-parametric human arm models, thus, early steps are provided in this chapter.

5.1.2 Measurements

Various sensors are used to accommodate the *online* identification of a model for the human arm. Usually high-precision position encoders and force measurements are employed to measure the position/orientation and the force/torques applied by the human

arm attached to the handle of a haptic device. The acquired data are then used in standard identification techniques, e.g. least-squares fit, to estimate the effective human arm characteristics usually as a mechanical impedance. In [43, 111] apart from the force and position data, electromyogram signals collected from upper arm muscles were also collected from electrodes attached at specific positions on the skin of the human operator. Although, this technique gives much more information on the muscle activity than simple position-force measurements, it is considered rather invasive as the electrodes have to be attached to each human operator. Furthermore, most electromyogram-based approaches require precise positioning of the sensors on each human arm, extensive calibrations and advanced signal processing.

It was only recently in [95] and in [59] where first insights appear that the grip (or grasp) force correlates with the impedance of the human arm and, hence, might help estimate it. Consequently, the measurement of the grip force could aid the development of haptic applications. As the field is rather immature a few grip force sensing devices exist. In [95] and in [59] simple forcing elements and rotational load cells were used. Similar approach is used later on in this chapter where a simple force sensor is positioned at the handle of the HSI to measure the grip force. Commercially available devices exist, at a rather early stage, such as the Grip Force Sensing Glove in [164] consisting of multiple flexible force sensors. Empirically, the accuracy and repeatability of the device is criticized. Recently, e-skin concepts made their appearance either as acting or sensing elements able to replicate the human skin behavior [159, 46]. In [46] a pressure sensitive skin is presented, able to adapt to the geometry of the object attached can offer reliable contact measurements. Those devices are yet not commercially available.

5.1.3 Human arm impedance identification

In the following we treat with parametric human models and therefore discuss techniques that are used to identify the human arm impedance in human-robot interaction setting. The basis of the identification techniques discussed here are the works of Hogan, Flash, and Mussa-Ivaldi in [79, 114]. They study the elastic force field which is generated to restore the human arm when displaced from an equilibrium posture by an external disturbance. The stiffness computed from this elastic force is represented as an ellipse characterized by three parameters: magnitude (the area), shape (the ratio of axis) and orientation (direction of the major axis). This representation captures the main geometrical features of the elastic force field associated with posture. It is also found that the conservative components of this elastic force field are much larger than the non-conservative part and the behavior of the neuromuscular system of the multiarticular arm is predominantly spring-like. It is finally then also found, that the results are strongly dependent on the arm configuration.

A linear least squares regression algorithm is applied in [43] to identify this stiffness during maintained posture with the foremost goal of understanding, by further knowledge of the human arm mechanics, the reason for this variation. It is shown, that the spatial variations of the hand stiffness ellipses in the horizontal place could be explained by a covariation between the shoulder stiffness and the stiffness component provided by two-joint muscles. They also found out that these stiffness parameters remained invariant over time.

Tsuji *et al.* in [168] studied *damping* and *inertia* amongst stiffness parameters in multi-joint arm movements using the same identification approach. Their results are summarized as follows: (1) the estimated inertia matrices of the human hand well agrees with computed values using a two-joint arm model, (2) spatial variations of the stiffness ellipses are consistent with the experimental results of Muss-Ivaldi in [114], (3) hand stiffness and damping increase with the grip force of the subject, and (4) damping and stiffness ellipses tend to have similar orientation.

Consequently, we use the same approach of [168] and [114] to identify the human arm end-point impedance by maintaining the posture. Small external disturbances are applied to the human arm, as seen in Figure 5.1, and a least-squares regression algorithm is employed to identify the apparent impedance parameters.

5.2 The human grip force towards impedance estimation

5.2.1 Idea

The human grip force, as discussed, is first explored in the works of Kuchenbecker *et al.* who found a positive linear correlation between grip force and *wrist* impedance in [95] and by Husser and Cutkosky who found out in [59] that the hand damping is steadily increasing with increasing pinch grasp force using two fingers. Also Tsuji *et al.* indicated in [168] that the grasp of the handle increased their identified impedance values.

We therefore, here, acknowledge for this extra degree-of-freedom - the grip force - and study it with the foremost goal of finding a relationship between the grip force intensity and the end-point human arm impedance. From now, as grip force, the measured force in the palm of the human operator grasping the haptic handle is considered. In the following, we present how a possible relationship between the grip force and the arm impedance during maintained postured is identified. The findings will be later employed for the according adaptive control mechanisms.

5.2.2 Impedance identification during maintained posture and grasping

The human arm impedance characteristics are examined here, including inertia and damping as well as stiffness, in multi-joint arm movements. For our work, only the apparent end-point impedance will be exploited, therefore no joint impedance values will be considered. The following impedance model is assumed

$$M(t)\ddot{x}(t) + D(t)\dot{x}(t) + K(t)(x(t) - x_v(t)) = -f(t) \tag{5.1}$$

where $M(t)$, $D(t)$ and $K(t) \in \Re^{l \times l}$ represent the arm end-point inertia, damping and stiffness matrices, respectively. $x(t) \in \Re^l$ is the hand position vector, $x_v(t)$ represents a virtual equilibrium point, and $f(t) \in \Re^l$ is the *interaction force* (not to be confused with the grip force) measured by the force sensor of the haptic device. l is the dimensionality of the task space; in this work the impedance was investigated in a planar setting, hence $l = 2$,
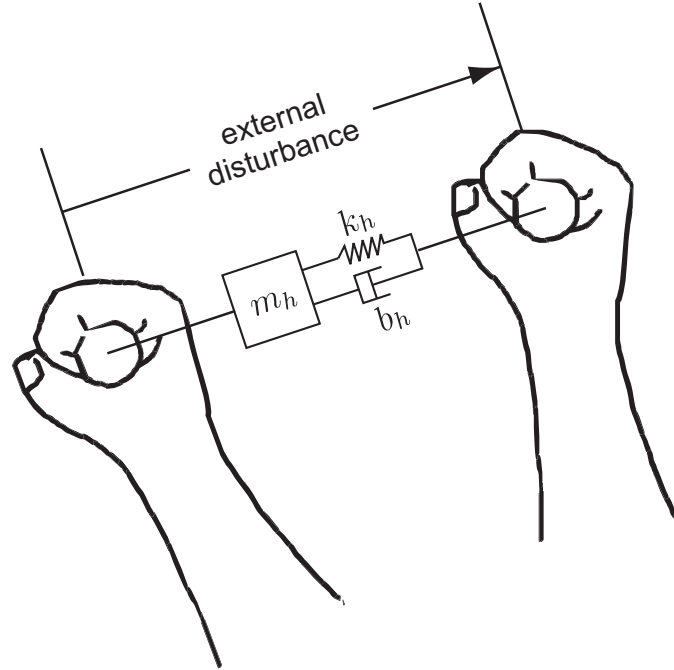
Fig. 5.1: Description of arm impedance. Adopted from [168]. If the human arm is externally disturbed it displays an impedance similar to that of a mechanical mass-spring-damper system.

the impedance model can be, however, straightforwardly extended to more dimensions. The impedance parameters can be joined in a parameter matrix $\mathbf{P} = [M \quad D \quad K]$.

The grip force $f_g(t) \in \Re$ of the human operator grasping the handle of the HSI is measured from a simple self-constructed device using one sensor element in the force range of 0-110 N, see Figure 5.2. For more technical details the reader is referred to Appendix A.3. The human operator grasps the haptic device handle in such a way that the force sensing element and the aluminum bar on top of it is in contact with the intermediate phalanges (middle area) of the index, middle and ring finger. Goal of the study is to investigate potential relationship between this grasping force $f_g(t)$ and the parameter matrix $\mathbf{P}$ when a posture is maintained in a planar setting, in other words the existence of a mapping function

$$h : f_g \rightarrow \mathbf{P}. \tag{5.2}$$

For this reason a pilot study is conducted using the methodology described below to identify - if any - the existence of such a mapping function.

Impedance identification method

While a subject maintains a given hand location and posture, small external disturbances are applied to his arm by a manipulandum in order to estimate the its impedance, see Figure 5.1. A force is generated to restore the arm to its original position and the corresponding force-displacement vectors are measured and sampled over time in order to estimate the arm impedance by means of a second-order linear model. A small size of the disturbance is necessary in order to assume the approximate constancy of M, D and K,

Fig. 5.2: Prototype of the grip force sensing device using one force sensor.

which are known to depend on posture only in a smooth way. The short duration of the disturbance is demanded by the need to avoid a variation of the virtual equilibrium point x_v during the measurement due to voluntary neural feedback. As a result, the arm inertia, damping, stiffness and the virtual equilibrium point are assumed to be constant after the onset of the disturbance. It is then possible to assume constancy of the second-order, linear impedance model of the arm dynamics for small motions around an equilibrium posture.

Since the equation is linear, the estimation problem can be solved by means of the standard least square procedure. At each set of displacement and force vectors the parameters of the impedance matrices is estimated by linear squares regression algorithm applied to the following equation

$$-f(t) = K\Delta x(t) + D\dot{x}(t) + M\ddot{x}(t) \tag{5.3}$$

where $f = [f_{x_1}, f_{x_2}]^T$, $\Delta x = [\Delta x_1, \Delta x_2]^T$, $\ddot{x} = [\ddot{x}_1, \ddot{x}_2]^T$. Only 6 parameters are each time estimated as the displacements are either only along the horizontal x_1 or only along the vertical x_2 axes keeping the other component each time at zero. The linear regression algorithm is applied independently to the two equations and no restriction (constrain) is used. The system is overdetermined as the mass, damping and stiffness matrices are considered constant.

Arm impedance representation

As a result an estimated $\hat{\mathbf{P}} = [\hat{M} \quad \hat{D} \quad \hat{K}]$ matrix is acquired. The identified matrices represent the relationship between a force vector and a displacement vector or one of its time derivatives, and are thus descriptive of force fields. Each two-dimensional impedance

(a)

(b)
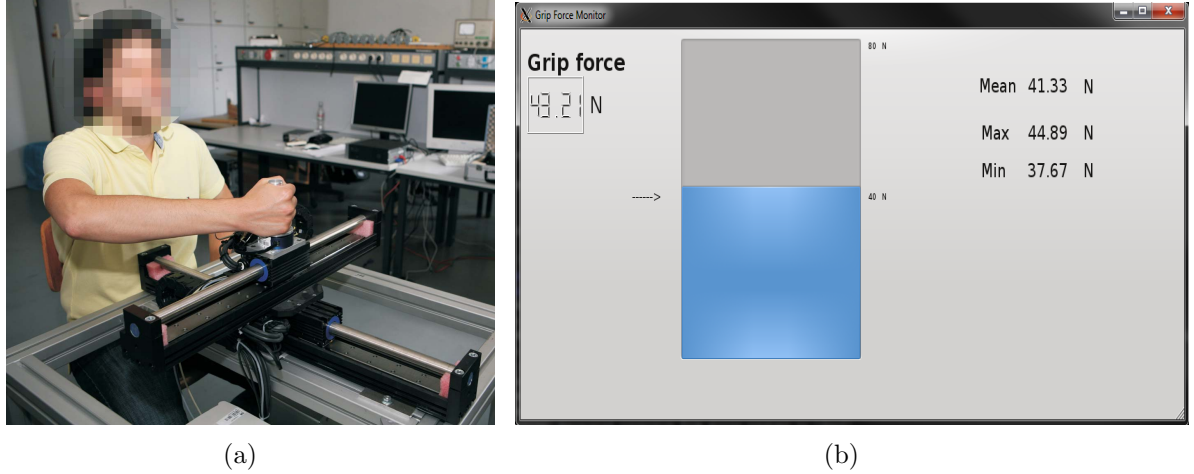
Fig. 5.3: (a) The subject grasping the manipulator. (b) The visual feedback the subjects were provided. They were instructed to use their grip force intensity to control the progress bar as closely as possible to the instructed value. At the end of the experiment, mean, minimum and maximum values were provided.

matrix may be written generally as

$$Z = \left[\begin{array}{cc} Z_{11} & Z_{12} \\ Z_{21} & Z_{22} \end{array} \right],$$

and may be decomposed into symmetric, Z_s, and antisymmetric, Z_a, parts

$$Z_s = \frac{1}{2}(Z + Z^T), \tag{5.4}$$

$$Z_a = \frac{1}{2}(Z - Z^T). \tag{5.5}$$

A concise graphical means of representing the symmetric component of such a matrix is as an ellipse whose contour is the locus of force vectors produced by rotating a fixed-length displacement vector (or one of its derivatives, for the dynamic impedance components) about the origin [79, 34]. Such an ellipse is characterized by size, shape, and orientation. The size is proportional to the determinant, the shape is given by the ratio of the larger to the smaller eigenvalue, and the orientation by the angle made by the principal eigenvector with the x_1-axis. The following equations transform the elements of the symmetric two-dimensional matrix [34]

$$Z_s = \left[\begin{array}{cc} s_1 & s_2 \\ s_2 & s_3 \end{array} \right], \tag{5.6}$$

into size, shape and orientation values

$$\lambda_{2,1} = \frac{1}{2}[(s_1 + s_3) \pm \sqrt{(s_1 + s_3)^2 + 4(s_2^2 - s_1 s_3)}], \tag{5.7}$$

$$A = \pi \lambda_1 \lambda_2, \tag{5.8}$$

$$R = \frac{\lambda_2}{\lambda_1}, \tag{5.9}$$

$$\theta = tan^{-1}\frac{\lambda_2 - s_1}{s_2} = tan^{-1}\frac{s_2}{\lambda_2 - s_3}, \tag{5.10}$$

where λ_i are the eigenvalues ($\lambda_2 \geq \lambda_1$), and A, R, and θ are the size (area), shape (aspect ratio), and orientation values, respectively.

Participants

5 male subjects participated in the experiment (mean age = 27.8 years, std. deviation = 2.05 years), all of whom were right-handed and naive to the purpose of the experiment and the experimental setup.

Apparatus

To measure the impedance parameter of the human arm manipulating a planar manipulandum a 2-DoF linear device is used as experimental testbed. The handle is equipped with the grip force sensing handle of Appendix A.3 and is able to measure forces up to 110 N with 1% accuracy. Both actuators are tubular linear motors, one Thrusttube 2504 and one 2510 both from Copley Controls Corp.. The linear devices were placed in a cross-configuration with the motor able to display the highest torque on the lower part. The device was equipped with a JR3 6-DoF force sensor to measure the applied arm interaction - and not grip - forces. The device is able to display 312 N of peak force in the direction of movement of the upper motor and 780 N in the direction of movement of the lower one. Both motors were connected to a digital servo drive Xenus XTL, also from Copley Controls Corp.. The digital servo operated in current control; thus, we can consider the signal input to be approximately proportional to the applied motor force. The position was measured by an optical incremental encoder with a precision of $1\mu m$. The entire haptic interface was controlled by a PC running a real-time Linux operating system. The digital servo was connected to the PC through a Sensoray I/O card. The overall haptic device was controlled by a high-gain position controller which compensated for viscous and Coulomb friction as well as for external forces. The sampling rate of the haptic signals and the local control loops was 1 kHz.

Experimental design

The subjects took a seat in front of the robot and were instructed to grasp a planar robot manipulandum with a specified pre-instructed grip force level, see Figure 5.3(a). Five different grip force levels $f_g \in \{10, 20, 40, 60, 80\}$ were given in random order as an instruction. A monitor was used to indicate the current grip force of the user using a progress bar and an arithmetic indication, see Figure 5.3(b). Each trial was repeated if the human subject failed to keep the indicated grip force approximately constant. Particularly, the mean value $\mu_{f_g(t)}$ and the standard deviation $\sigma_{f_g(t)}$ of the grip force were computed after each trial and displayed on the screen. If they exceeded the predefined tolerance thresholds the experiment was repeated. Particularly the mean and standard deviation
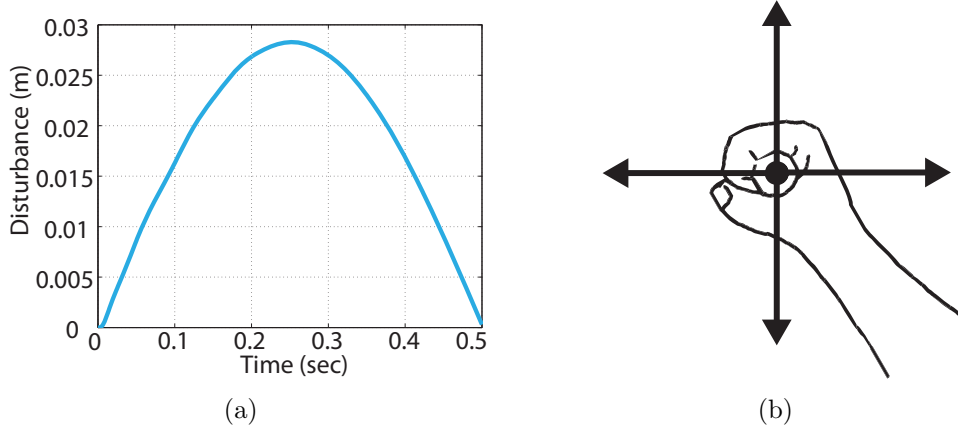
Fig. 5.4: (a) A disturbance profile with a 500 ms duration and an RMS value of 20mm. It is applied at a random time to the constant position held by the subject. (b) The direction along which disturbances randomly occurred. The relative angle of the arm to the axis is $45°$.

should not exceed more than 20% the instructed grip force level.

The robot was positioned at the starting position using a feedback control law. The subject was asked to keep his hand at the initial position. An external disturbance was then applied to his hand by the robot, see Figure 5.4(a) for a profile of the disturbance pattern. The disturbance had an amplitude of about 15 mm and returned to the initial position in about 500 ms. This should eliminate any significant influence of voluntary responses of the subject on the measurements performed. Moreover, in order to avoid prediction by the subject, the time onset of the disturbance and its direction (among four possible ones, see Figure 5.4(b)) were chosen in random way. For each disturbance direction 5 repetition were required resulting in a $5 \times 4 = 20$ set of trials for each grip force level. The hand displacements $dx(t)$, the acceleration $\ddot{x}(t)$ and hand force $dF(t)$ were recorded. The derivative of the hand displacement $\dot{x}(t)$ was used as an estimation of the velocity. The arm impedance parameters, M, D, K, were estimated for a set of data corresponding to four disturbances with different directions. Mean values and standard deviations of the parameters of the arm impedance for the data sets (each trial) were used in the following analysis.

Evaluation

In [79, 114] it is shown that for a stiffness matrix acquired from a human impedance identification experiment during maintained posture only the conservative part of the matrix is largely predominant and therefore the symmetrical part of the stiffness matrix was calculated, as described in (5.4), and illustrated as an ellipse. Later, in [168] it is found, that similar to the stiffness matrix, the estimated inertia $\hat{M}$ and damping $\hat{D}$ matrices display also similar behavior. The conservative parts of the matrices are much larger than the non-conservative ones, and therefore only the symmetrical part is considered.

This rationale is considered also in the evaluation of our pilot study. Hence, the area (size), shape, and orientation of each impedance ellipse is computed after each set of 20

trials for each grip force level.

Results

The mean of the conservative part of each estimated impedance parameter matrix, i.e. $\hat{M}$, $\hat{D}$ and $\hat{K}$, is first computed for each grip level over all 20 repetitions. The size (area) of each ellipse can then be computed for each subject, and Figure 5.5 summarizes the findings of the pilot study by illustrating the mean size of the ellipse, together with the standard deviation for each impedance parameter at each grip force level. Figure 5.6 exemplarily shows the results in ellipse size for one random subject.

The results of the study are summarized in the following:

- The most important finding is that *the size of the damping ellipses significantly increases with increasing grip force*, see Figure 5.5(b). It is also observed, that the relationship is very close to linear. This knowledge can lead to significant performance increase as will be discussed in Section 5.3.

- The stiffness ellipse size did not *significantly* increase, see Figure 5.5(c). Although further insight is needed on that, this fact might be explained by the predefined specified human arm maintained posture we used in our experiment, see Figure 5.4(b). To no surprise, this result is aligned to the findings in [168], where the hand stiffness with and without grasping of the manipulandum is compared in an experiment with many maintained postures. It is observed, that in the same posture used in our experiments, no significant increase of the stiffness ellipse occurred as well, although the stiffness did significantly increase at other postures. However, that experiment used a molded plastic cast to fix the wrist and this result cannot straightforwardly be compared with our setting; future investigation with multiple postures should evaluate that.

- Finally, the inertia ellipse in our experiment, decreases with increasing grip force intensity, see Figure 5.5(a). Without any further insight, it is assumed that this behavior is a result of the more rigid contact that the human arm establishes when grasping the handle of the device tighter, which in turns reduces the apparent inertia. The study in [95], assumes the apparent inertia to be independent of the grip force and identifies one single value which is then used throughout all identification experiments. However, a more extensive study should further consider whether this leads to better impedance identification.

In Figure 5.5(d) the corresponding grip force levels are indicated for all subjects over all trials. Trials that exceeded the predefined thresholds were excluded from the study, and the trial was repeated. Therefore, the mean grip force of the subjects was very close to the instructed values, without any statistically significant overlap.

5.2.3 Discussion

The main result of this part is that the human arm end-point damping, in a second-order mechanical impedance model, highly correlates - almost linear - with the grip force. This
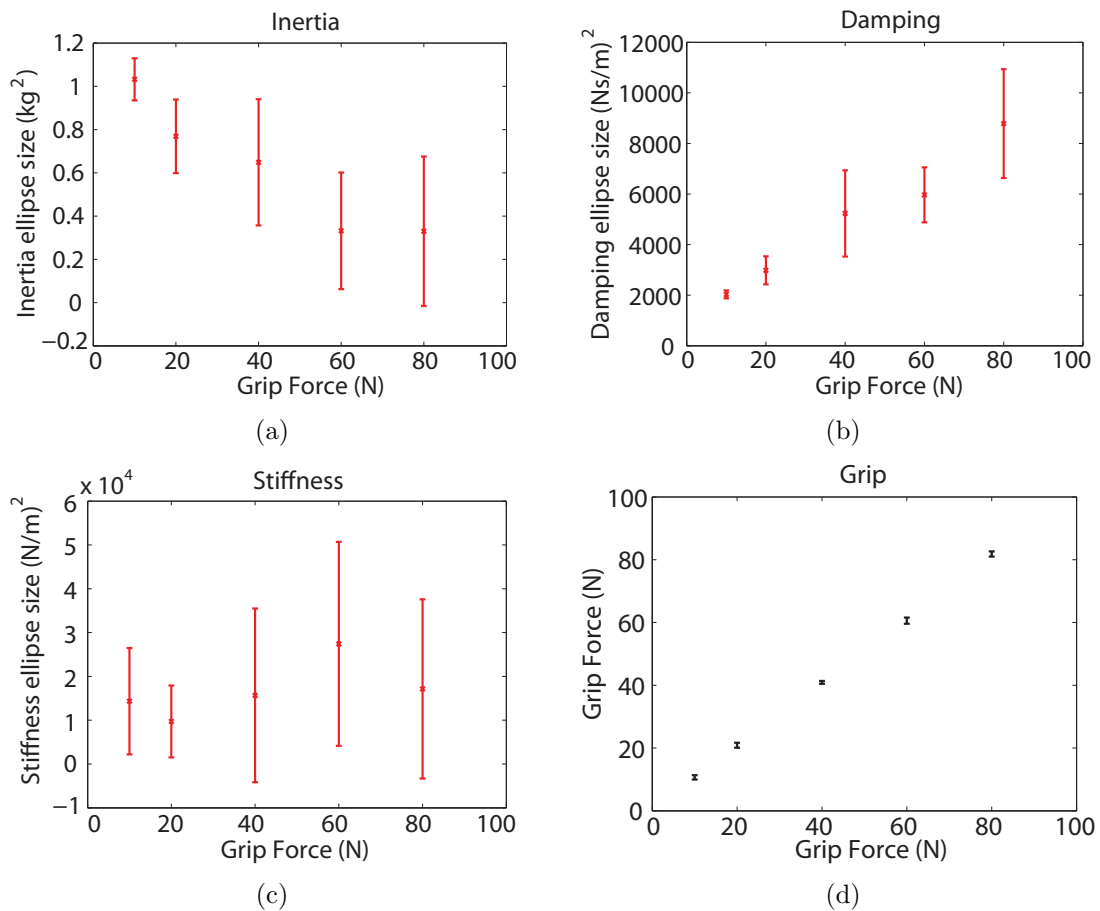
Fig. 5.5: The size of the impedance parameters ellipses for 5 different grip force levels. (a) The inertia ellipse size did not have a statistically significant change with increasing grip force. (b) The size of the damping ellipses is increasing, almost linearly, with the grip force level. This is an important finding which can be used at the controller design. (c) The size of the stiffness ellipse remained almost constant, indicating that the stiffness is eventually more influenced by the maintained pose rather than the maintained grip force. (d) The grip force intensity (mean and standard variation) of the subjects at the moment of the disturbance.

(a)

(b)

(c)
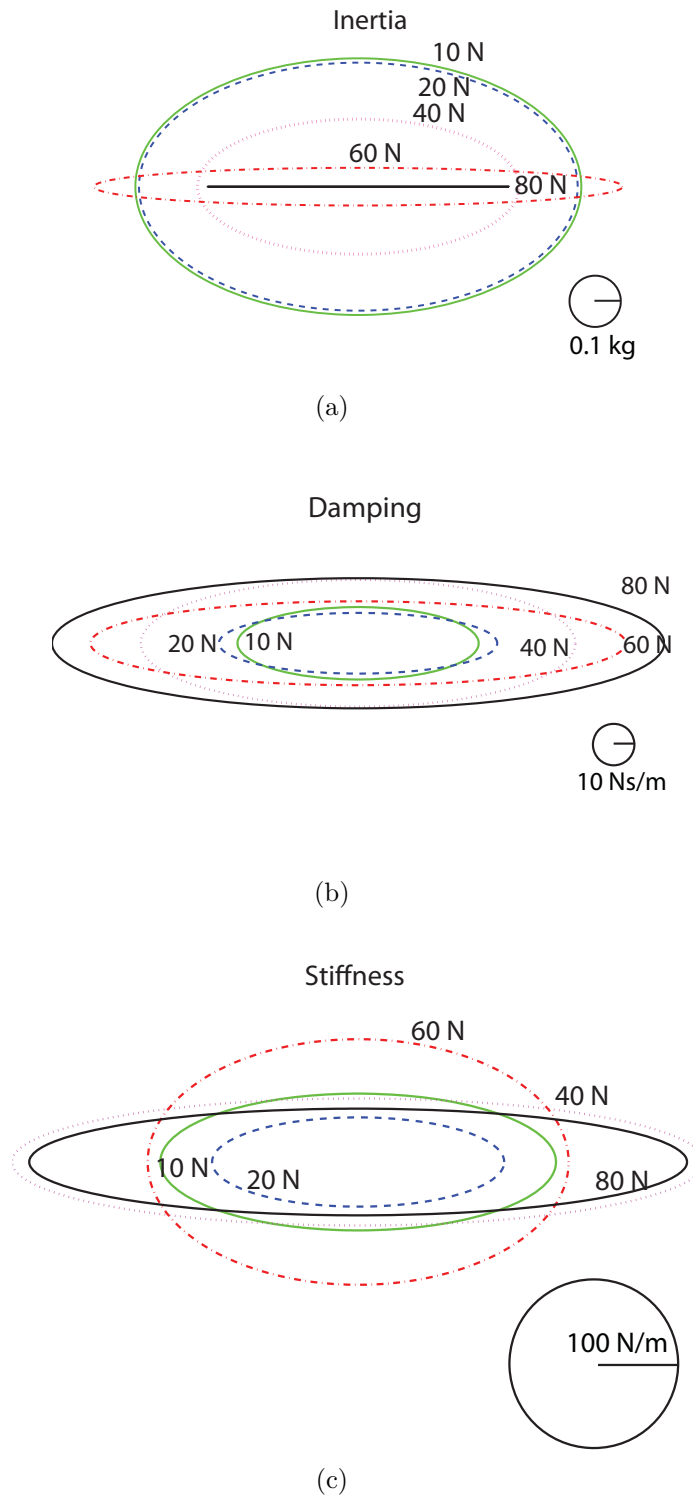
Fig. 5.6: The identified ellipses for the five grip force levels, 10, 20, 40, 60 and 80 N for a randomly chosen subject (No. 4). (a) The inertia ellipse size reduces with increasing grip force. (b) The damping increases for increasing grip force. Note however that no significant change occurred between 10 and 20 N grip. (c) Strange pattern for the stiffness ellipse size as it is for small grip forces decreasing, but higher grip forces lead to higher arm stiffness. Note that the non-elastic forces were ignored for all identified parameters, hence the ellipses cannot rotate. However, note that the principal axis in *all* ellipses over all parameters is always horizontally aligned due to the specific maintained posture that this experiment had. This agrees with the findings in [168].

result, for the time being, holds only for a planar environment at the given maintained posture. We hope that our pilot study, can further inspire studies from physiologists to provide solid results to be used from control engineers.

The pilot study poses several challenges. Despite the similarities with previous approaches, the presented one differs from what has been known so far and comparison with published results should be done with care. Particularly, in the study in [168] the wrist and the hand were fixed by a molded plastic cast tightly attached to the robot handle for the purpose of the experiment. In the present study, focusing on the effect of the grip force intensity in the overall apparent human arm impedance, the wrist was allowed to move freely and users were just instructed to keep it at the beginning of the experiment aligned with the forearm. Moreover, results are expected to be task- and device-dependent; the latter plays an important role in the identification process. Gomi *et al.* in [49] came up with five important factors for a reliable human arm stiffness measurement in *dynamic* environments. In detail, stiffness measurement invokes application of external forces to the arm by a manipulandum and measurement of the resulting trajectory perturbations. If the perturbation is too strong or the manipulandum is too heavy, the subject cannot complete natural movements, and arm stiffness increases to prevent failure. On the other hand, if the perturbation is too small, a reliable estimate cannot be obtained. The manipulandum needs to be (1) fast and light enough to minimize movement interference, while also being (2) strong enough to transmit large forces, and (3) rigid enough to be controlled at high frequencies. It is also necessary to (4) support the human arm on a horizontal plane to be free from the force of gravity and to reduce fatigue. Additionally, (5) nonlinear forces due to manipulandum dynamics should be reduced so as not to disturb the arm movements. Our high-fidelity equipment is assumed to satisfy almost all requirements, being able to be fast, display high forces, and approximating a linear behavior (physically and through friction compensation). On the other hand, it is a large and heavy device and it would be interesting to evaluate the results also with a lightweight impedance-type device.

5.3 Benefits of increased human arm damping and its online estimation

In the following, four distinct applications areas where the previous findings can be beneficial are discussed together with an illustration of the approach benefits. Direct thoughts towards a human-centered control design for teleoperation systems are also given.

5.3.1 Human-centered adaptive control

It is well known that in the presence of even small communication delay, a bilateral controller may become unstable. To increase the stability robustness, artificial damping can be added to the master controller to absorb the energy that is generated by the non-passive communication channel. As a result the control action consists not only of the delayed force-feedback but an extra damping term $f_{vd} = f_e e^{-sT_d} + b_d \dot{x}_h$ where b_d represents the constant damping of the HSI device. Although, this damping term provides stability in

practice it creates a mushy feeling for the operator. It is therefore desirable to keep it as low as possible, as often as possible.

Furthermore, as discussed in Chapter 3, the human arm damping contributes together with the device inherent damping to the stabilization of the overall haptic system. It is hence expected that a high human arm damping will stabilize the system and a lower one will put stability at risk. Actually, variable damping has been proposed to guarantee stability during contact actions in [102, 141, 36]. Although these methodologies are primarily stability-based designs, they do not include the operator's dynamics in their adjustment schemes. A loose grasping, to use the grip force framework, can result in a system more vulnerable to instability than a firm grasp. On the other hand, the use of a conservative and excessive choice for the damping, as discussed above, will affect the realism of the haptic interaction.

The work of Mobasser and Hashtrudi-Zaad in [110] builds upon this principle based on their impedance identification work in [111] and proposes a variable damping teleoperation controller. It adjusts the master artificial damping based on the arm *online identified* natural damping to maintain a constant level of total damping. Practically this means, that when the human arm impedance, mainly the arm damping, reduces, additional damping is injected by the controller preserving the stability of the haptic system. When the human operator grasps the device firmly, with a higher effective damping, the extra damping is removed. Mobasser *et al.* manage to estimate the human arm impedance using 4 EMG signals. However, they require user-specific training of their classifiers plus extensive calibration and positioning of the EMG sensors. Our approach can avoid that, with the use of an grip-force-based damping estimation. Moreover, their work, and their identification technique is only appropriate for a 1-DoF system. The following example illustrates this adaptive approach.

Example 5.1 (Variable damping controller)
In this simulation study the effect of the human arm damping as a stabilizing factor is demonstrated for a basic haptic telepresence control architecture. A system with 1-DoF is considered and velocity is commanded from the HSI to the TO, the sensed environmental force is fed back to be displayed by the HSI. The time delay is 15 ms in both channels. The human operator applies a sinusoidal force with amplitude of 3 N and frequency 2 rad/s on the HSI. The HSI is simulated as an inertial device of 1 kg. By local control a damping b_m can be injected. The TO is second-order system with mass 1 kg and damping 5 Ns/m and is controlled by a proportional-integral controller with the P-gain 300 Ns/m and the I-gain 4000 N/m. The environment is represented by a spring with constant 100 N/m.

The results are illustrated in Figure 5.7. In Figure 5.7(a) we observe a stable contact resulting from the firm grasp of the human, i.e. $b_h = 50 Ns/m$. Instability occurs when the human arm damping is reduced in Figure 5.7(b). If the reduction of the human arm damping is quickly recognized, e.g. with a grip force estimator, extra damping can be injected to stabilize the system as shown in Figure 5.7(c). Hence, stability is achieved without over-conservatism; the extra injected damping that might influence the haptic rendering is removed as long as the human operator grasps the haptic device firmly again and it is not used at all times.
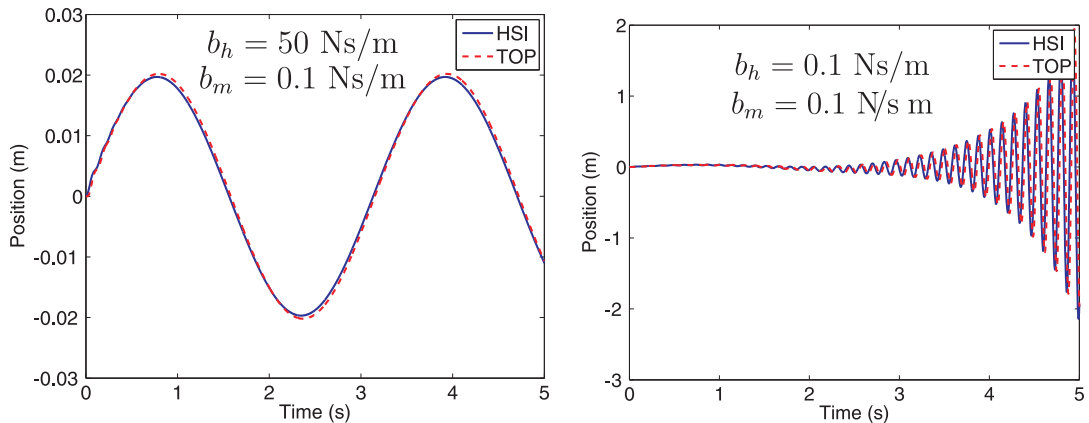
(a) Tight grasp guarantees a stable contact.

(b) Loose grasp, namely low human arm damping, destabilizes the system.
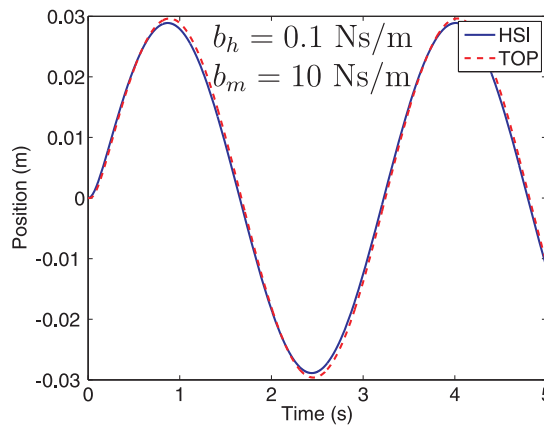
(c) Fast recognition of the lower human arm damping injects extra damping to stabilize it again.

Fig. 5.7: Simulation of a haptic teleoperation system in contact with a virtual environment represented by a spring with 100 N/m spring constant. (a) A firm human grasp ($b_h = 50Ns/m$) maintains a stable contact. (b) A loose grasp ($b_h = 0.1Ns/m$) makes the system unstable. (c) A variable damping of $10Ns/m$ is added at the moment of the loose grasp and the system remains stable.
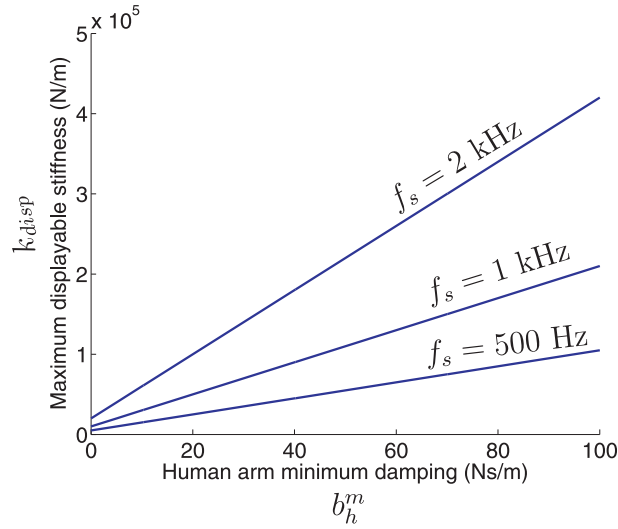
Fig. 5.8: The maximum displayed stiffness increases with the lower human arm damping. This can lead to either more stable systems or lowest required sampling frequency, thus data reduction and efficiency in networked systems.

5.3.2 Higher fidelity in haptic rendering

The role of friction in haptic devices was early recognized as important in [48] as it plays a key role in dissipating surplus energy to maintain passivity of the haptic system when a haptic environment is rendered. It is also well known that the maximum achievable stiffness of a haptic system varies widely, mainly depending on sampling rate, quantization error, computational delay and amplifier dynamics [33]. Woo and Lee in [176] however, show that the effective viscous coefficient depends on the degree of human arm impedance as well as the physical friction, as the human stiffness and damping is applied in conjunction with the device parameters [33]. This implies, as also seen in Chapter 3, that the energy generated in a haptic system can be also dissipated by the human damping as well.

Particularly, they show that a necessary and sufficient condition for the maximum virtual wall stiffness displayable under the passivity setting is

$$k_{disp} \leq \frac{2(b_h^m + b_d)}{T_s}. \tag{5.11}$$

where b_h^m the minimum damping coefficient of the human arm, b_d the device damping and T_s the sampling time. This is a very important finding, highlighting that approximate knowledge of the human arm damping can lead to large benefits in haptic rendering, either higher displayed stiffness or relaxed requirements on the sampling frequency can be achieved. The relationship (5.11) is illustrated in Figure 5.8 indicating how a higher lower bound of human damping will allow for either higher stiffness for the same sampling rate, or lower required sampling frequency for the same amount of maximum displayable stiffness.
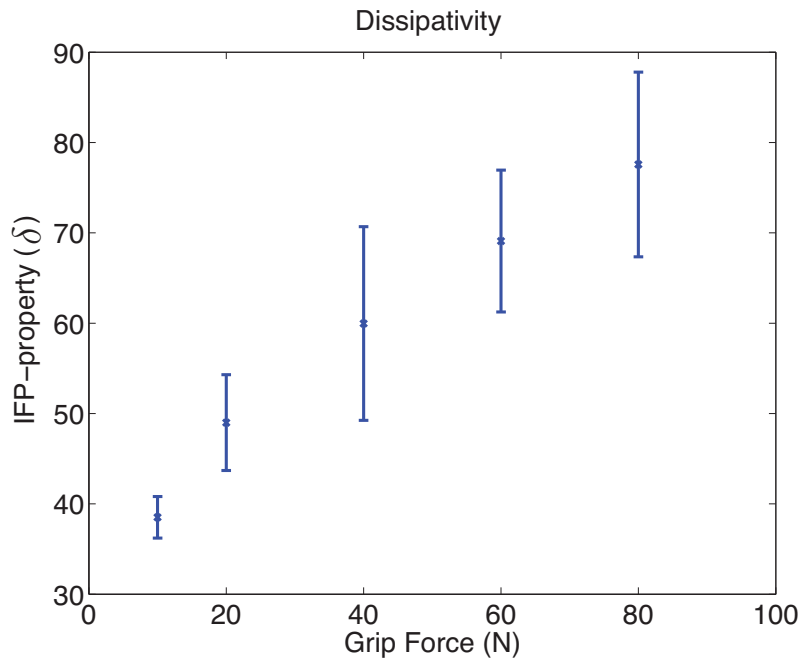
Fig. 5.9: Means and standard deviation of the IFP(δ) parameter of the human arm for the 5 subjects that participated in the pilot study. An almost linear correlation of the grip force intensity and the parameter δ is observed. Extending this result might lead to fast and reliable dissipativity estimation without requiring the direct energy observation or the online solution of complex and processing power consuming optimization problems.

5.3.3 Estimating dissipative properties of human arm online

Chapter 3 dealt with the exploitation of dissipative energetic characteristics of different subsystems of the teleoperation architecture in order to guarantee stability and improve the transparency in haptic telepresence systems. For the human, in most cases and as shown in Section 3.1.3, the (Q, S, R)-dissipative parameters are assumed to be acquired offline, either by estimating lower damping bounds in simple IF-OFP systems or by solving LMIs such that the (Q, S, R)-dissipative inequality (2.3.9) is satisfied; for more details on solving the LMIs see [105].

To avoid the use of energy observers and the process-power consuming online solution of LMIs, but also to study the dissipative characteristics of the human arm from the data collected in the pilot study conducted for this chapter, Figure 5.9 illustrates the IFP(δ) property for the human arm considering the velocity/force as input/output pair. It is observed that for all grip forces the human arm of the subjects showed an apparent dissipative behavior which increased, almost linearly, with increasing grip force intensity. This indicates larger energy dissipation for larger grip forces, and consequently the grip force measurement can be utilized, in particular applications, as a good online dissipativity-estimator.

5.3.4 Transparency improvements in telepresence with communication unreliabilities

The benefit of an increased damping for a system with communication unreliabilities is sketched analytically in Chapter 3 and the corresponding transparency analysis is shown in Section 3.4. The identification of the human damping lower bound is important as higher values might lead to significant performance improvement. However, only static lower bounds were discussed. In fact, an online estimation of the human arm damping can further improve the transparency of the system; this would require dynamic transformations based on the online estimation of the damping/energetic behavior. The synchronization of both sides of the generalized scattering transformation poses significant challenges, so from a first point of view the generalized scattering transformation control scheme can only hope on minor or no benefit from an approximation of the lower damping of the human arm online.

Looking closer though, one can expect performance benefits in the generalized scattering transformation schema as well. Taken for granted that the grip force will give an approximate estimate of the human arm damping one could avoid over-conservative choices of the lower damping bound by injecting extra damping when needed, as done in Section 5.3.1, which in turn can increase the transparency of the overall haptic telepresence system. The following example illustrates these cases.

Example 5.2 (Variable damping controller for the GST architecture)
Assume a haptic interaction session with a stiff environment (spring constant 300 N/m) displayed over a delayed channel (50 ms in each direction) through the generalized scattering transformation architecture of Chapter 3. The haptic sessions employs firm grasp of the human with the HSI at the 90% of the session time and loose grasp at the rest 10%. Without fast human damping estimation the loose grasp leads to an overconservative choice based on this 10% of the time which the human maintained a loose grasp of the haptic device and consequently had a low damping. The dissipativity of the lefthandside architecture is thus selected as $\epsilon_l = 0$ resulting in an overconservative choice of $\theta = 45°$, namely the scattering transformation. The displayed stiffness, computed by the least squares stiffness estimate of the mechanical impedance in (3.24), is in this case 31.83 N/m. Alternatively, it can be computed (with an Pade-approximation induced error) by (3.28). Considering now, that the lefthand side is a dissipative system where the energy dissipating damping term is always preserved at a high level, e.g. $\epsilon_l = 30$, and further assuming a fast identification of the loose grasp and injection of the extra missing damping as in Section 5.3.1 takes place, allows for a broader range of transformation angles in $[2°, 45°]$ instead of just $\theta = 45°$. Choosing $\theta = 10°$ results in a displayed stiffness of 172.71 N/m, pointing out that a fast recognition of human damping and a non worst-case choice of transformation angle with the help of a variable damping controller can lead to significant control performance increase at the expense of damping injection in a small period of time.

5.4 Open problems - Vistas

Acquiring knowledge of the human dynamics or the human energetic behavior and using it for adaptive control actions is only one step towards what we envision as human-centered control design. A range of improvements that were sketched out in the previous sections give further insight for the direction that a future research can take on that. Aside from the implementation-specific issues of the grip force sensing impedance estimator a number of problems remain still open and further research should concentrate on them.

- First of all, it should be pointed out that a simple linear time-invariant parametric model is considered in our study. To treat with dexterous human arm movements, in a 6-dimensional space, more complicated human arm impedance models have to be employed in the future and the studies should be elaborated to more complex environments than just a planar setting.

- A major point in the presented study is that only static grip forces are employed, as users were instructed to preserve a constant grip force. Furthermore, the human arm dynamics were also considered constant, even in the parametric model. Therefore, further research should point out whether the human grip dynamics correlate with the human arm ones in a *dynamic* setting. Practically, there is an imperative need for better tools to identify the human arm characteristics dynamically, up to now studies on stiffness during human arm movements have been made [49, 163, 34, 50].

- The lower bound of the damping term is, unfortunately, through a single grip force measurement not guaranteed. Hence, the control strategies should take that into consideration. Up to now, no robust controller has been proposed in this setting. Interesting enough, are also Markov-based approaches which can use the grip force as a classification future for specific *behavioral* states of the human arm. Stochastic exponential stability of the overall system could then be studied.

- Human-centered knowledge acquired online will definitely lead to adaptive control actions. From a human-centered point of view, adaptive controllers are not a panacea. Quite a few studies, e.g. in [134], exist on the transparency of adaptive control actions, particularly when this affects the displayed dynamics to the human. User studies to evaluate up to which point are time-varying displayed dynamics desired to increase the task performance are necessary.

- Finally, a general control theoretic formulation of the grip-force-based haptic system in terms of stability, reachability and detectability will build the fundamental for future research.

5.5 Discussion

The human operator grip force is a significant degree of freedom neglected so far in haptic rendering or teleoperation settings. The system presented in this chapter utilizes this

information to provide an innovative haptic teleoperation system that is affected by the human and adapted correspondingly online. The approach hopefully paves the way for other human-centered control designs for haptic systems.

Particularly, a pilot study is conducted to identify possible correlation between the human operator grip force and the human arm impedance. Results from a user study in a planar experiment with maintained arm posture, interestingly enough, indicate some linear correlation of the grip force with the effective end-point human arm viscosity (damping) and furthermore with the human arm dissipativity. Taken that, adaptive control schemes could be given and directions on how this knowledge of human arm dynamics, acquired in a fast way, can lead to better performing controllers are sketched. Actually, a variable damping controller which observes the human arm apparent damping is given. By injecting damping only when needed, stability can be guaranteed, even e.g. when the human does not touch a high-tuned system; transparency can also be improved. The idea is further transferable to time-delayed telepresence systems as the one studied in Chapter 3, an example is provided. Furthermore, along with previous research findings, we illustrate how the knowledge of the minimum human arm damping can lead to lower required sampling rate, thus, haptic data reduction.

Finally, open problems are discussed and, based on the promising results, future research directions are given, mainly in a two-fold way: First, knowledge of the dexterous human dynamics should be further incorporated online on the control schemes, and secondly, control schemes should allow for further adaptability, i.e. dynamic transformations. A better control-theoretic formulation is also required to extend the usage of the approach.

6 Conclusions and future directions

6.1 Concluding remarks

The focus of this dissertation is on *human-centered* control design for haptic telepresence systems over communication networks. Conceptually unique is the consideration of the human as the common reference point throughout the whole design process, i.e. i) at bilateral controller that will guarantee a safe and stable interaction, ii) at the data reduction algorithms for efficient network resources usage, and iii) at the appropriate techniques that will augment the system to improve its realism. The main approaches along with the major result are highlighted in the following.

What makes haptic telepresence systems so unique is that a control loop is closed over two highly uncertain and unpredictable systems, the human operator and the environment. Moreover, all data is transmitted over a communication network which is known to influence networked control systems and their stability. In order to achieve stability, the control community came up with a broad range of controller schemes, the most important thereof, being approaches that could guarantee stability for an almost unknown human operator and in an almost unknown and unexplored environment. Avoiding the exact modeling of the human operator is the key aspect, as most approaches that tried to use an exact dynamical model failed to be employed in haptic telepresence scenarios with relatively different human dynamics. This, however, led to an over-conservative, in terms of control performance, passivity-based design. Chapter 3 aims to circumvent exactly this problem. Equipped with the background knowledge of Chapter 2 a new control design approach is given for haptic telepresence system based on *only approximate knowledge* of the human operator, the environment, or the controlled robotic manipulators. The theory of (Q, S, R)-dissipative systems is employed to avoid exact modeling of the subsystems. Only input-output properties of the involved subsystems is required. Any further knowledge available can, however, easily get integrated in the design. The whole design approach is also modular, fulfilling thus the requirement of studying each subsystem independently. To circumvent the challenges posed by communication unreliabilities, such as time delay and packet loss, the generalized scattering transformation, which applies to (Q, S, R)-dissipative systems, is employed. As a result *finite gain $\mathcal{L}_2$-stability* can be deduced and a small gain condition is satisfied in the communication network. Additionally, a transparency analysis of the proposed approach shows *improved performance*, in terms of displayed mechanical properties, compared to the standard scattering transformation, highlighting the impact that the presented approach can have in the overall field of the passivity-based designs that dominated the control-theory the last years.

The role of the human operator, is early acknowledged in this thesis. However, from the engineering point of view, it is usually assumed that this knowledge, whether of its perceptual system or its physiology is existent or acquired offline. Chapter 5 goes beyond

that and proposes an innovative way of acquiring knowledge of the human arm dynamics simply and quickly. The main idea is here, that the human arm end-point impedance correlates with the grip force intensity. The more firm or tight the human grasps the human system interface, the higher the arm impedance or some parameters thereof. This knowledge could be exploited as a fast estimator of the human arm impedance. A pilot study is conducted, and a second-order model of the human arm impedance is estimated for 5 different grip force levels in a planar manipulator and by maintaining a constant posture. Interestingly enough, the damping of the human arm increases almost linearly with the grip force intensity. Without any further measures and using cheap and reliable sensing one has a coarse estimation of the damping that could be beneficial in both haptic telepresence or haptic rendering scenarios; some of them are demonstrated.

Finally, not only human motor skills are in this work incorporated. The human haptic perception is also considered in the global control loop. First of all, performance is in all phases of the thesis measured in a perception-oriented manner. The use of metrics such as transparency, or the degree thereof, validate this and focus is mainly given at distortions that may degrade the human feeling of presence. Psychophysical studies validate the performance of the controllers in many phases to further enhance this. Besides that, in Chapter 4 the perceptual characteristics of the human operator further inspire and influence the system design. Particularly, the communication network is studied. Fact is, that the controllers will require high sampling rate and rapid data transmission to perform as best as possible. This can lead to severe problems in the network. Network congestion, from the thousands of packets triggered per second, is only one. High bandwidth requirements, especially in application areas where broad bandwidth is very expensive or even unavailable (e.g. underwater, wireless/space), is another. A range of *haptic data reduction techniques*, applicable in different scenarios, is proposed in Chapter 4. All share the same perception-inspired idea, the deadband approach. Deadband is applied in time-delayed systems, in systems with multiple degrees of freedom, and even further extended, i.e. adaptive deadband-based reduction. Psychophysical studies were conducted to validate the approach.

In summary, the ideas, concepts and approaches developed here significantly advance the state-of-the-art in haptic telepresence system and pave the way to more human-centric schemes. Moreover, the generic methodology applied overcomes the haptic community and is hoped that this work is transferable and will inspire research in other disciplines as well.

6.2 Outlook

Haptic telepresence system have the ultimate goal of true immersion in the remote/scaled side. Further research should close the gap between the theory and praxis and enable humans to solve challenging real-world problems better, faster and safer. The human-centered control design presented in this thesis further elaborates the developments in this area towards an absolute transparent but also stable system. It considers current challenges and state-of-the-art methods and introduces new dimensions with the dissipativity-based framework. There is a number of exciting research directions directly emerging from this results that could be considered in the future, some are:

Multiple-inputs-multiple-outputs - From the control-theoretic point of view, the presented framework, can be extended to systems with multiple-inputs-multiple-outputs (MIMO). This can further reduce the restrictions required by each subsystem of the overall teleoperation architecture and hence lead to improved performance.

Psychophysical findings in multi-/dimensional/modal spaces - With respect to the reduction schemes of haptic data, the psychophysical findings in multidimensional perception should be elaborated and expanded. It was early recognized in this thesis, that the knowledge of the human perception in multi-dimensional spaces is inadequate. A few is only known, on the cross-effects that different simultaneous stimuli have on the human operator perception. Any further finding could greatly benefit the developed haptic data reduction schemes and the presented idea for multi-DoF deadband could be further elaborated.

Knowledge-based control - The use of the subsystems' dissipation on the one side, and the use of the grip force on the other highlight just two examples in the haptic telepresence setting, where further, not necessarily dynamic, model knowledge can lead to either more stable or better performing control systems. Acquiring knowledge, instead of a priori assuming it, is the key in the methods presented here and carves the path for other applications as well. A control-theoretic framework able to address the challenges of stability, reachability and detectability of them is a goal to achieve.

Behavioral-based control - Stochastic theory offers a set of tools, e.g. Markov-based approaches, which could be employed to mitigate the high uncertainty of human actions. Measurements such as the grip force, could classify the human to specific behavioral states and stochastically predict his future actions. From the control perspective, stochastic exponential stability could be also studied.

We are confident, that solutions can be met in the near future and haptic telepresence systems will very soon find their way in medicine, space and large-scale dangerous or hazardous operations and probably later on might enter the consumer market.

A Appendix - Experimental setups

A.1 Linear haptic device

This experimental testbed consists of two identical 1-DoF tubular linear motors, Thrust-tube 2510 from Copley Controls Corp., shown in Figure A.1, each equipped with a Burster Corp. 8524-5500 force sensor and a PC. The linear motor is able to display peak forces of up to 780 N and continuous stall forces of up to 104.3 N and is connected to a digital servo drive Xenus XTL, also from Copley Controls Corp. The digital servo operates in current control; thus, we can consider the signal input to be approximately proportional to the applied motor force. The position is measured by an optical incremental encoder with a precision of 1 μm. The force sensor has a measurement range of 0 ± 500 N with an accuracy of 0.25% in full scale. The system is characterized by its linearity. No trigono-metric functions are necessary to compute the position of the end-effector as e.g. necessary when using rotary joints. Moreover, due to its simplicity, exact mathematical models can be found which describe the system. Hereby, the dynamics of the telemanipulation can be identified as a mass-damper system with standard system identification techniques. The corresponding parameters are shown in Table A.1.

Two different control modes are used to realize different teleoperation architectures, the force and the velocity control mode, and are discussed in the following.

Force control mode The entire haptic interface is controlled by a PC running a real-time Linux operating system. The digital servo is connected to the PC through a Sensoray I/O card. The overall haptic device is controlled by a high-gained force controller which compensates for viscous and Coulomb friction as well as for external forces. A force proportional P-gain= 4 is chosen and results in reduced device dynamics displayed to the human, i.e. 0.35 kg inertia and 3.01 Ns/m damping. All the control functions are implemented by Simulink blocksets. The sampling rate of the haptic signals and the local control loops is 1 kHz.

Tab. A.1: Dynamics of the linear device in current control mode

parameter	value
mass m	2.386 kq
damping d	20 Ns/m
motor electrical time constant T_α	0.00065 s
force sensor time constant T_f	0.0032 s
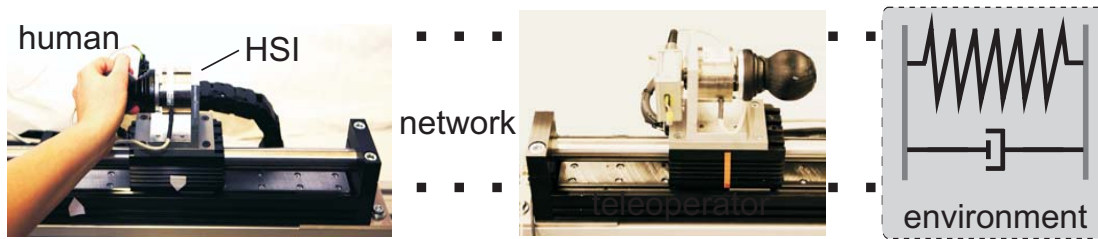
Fig. A.1: A linear haptic 1-DoF device as a Human-System-Interface and as teleoperator (similar kinematics). The human is grasping a handle which is attached to a force sensor parallel to the direction of the rod. The teleoperator can interact with real or even virtual environments.

Velocity control mode The teleoperator is velocity-controlled with a proportional-integral controller with the P-gain 8000 Ns/m and the I-gain 40000 N/m. The sampling rate of the haptic signals and the local control loops is $1\ kHz$.
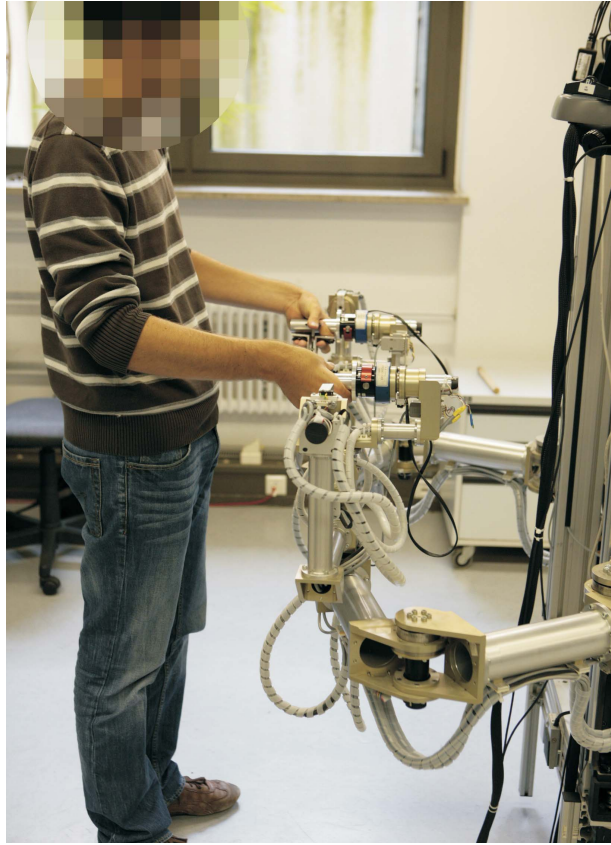
Fig. A.2: A human operator using the ViSHaRD7 human system interface.

A.2 Multi-DoF haptic telepresence setup

This experimental testbed consists of an admittance-type haptic interface for bimanual manipulation as presented in [127], the ViSHaRD 7, and a human-scaled 7-DoF mobile teleoperator [16].

A.2.1 ViSHaRD7

The Virtual Scenario Haptic Rendering Device has two arms each with 7 actuated DoF, the first one being a linear axis and the remaining 6 being revolute joints. It has hence full 6-DoF capability; it is illustrated on Figure A.2. Each arm is also employed with 6-DoF force/torque sensor mounted on its end effectors. Both arms are admittance-type devices and are thus controlled using position-based admittance control schemes as presented in [126], i.e. a inner-position controller is employed to cancel the nonlinear dynamics and friction, and an outer admittance loop to render dynamics and provide more robust stability. The control parameters are listed in Table A.2. The mobile platform of the device, allowing it to move in the room, was not used in our experiments. For a detailed extensive analysis of the design, the output capability and for an evaluation of the device the reader is encouraged to read [126, 127].

Parameters	Master
$\mathbf{K}_p$	$\mathrm{diag}\,(100000, 64, 64, 4, 8, 5, 2)$
$\mathbf{K}_d$	$\mathrm{diag}\,(640, 0.12, 0.12, 0.12, 0.008, 0.004, 0.05)$
$\mathbf{M}_t[Kg]$	$\mathrm{diag}\,(10, 10, 10)$
$\mathbf{M}_o[Kgm^2]$	$\mathrm{diag}\,(0.2, 0.2, 0.2)$
$\mathbf{D}_t$	$\mathrm{diag}\,(11, 11, 11)$
$\mathbf{D}_o$	$\mathrm{diag}\,(0.5, 0.5, 0.5)$

Tab. A.2: Robot control parameters for the ViSHaRD7 haptic rendering device.

A.2.2 Teleoperator

The teleoperator is a human-scaled redundant bimanual robot. It consists of two identical, human-scaled arms, whereby each arm further consists of two spherical joints with 3-DOF at shoulder and wrist, and one revolute joint at the elbow as designed in [155, 154]. A 6-DoF force/torque sensor is employed in each arm. It is characterized by accurate position control, dexterous free space motion, and singularity robust kinematic transformations. It is also equipped with a camera head and a mobile platform which were not used in our experiments.

Both arms are again admittance-type devices and are thus controlled using position-based admittance control schemes as presented in [126], i.e. a inner-position controller is employed to cancel the nonlinear dynamics and friction, and an outer admittance loop to render dynamics and provide more robust stability. The control parameters are listed in Table A.3.

Parameters	Teleoperator
$\mathbf{K}_p$	$\mathrm{diag}\,(6000, 6000, 6000, 6000, 3000, 3000, 3000)$
$\mathbf{K}_d$	$\mathrm{diag}\,(0.25, 0.25, 0.25, 0.25, 0.1, 0.1)$
$\mathbf{M}_t[Kg]$	$\mathrm{diag}\,(10, 10, 10)$
$\mathbf{M}_o[Kgm^2]$	$\mathrm{diag}\,(0.2, 0.2, 0.2)$
$\mathbf{D}_t$	$\mathrm{diag}\,(11, 11, 11)$
$\mathbf{D}_o$	$\mathrm{diag}\,(0.5, 0.5, 0.5)$

Tab. A.3: Robot control parameters for the 7 DoF telemanipulator.

A.3 Grip force sensing handle

To measure the force which the human user applies when grasping the handle of the haptic device a low-noise load cell FC22 from Measurement Specialists is used. The load cell is able to measure forces up to approximately 110 Newton (25 lbf) with an accuracy (non linearity, hysteresis, and repeatability) of 1%. The sensor housing is mounted *in* the aluminum handle as illustrated in Figure A.4 with the sensing element coming out of it. A rigid aluminum bar is attached on top of the load cell, increasing thus the effective plane that the human palm/fingers can press/squeeze. The force created by the pivot effect that
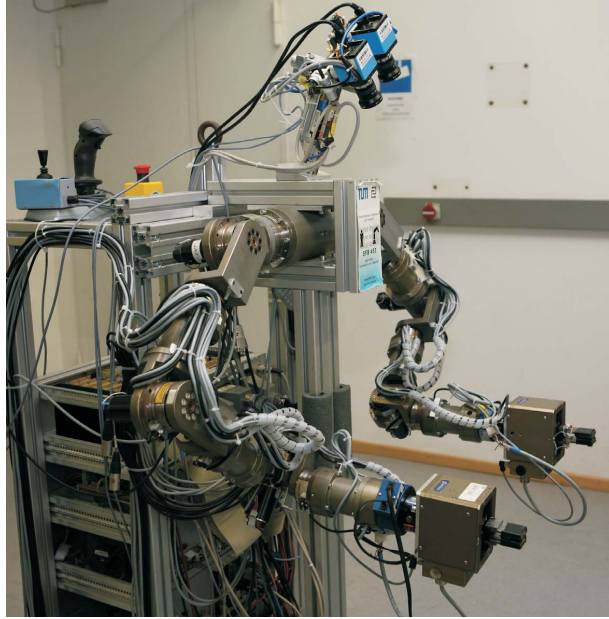
Fig. A.3: The anthropomorphic 7-DoF teleoperator.

the sensor and the aluminum bar cause is for simplicity here ignored; we assume that the measured force applies homogeneously along the aluminum bar.
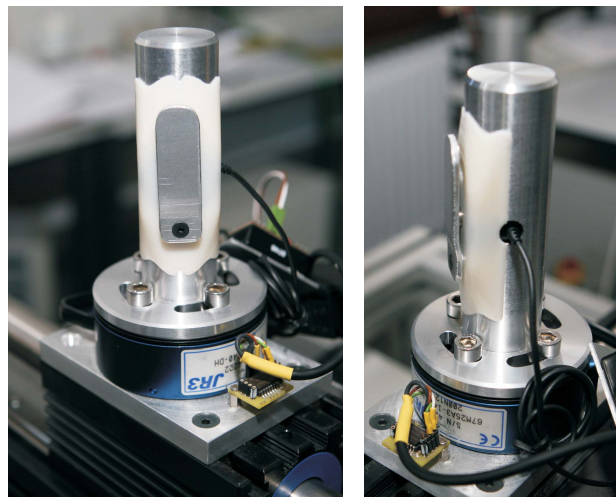
(a) Front view　　　(b) Side view

Fig. A.4: The self-made grip force sensing device. A sensor element is built in the handle that the human user grasps.

B Appendix - Aspects of robotic manipulators control

Although the telerobotics research has gained significance the last two decades, the problems of robotic control that have to do with telerobotics are poorly discussed in telerobotics literature. Moreover, most of the algorithms, or even stability guaranteeing control architectures that are proposed, tend to ignore fundamental robotic problems by only treating 1-DoF cases. Here, the most important problems that were faced during the implementation of our algorithms in a real telerobotic multi-DoF equipment are discussed.

Motion controllers are used in teleoperation systems for both the HSI and the teleoperator in the velocity-velocity architecture and for the teleoperator in the velocity-force architecture. Motion control ensures the tracking of a desired velocity or position. A PI-controller is widely used in teleoperation systems in case of velocity control [117]. Combining a PI-controller with dynamic controllers compensates the robot dynamics and improves the performance of the motion controller.

Kinematically similar manipulators can be controlled in joint level with independent joint controllers. However, task space control is considered in most of telerobotic scenarios for the motion control because in most of the cases the HSI and teleoperator manipulators differ kinematically. Besides that, in passivity-based control, Cartesian-based implementations seem to be less conservative than independent passive joint controllers [63]. However, in velocity-based architectures, as most passivity-based techniques are, Cartesian-based control poses some challenges as the variables are transmitted through a network to another system.

Two of those are discussed here. First of all, although position (translation) control is trivial, the orientation is challenging due to the singularities some orientation representations pose. The problem becomes more challenging in teleoperation systems due to the derivation and integration that velocity-based techniques require. The integration of the angular velocity, that is transmitted through the communication channel for example, would not have a physical meaning when dealing with finite rotations. Secondly, the drifting phenomena and ways to mitigate such problems are also discussed in the second part of this appendix. Apart from the drifting that numerical integration can add in the velocity-based approaches, this part is very important in our work, due to the data reduction-related error that is added by the techniques of Chapter 4. Methods on the correction of this pose drift are already discussed in Section 4.6.4, here, we only touch the stability of these approaches.

B.1 Orientation control

The angular velocity vector $\boldsymbol{\omega}$ is the most intuitive representation of the rotational velocity [144]. The main problem of using $\boldsymbol{\omega}$ in robotics control is, however, the fact that $\int \boldsymbol{\omega}$ has no physical meaning when dealing with finite rotations since those can not be added like vectors. $\boldsymbol{\omega}$ can thus not be used in a closed kinematic control or in PI operational space control directly.

One solution is to assume that the rotations are infinitesimal and thus can be added. Since control loop normally have very small sample time, the rotation caused by the human operator in a sample time can be considered infinitesimal. So we could assume that by integrating $\boldsymbol{\omega}$ we get the orientation which can be used in control. This method is though problematic in the passivity framework since it can not be determined to what extent the approximation errors in calculating $\int \boldsymbol{\omega}$ may generate energy and violate the passivity condition.

To overcome this issue, $\boldsymbol{\omega}$ is mapped to a representation of rotation like the Euler angles or the quaternions discussed here.

B.1.1 Euler angles

The Euler angles are a very common representation of orientation in robotics. They are named after Leonard Euler, who proved that the the rotation between any two independent orthonormal coordinate frames can be described by no more than three rotations around the coordinates axes [17]. These rotations are represented by the Euler angles α, β and γ. There exists, however, several conventions, 12 to be precise, depending on the order of rotation axes.

$$\boldsymbol{\phi}\left(\alpha, \beta, \gamma\right) = \begin{pmatrix} \alpha \\ \beta \\ \gamma \end{pmatrix} \in M^3 \equiv \Re^3.$$

For a given convention and Euler angles, the resulting rotation is unique. However, the inverse problem, i.e determining the Euler angles for a given rotation, is not always unique since Euler angles inherently have singularities. Despite their singularities, Euler angles are commonly used in robotics. One of the reasons behind this, is that the orientation error can be calculated simply by subtracting the current Euler angles from the desired ones,

$$e_o = \phi_d - \phi.$$

Euler angles are part of the so-called operational space. The joint space configuration and the operational space configuration are related by the analytical Jacobian J_A which has the following relation to the geometrical Jacobian J,

$$J = T_A\left(\phi\right) J_A,$$

with

$$\boldsymbol{\omega} = T_A(\boldsymbol{\phi})\,\dot{\boldsymbol{\phi}}, \qquad\qquad (B.1)$$

$$\text{where } T_A(\alpha, \beta, \gamma) = \begin{pmatrix} 0 & -\sin(\alpha) & \sin(\beta)\cos(\alpha) \\ 0 & \cos(\alpha) & \sin(\beta)\sin(\alpha) \\ 1 & 0 & \cos(\beta) \end{pmatrix}.$$

The inverse problem, i.e. finding the $\boldsymbol{\phi}$ corresponding to a given $\boldsymbol{\omega}$, has a solution only if T_A is invertible. This is however not always the case, since

$$\det(T_A) = \sin(\beta),$$

which is equal to zero if $\beta = 0$ or $\beta = \pi$. Other Euler angle sequences also have their singularities, which is the main disadvantage of this representation.

B.1.2 Quaternion

Unit quaternions help overcome the singularity issues of the Euler angles representation. Quaternions are the immediate extension to complex numbers. They were first proposed by Hamilton in 1843. A quaternion $\mathcal{Q}$ is a described by a set of 4 real numbers $\mathcal{Q} = [\mathcal{Q}_0 \; \mathcal{Q}_1 \; \mathcal{Q}_2 \; \mathcal{Q}_3]$

$$\begin{aligned} \mathcal{Q} &= \mathcal{Q}_0 + \mathcal{Q}_1 i + \mathcal{Q}_2 j + \mathcal{Q}_3 k \\ &= (\eta, \boldsymbol{\epsilon}), \end{aligned}$$

with $\eta = \mathcal{Q}_0$ and $\boldsymbol{\epsilon} = [\mathcal{Q}_1, \mathcal{Q}_2, \mathcal{Q}_3]$. Good introductions to the mathematical properties of quaternions can be found in [58] and [166].

Quaternion orientation error

In oder to devise an inverse kinematics algorithm based on the unit quaternion a suitable orientation error shall be defined. The orientation error is computed by means of the quaternion product between the desired quaternion $\mathcal{Q}_d$ and the inverse of the quaternion representing the current orientation $\mathcal{Q}$

$$\begin{aligned} \Delta\mathcal{Q} &= \mathcal{Q}_d \otimes \mathcal{Q}^{-1} \\ &= (\Delta\eta, \Delta\boldsymbol{\epsilon}), \end{aligned}$$

where the $\otimes$ operation represents the quaternion product. The orientation error corresponds to the imaginary part of $\Delta\mathcal{Q}$ [144]

$$e_o = \Delta\boldsymbol{\epsilon}$$

As in the operational space, a mapping is needed between $\boldsymbol{\omega}$ and the quaternion space.

For this purpose a representation Jacobian for the task space controller is to be defined

$$\begin{bmatrix} \dot{\eta} \\ \dot{\boldsymbol{\epsilon}} \end{bmatrix} = \mathcal{E}\left(\eta, \boldsymbol{\epsilon}\right) \boldsymbol{\omega}, \tag{B.2}$$

where $\mathcal{E}\left(\eta, \boldsymbol{\epsilon}\right)$ has the following form

$$\mathcal{E}\left(\eta, \boldsymbol{\epsilon}\right) = \frac{1}{2} \begin{bmatrix} -\boldsymbol{\epsilon}^T \\ \eta I - S\left(\boldsymbol{\epsilon}\right) \end{bmatrix} \in \Re^{4 \times 3},$$

where $I \in \Re^{3 \times 3}$ is the unit matrix and the operator $S\left(\right)$ is the skew-symmetric operator such that, for a given vector $x = [x_1 \ x_2 \ x_3]^T$

$$S\left(x\right) = \begin{pmatrix} o & -x_3 & x_2 \\ x_3 & 0 & -x_1 \\ -x_2 & x_1 & 0 \end{pmatrix}.$$

The main challenge in applying task space control is that the corresponding quaternion for a given Ω has to be determined in order to compute the orientation error. This can be reached by integrating $\dot{\mathcal{Q}}$, which is equivalent to solving the first order differential (B.2). Close solutions for this equation may exist under certain assumptions. The simplest assumption is that $\boldsymbol{\omega}$ is constant over the integration step, which corresponds to a zeroth order quaternion integration [166]. For an integration step Δt, the zeroth order integral form can be defined as

$$\mathcal{Q}\left(t + \Delta t\right) = \begin{bmatrix} \frac{\boldsymbol{\omega}}{\|\boldsymbol{\omega}\|} \sin\left(\frac{\|\boldsymbol{\omega}\|}{2} \Delta t\right) \\ \cos\left(\frac{\|\boldsymbol{\omega}\|}{2} \Delta t\right) \end{bmatrix} \otimes \mathcal{Q}\left(t\right). \tag{B.3}$$

The derivation of (B.3) can be found in [166]. It is also possible to apply higher order integration, which leads to more complex forms.

B.2 Inverse kinematics drift

A reconstruction of joint variables q is entrusted to a numerical integration which involves *drift* phenomena of the solution; as a consequence, the end-effector location corresponding to the computed joint variables differs from the desired one. This inconvenience can be overcome by resorting to a solution scheme that accounts for the operational space error between the desired and the actual end-effector position and orientation [144]. Let

$$e = x_d - x = x_d - k(q) \tag{B.4}$$

be the expression of such error, where the vector $k()$-nonlinear in general-allows computation of the operational space variables by knowing the joint space variables. Consider the time derivative of (B.4)

$$\dot{e} = \dot{x_d} - \dot{x} \tag{B.5}$$

which, according to differential kinematics, can be written as

$$\dot{e} = \dot{x}_d - J_A(q)\dot{q} \tag{B.6}$$

which, gives a differential equation describing error evolution over time. Nonetheless, it is necessary to choose a relationship between $\dot{q}$ and e that ensures convergence of the error to zero.

Having formulated the inverse kinematics problem in an algorithmic fashion implies that the joint variables q corresponding to the assigned end-effector posture x_d are accurately obtained only when the error e is below a given tolerated threshold.

Jacobian (Pseudo-)Inverse   On the assumption that matrix J_A is square and nonsingular, the choice

$$\dot{q} = J_A^{-1}(q)(\dot{x}_d + Ke) \tag{B.7}$$

leads to the equivalent linear system

$$\dot{e} + Ke = 0. \tag{B.8}$$

If K is a positive definite (usually diagonal) matrix, the system (B.8) is *asymptotically stable* [144]. The error tends to zero along the trajectory with a convergence rate that depends on the eigenvalues of matrix K; the larger the eigenvalues, the faster the convergence. In practice, since the inversion scheme is to be implemented in discrete-time, there is an upper bound on the norm of K with reference to the adopted sampling time.

Bibliography

[1] R. Adams and B. Hannaford. Stable haptic interaction with virtual environments. *IEEE Transactions on Robotics and Automation*, 15(3):465–474, 1999.

[2] I. F. Akyildiz, D. Pompili, and T. Melodia. Challenges for efficient communication in underwater acoustic sensor networks. *SIGBED Rev.*, 1(2):3–8, 2004.

[3] S. Allin, Y. Matsuoka, and R. Klatzky. Measuring just noticeable differences for haptic force feedback: implications for rehabilitation. In *Proceedings of the 10th Symposium on Haptic Interfaces for Virtual Environment and Teleoperator Systems*, pages 299–302, Orlando, FL, USA, 2002.

[4] R. J. Anderson and M. W. Spong. Bilateral control of teleoperators with time delay. *IEEE Transactions on Automatic Control*, 34(5):494–501, May 1989.

[5] P. Arcara and C. Melchiorri. Control schemes for teleoperation with time delay: A comparative study. *Robotics and Autonomous Systems*, 38(1):49–64, January 2002.

[6] J. Artigas, C. Preusche, G. Hirzinger, G. Borghesan, and C. Melchiorri. Bilateral energy transfer in delayed teleoperation on the time domain. In *Robotics and Automation, 2008. ICRA 2008. IEEE International Conference on*, pages 671 –676, May 2008.

[7] J. Artigas, J.-H. Ryu, and C. Preusche. Time domain passivity control for position-position teleoperation architectures. *Presence: Teleoper. Virtual Environ.*, 19:482–497, 2010.

[8] J. Baillieul and P.J. Antsaklis. Control and communication challenges in networked real-time systems. *Proceedings of the IEEE*, 95(1):9 –28, Jan. 2007.

[9] P. Berestesky, N. Chopra, and M. W. Spong. Discrete time passivity in bilateral teleoperation over the internet. In *Proceedings of the 2004 IEEE International Conference on Robotics and Automation, ICRA '04*, volume 5, pages 4557 – 4564, April 2004.

[10] P. Berestesky, N. Chopra, and M.W. Spong. Theory and experiments in bilateral teleoperation over the internet. In *Control Applications, 2004. Proceedings of the 2004 IEEE International Conference on*, volume 1, pages 456–463 Vol.1, 2-4 Sept. 2004.

[11] C. W. Borst. Predictive coding for efficient host-device communication in a pneumatic force-feedback display. In *Proceedings of the First Joint Eurohaptics Conference and Symposium on Haptic Interfaces for Virtual Environment and Teleoperator Systems, World Haptics*, pages 596–599, Pisa, Italy, March 2005.

[12] C. Braun, M. Haug, K. Wiech, N. Birbaumer, T. Elbert, and L. E. Roberts. Functional organization of primary somatosensory cortex depends on the focus of attention. *Neuroimage*, 17:1451–1458, 2002.

[13] S. P. Buerger and N. Hogan. Relaxing passivity for human-robot interaction. In *Proceedings of the IEEE/RSJ International Conference on Intelligent Robots and Systems*, pages 4570–4575, October 2006.

[14] S. P. Buerger and N. Hogan. Complementary stability and loop shaping for improved human-robot interaction. *Robotics, IEEE Transactions on*, 23(2):232 –244, April 2007.

[15] G. C. Burdea. *Force and Touch Feedback for Virtual Reality*. Wiley, 1996.

[16] M. Buss, A. Peer, T. Schauss, N. Stefanov, U. Unterhinninghofen, S. Behrendt, J. Leupold, M. Durkovic, and M. Sarkis. Development of a multi-modal multi-user telepresence and teleaction system. *International Journal of Robotics Research (IJRR)*, 29(10):1298–1316, September 2010.

[17] R. Campa and H. De La Torre. Pose control of robot manipulators using different orientation representations: a comparative review. In *ACC'09: Proceedings of the 2009 conference on American Control Conference*, pages 2855–2860, Piscataway, NJ, USA, 2009. IEEE Press.

[18] R. Campa, R. Kelly, and E. Garcia. On stability of the resolved acceleration control. In *Robotics and Automation, 2001. Proceedings 2001 ICRA. IEEE International Conference on*, volume 4, pages 3523 – 3528 vol.4, 2001.

[19] F. Castanos and R. Ortega. Energy-balancing passivity-based control is equivalent to dissipation and output invariance. *Systems & Control Letters*, 58(8):553 – 560, 2009.

[20] C.-C Chen. *Performance-Oriented Control and Co-Design for Stochastic Networked Control Systems*. PhD thesis, Technische Universität München, 2010.

[21] Hyun Chul Cho and Jong Hyeon Park. Impedance controller design of internet-based teleoperation using absolute stability concept. In *IEEE/RSJ Intl. Conference on Itelligent Robots and Systems*, pages 2256 – 2261, October 2002.

[22] N. Chopra, M. W. Spong, S. Hirche, and M. Buss. Bilateral teleoperation over the internet: the time varying delay problem. In *American Control Conference, 2003. Proceedings of the 2003*, volume 1, pages 155–160, 4-6 June 2003.

[23] E. Colgate and G. Schenkel. Passivity of a class of sampled-data systems: Application to haptic interfaces. *Journal of Robotic Systems*, 14:37–47, 1997.

[24] J. E. Colgate and J. M. Brown. Factors affecting the z-width of a haptic display. In *Robotics and Automation, 1994. Proceedings., 1994 IEEE International Conference on*, pages 3205 –3210 vol.4, May 1994.

[25] J. E. Colgate and N. Hogan. Robust stability of dynamically interacting systems. *International Journal of Control*, 48:65–88, 1988.

[26] J. E. Colgate, M. C. Stanley, and G. G. Schenkel. Dynamic range of achievable impedances in force-reflecting interfaces. In Won S. Kim, editor, *Telemanipulator Technology and Space Telerobotics*, volume 2057, pages 199–210. SPIE, 1993.

[27] Shadow Robot Company. Shadow robot dextrous hand.

[28] Controller Area Network (CAN). http://www.can-cia.de/.

[29] M. R. Cutkosky and R. D. Howe. Human grasp choice and robotic grasp analysis. In *Dextrous robot hands*, pages 5–31. NewYork:Springer, 1990.

[30] R. M. Daoud, H. H. Amer, H. M. Elsayed, and Y. Sallez. Ethernet-based car control network. In *Electrical and Computer Engineering, 2006. CCECE '06. Canadian Conference on*, pages 1031 –1034, May 2006.

[31] J. T. Dennerlein, D. B. Martin, and C. J. Hasser. Force-feedback improves performance for steering and combined steering-targeting tasks. *Proceedings of the SIGCHI conference on Human factors in computing systems, The Hague, The Netherlands*, pages 423–429, 2000.

[32] N. Diolaiti, C. Melchiorri, and S. Stramigioli. Contact impedance estimation for robotic systems. *Robotics, IEEE Transactions on*, 21(5):925 – 935, Oct. 2005.

[33] N. Diolaiti, G. Niemeyer, F. Barbagli, and J.K. Salisbury. Stability of haptic rendering: Discretization, quantization, time delay, and coulomb effects. *Robotics, IEEE Transactions on*, 22(2):256 –268, April 2006.

[34] J. M. Dolan, M. B. Friedman, and M. L. Nagurka. Dynamic and loaded impedance components in the maintenance of human arm posture. *Systems, Man and Cybernetics, IEEE Transactions on*, 23(3):698 –709, May/June 1993.

[35] J. Droesler. An n-dimensional weber law and the corresponding fechner law. *Journal of Mathematical Psychology*, 44:330–335, 2000.

[36] R. Dubbey, T. Chang, and S. Everret. Variable damping impedance control of a bilateral telerobotic system. *IEEE Control Systems Magazine*, 17:37–45, 1997.

[37] L. Eusebi and C. Melchiorri. Force reflecting telemanipulators with time-delay: stability analysis and control design. *Robotics and Automation, IEEE Transactions on*, 14(4):635 –640, August 1998.

[38] M. W. Eysenck and M. T. Keane. *Cognitive Psychology. A student's handbook*. Psychology Press, 2000.

[39] W. R. Ferrell. Remote manipulation with transmission delay. *IEEE Transactions on Human Factors in Electronics*, HFE-6:24–32, September 1965.

[40] W. R. Ferrell. Delayed force feedback. *Human Factors: The Journal of the Human Factors and Ergonomics Society*, 8:449–455(7), October 1966.

[41] P. Fiorini and R. Oboe. Internet-based telerobotics: problems and approaches. In *Advanced Robotics, 1997. ICAR '97. Proceedings., 8th International Conference on*, pages 765 –770, July 1997.

[42] T. Flash and N. Hogan. The coordination of arm movements: An experimentally confirmed mathematical model. *The Journal of Neuroscience*, 5(7):1688–1703, July 1985.

[43] T. Flash and F. Mussa-Ivaldi. Human arm stiffness characteristics during the maintenance of posture. *Experimental Brain Research*, 82:315–326, 1990. 10.1007/BF00231251.

[44] M. Franken, S. Stramigioli, R. Reilink, C. Secchi, and A. Macchelli. Bridging the gap between passivity and transparency. *Proc. of Robotics: Science & Systems*, 2009.

[45] D. Franklin, E. Burdet, R. Osu, M. Kawato, and T. Milner. Functional significance of stiffness in adaptation of multijoint arm movements to stable and unstable dynamics. *Experimental Brain Research*, 151:145–157, 2003. 10.1007/s00221-003-1443-3.

[46] M. Fritzsche, N. Elkmann, and E. Schulenburg. Tactile sensing: a key technology for safe physical human robot interaction. In *Proceedings of the 6th international conference on Human-robot interaction*, HRI '11, pages 139–140, New York, NY, USA, 2011. ACM.

[47] G. A. Gescheider. *Psychophysics.* Lawrence Erlbaum, 1985.

[48] R. B. Gillespie and M. R. Cutkosky. Stable user-specific haptic rendering of the virtual wall. In *Proceedings of the International Mechanical Engineering Comgress and Exhibition*, volume 61, pages 85–92, November 1995.

[49] H. Gomi and M. Kawato. Human arm stiffness and equilibrium-point trajectory during multi-joint movement. *Biological Cybernetics*, 76:163–171, 1997. 10.1007/s004220050329.

[50] H. Gomi, Y. Koike, and M. Kawato. Human hand stiffness during discrete point-to-point multi-joint movement. In *Engineering in Medicine and Biology Society, 1992. Vol.14. Proceedings of the Annual International Conference of the IEEE*, volume 4, pages 1628 –1629, Oct. 1992.

[51] G. C. Goodwin and K. S. Sin. *Adaptive Filtering Prediction and Control.* Prentice-Hall, 1984.

[52] J. D. Greenspan and S. J. Bolanowski. *The Psychophysics of Tactile Perception and Its Peripheral Physiological Basis, In: L. Kruger (Ed.). Pain and Touch.* Academic Press Inc., 1996.

[53] G. S. Guthart and Jr. Salisbury, J. K. The intuitivetm telesurgery system: overview and application. In *Robotics and Automation, 2000. Proceedings. ICRA '00. IEEE International Conference on*, volume 1, pages 618 –621 vol.1, 2000.

[54] U. Hagn, T. Ortmaier, R. Konietschke, B. Kubler, U. Seibold, A. Tobergte, M. Nickl, S. Jorg, and G. Hirzinger. Telemanipulator for remote minimally invasive surgery. *Robotics Automation Magazine, IEEE*, 15(4):28 –38, Dec. 2008.

[55] A. Z. Hajian and R. D. Howe. Identification of the mechanical impedance at the human finger tip. *Journal of Biomechanical Engineering*, 119(1):109–114, 1997.

[56] B. Hannaford. Stability and performance tradeoffs in bi-lateral telemanipulation. In *Robotics and Automation, 1989. Proceedings., 1989 IEEE International Conference on*, pages 1764 –1767 vol.3, May 1989.

[57] B. Hannaford, L. Wood, D.A. McAffee, and H. Zak. Performance evaluation of a six-axis generalized force-reflecting teleoperator. *Systems, Man and Cybernetics, IEEE Transactions on*, 21(3):620–633, May/Jun 1991.

[58] A. J. Hanson. *Visualizing Quaternions (The Morgan Kaufmann Series in Interactive 3D Technology)*. Morgan Kaufmann Publishers Inc., San Francisco, CA, USA, 2006.

[59] C.J. Hasser and M.R. Cutkosky. System identification of the human hand grasping a haptic knob. In *Haptic Interfaces for Virtual Environment and Teleoperator Systems, 2002. HAPTICS 2002. Proceedings. 10th Symposium on*, pages 171 –180, 2002.

[60] K. Hastrudi-Zaad and S.E. Salcudean. On the use of local force feedback for transparent teleoperation. In *Robotics and Automation, 1999. Proceedings. 1999 IEEE International Conference on*, volume 3, pages 1863 –1869 vol.3, 1999.

[61] K. Hastrudi-Zaad and S.E. Salcudean. Analysis of control architectures for teleoperation systems with impedance/admittance master and slave manipulators. *The International Journal of Robotics Research*, 20(6):419–445, 2001.

[62] M. A. Heller, G. J. Roger, and C. L. Perry. Tactile pattern recognition with the optacon: Superior performance with active touch and the left hand. *Neuropsychologia*, 28:1003–1006, 1990.

[63] K. Hertkorn, T. Hulin, P. Kremer, C. Preusche, and G. Hirzinger. Time domain passivity control for multi-degree of freedom haptic devices with time delay. In *Robotics and Automation (ICRA), 2010 IEEE International Conference on*, pages 1313 –1319, May 2010.

[64] K. Hikichi, H. Morino, I. Fukuda, S. Matsumoto, Y. Yasuda, I. Arimoto, M. Iijima, and K. Sezaki. Architecture of haptics communication system for adaptation to network environments. In *Proceedings of the IEEE International Conference on Multimedia and Expo*, pages 563–566, Tokyo, Japan, August 2001.

[65] D. Hill and P. Moylan. The stability of nonlinear dissipative systems. *Automatic Control, IEEE Transactions on*, 21(5):708–711, Oct 1976.

[66] D. Hill and P. Moylan. Stability results for nonlinear feedback systems. *Automatica*, 13(4):377 – 382, 1977.

[67] M. D. Hill and G. Niemeyer. Real-time estimation of human impedance for haptic interfaces. In *EuroHaptics conference, 2009 and Symposium on Haptic Interfaces for Virtual Environment and Teleoperator Systems. World Haptics 2009. Third Joint*, pages 440 –445, 2009.

[68] P. Hinterseer, S. Hirche, S. Chaudhuri, E. Steinbach, and M. Buss. Perception-based data reduction and transmission of haptic data in telepresence and teleaction systems. *Signal Processing, IEEE Transactions on*, 56(2):588–597, Feb. 2008.

[69] S. Hirche. *Haptic Telepresence in Packet Switched Communication Networks*. PhD thesis, Technische Universitaet Muenchen, Institute of Automatic Control Engineering, 2005.

[70] S. Hirche and M. Buss. Packet loss effects in passive telepresence systems. In *Decision and Control, 2004. CDC. 43rd IEEE Conference on*, volume 4, pages 4010–4015 Vol.4, Dec. 2004.

[71] S. Hirche and M. Buss. Human perception oriented control aspects of networked telepresence and teleaction systems. In *Proceedings of the International Conference on Instrumentation, Control and Information Technology*, pages 3430–3435, Okayama, Japan, 2005.

[72] S. Hirche and M. Buss. Transparenz haptischer Telepräsenzsysteme mit konstanter Zeitverzögerung (Transparency of haptic telepresence systems with constant time delay). *Automatisierungstechnik*, 54(2):51–59, February 2006.

[73] S. Hirche and M. Buss. Transparent data reduction in networked telepresence and teleaction systems. part ii: Time-delayed communication. *Presence: Teleoperators & Virtual Environments*, 16(5):532–542, 2007.

[74] S. Hirche, M. Ferre, J. Barrio, C. Melchiorri, and M. Buss. *Advances in Telerobotics*, chapter Bilateral Control Architectures for Telerobotics Control, pages 163–176. STAR. Springer-Verlag, Berlin, 2007.

[75] S. Hirche, P. Hinterseer, E. Steinbach, and M. Buss. Towards deadband control in networked teleoperation systems. In *Proceedings of the IFAC World Congress*, Prague, Czech Republic,, 2005. Int. Federation of Autom. Control.

[76] S. Hirche, P. Hinterseer, E. Steinbach, and M. Buss. Transparent data reduction in networked telepresence and teleaction systems. part i: Communication without time delay. *Presence: Teleoperators & Virtual Environments*, 16(5):523–531, 2007.

[77] S. Hirche, T. Matiakis, and M. Buss. A distributed controller approach for delay-independent stability of networked control systems. *Automatica*, 45(8):1828 – 1836, 2009.

[78] N. Hogan. Controlling impedance at the man/machine interface. In *Robotics and Automation, 1989. Proceedings., 1989 IEEE International Conference on*, volume 3, pages 1626–1631, Scottsdale, AZ, 14-19 May 1989.

[79] N. Hogan. The mechanics of multi-joint posture and movement control. *Biological Cybernetics*, 52:315–331, 1985.

[80] P. F. Hokayem and M. W. Spong. Bilateral teleoperation: An historical survey. *Automatica*, 42(12):2035–2057, December 2006.

[81] P. F. Hokayem and M. W. Spong. Stability of quantized and delayed bilateral tele-operators. In *Proceedings of the 45th IEEE Conference on Decision & Control*, pages 4484–4489, San Diego, CA, USA, December 2006.

[82] D. Hristu-Varsakelis and W. S. Levine. *Handbook of networked and embedded control systems*. Birkhäuser, Boston, 2005.

[83] Y. Iguchi, Y. Hoshi, and I. Hashimoto. Selective spatial attention induces short-term plasticity in human somatosensory cortex. *Neuroreport*, 12:3133–3136, 2001.

[84] Immersion Corp. Cyberglove and cybergrasp exoskeleton.

[85] R. Isermann. *Identifikation dynamischer System I*. Springer, 2 edition, 1992.

[86] L. Jandura and MA. Srinivasan. Experiments on human performance in torque discrimination and contro. *Proc. of the ASME dynamic systems and control division*, 55-1:369–75, 1994.

[87] L. A. Jones. Matching forces: constant errors and differential thresholds. *Perception*, 18(5):681–687, 1989.

[88] L. A. Jones and I. W. Hunter. A perceptual analysis of stiffness. *Experimental Brain Research*, 79:150–156, 1990.

[89] L. A. Jones and I. W. Hunter. Human operator perception of mechanical variables and their effects on tracking performance. *ASME Advances in Robotics*, 53:42–49, 1992.

[90] L. A. Jones and I. W. Hunter. A perceptual analysis of viscosity. *Experimental Brain Research*, 94:343–351, 1993. 10.1007/BF00230304.

[91] J. Kammerl, R. Chaudhari, and E. Steinbach. Exploting directional dependencies of force perception for lossy haptic data reduction. In *In proceedings of the International Symposium on Haptic Audio-Visual Environments and Games*, 2010.

[92] C. Kao and A. Rantzer. Stability analysis of systems with uncertain time-varying delays. *Automatica*, 43(6):959 – 970, 2007.

[93] H. K. Khalil. *Nonlinear Systems*. Prentice Hall, 1996.

[94] K. Kosuge, Y. Fujisawa, and T. Fukuda. Control of mechanical system with man-machine interaction. In *Intelligent Robots and Systems, 1992., Proceedings of the 1992 lEEE/RSJ International Conference on*, volume 1, pages 87 –92, Jul. 1992.

[95] K. J. Kuchenbecker, J. G. Park, and G. Niemeyer. Characterizing the human wrist for improved haptic interaction. *ASME Conference Proceedings*, 2003(37130):591–598, 2003.

[96] M. Kuschel, P. Kremer, S. Hirche, and M. Buss. Lossy Data Reduction Methods for Haptic Telepresence Systems. In *Proceedings of the 2006 IEEE International Conference on Robotics and Automation*, pages 2933–2938, 2006.

[97] D. A. Lawrence. Stability and transparency in bilateral teleoperation. In *Decision and Control, 1992., Proceedings of the 31st IEEE Conference on*, pages 2649–2655 vol.3, 1992.

[98] D.A. Lawrence. Stability and transparency in bilateral teleoperation. In *Robotics and Automation, IEEE Transactions on*, volume 9, pages 624 –637, Oct. 1993.

[99] D. Lee and K. Huang. Passive set-position modulation approach for haptics with slow, variable, and asynchronous update. In *EuroHaptics conference, 2009 and Symposium on Haptic Interfaces for Virtual Environment and Teleoperator Systems. World Haptics 2009. Third Joint*, pages 541 –546, March 2009.

[100] Dongjun Lee and Ke Huang. Passive-set-position-modulation framework for inter-active robotic systems. *IEEE Transactions on Robotics*, 26(2):354 –369, April 2010.

[101] F. L. Lian, J. R. Moyne, and D. M. Tilbury. Performance evaluation of control networks: Ethernet, controlnet, and devicenet. *Control Systems Magazine, IEEE*, 21(1):66 –83, February 2001.

[102] L. Love and Book W. Force reflecting teleoperation with adaptive impedance control. *IEEE Transactions on Systems, Man and Cybernetics*, 34:159–165, 2004.

[103] R. Lozano, , N. Chopra, and M. Spong. Passivation of force reflecting bilateral teleoperators with time varying delay. In *in Proceedings of the 8. Mechatronics Forum*, pages 24–26, 2002.

[104] C. Mahlo, C. Hoene, A. Rosami, and A. Wolisz. Adaptive coding and packet rates for tcp-friendly voip flows. In *In Proc. of the Int. Symposium on Telecommunications, Shiraz, Iran*, 2005.

[105] T. Matiakis. *Stability and performance of networked control systems with a distributed controller approach*. PhD thesis, Technische Universitaet Muechen, 2009.

[106] T. Matiakis, S. Hirche, and M. Buss. Independent-of-delay stability of nonlinear networked control systems by scattering transformation. *American Control Conference, 2006*, pages 6 pp.–, June 2006.

[107] T. Matiakis, S. Hirche, and M. Buss. Networked control systems with time-varying delay - stability through input-output transformation (netzwerkregelungssysteme mit variabler totzeit - stabilität durch eingangs-ausgangs-transformation). *Automatisierungstechnik*, 56(1):29–37, 2008.

[108] B. Miller, E. Colgate, and R. Freeman. Guaranteed stability of haptic system with nonlinear virtual environments. *IEEE Transacions on Robotics and Automation*, 16(6):712–718, December 2000.

[109] S. K. Mishra, S. Z. Wang, and K. K. Lai. *Generalized Convexity and Vector Optimization*. Springer Verlag, 2009.

[110] F. Mobasser and K. Hashtrudi-Zaad. Adaptive teleoperation control using online estimate of operator's arm damping. In *Decision and Control, 2006 45th IEEE Conference on*, pages 2032 –2038, Dec. 2006.

[111] F. Mobasser and K. Hashtrudi-Zaad. A method for online estimation of human arm dynamics. In *Engineering in Medicine and Biology Society, 2006. EMBS '06. 28th Annual International Conference of the IEEE*, pages 2412 –2416, Aug. 2006.

[112] J. Mostow. Surrogates. Film, Touchstone Pictures, 2009.

[113] S. Munir and W.J. Book. Internet Based Teleoperation using Wave Variable with Prediction. *ASME/IEEE Transactions on Mechatronics*, 7(2):124–133, 2002.

[114] F. A. Mussa-Ivaldi, N. Hogan, and E. Bizzi. Neural, mechanical, and geometric factors subserving arm posture in humans. *The Journal of Neuroscience*, 5(10):2732–2743, October 1985.

[115] E. M. Navarro-Lopez. *Dissipativity and passivity-related properties in nonlinear discrete-time systems*. PhD thesis, Universidad Politecnica de Cataluna, 2002.

[116] G. Niemeyer. *Using Wave Variables in Time Delayed Force Reflecting Teleoperation*. PhD thesis, Massachusetts Institute of Technology, September 1996.

[117] G. Niemeyer, C. Preusche, and G. Hirzinger. *Telerobotics:*, chapter 31, pages 741–757. Springer, 2008.

[118] G. Niemeyer and J. E. Slotine. Stable adaptive teleoperation. *IEEE Journal of Oceanic Engineering*, 16(1):152–162, January 1991.

[119] A. Ortega and Y. Liu. Lossy compression of haptic data. In *Touch in Virtual Environments: Haptics and the Design of Interactive Systems*, chapter 6, pages 119–136. Prentice Hall, 2002.

[120] R. Ortega and E. Garcia-Canseco. Interconnection and damping assignment passivity-based control: A survey. *European Journal of Control*, 10:432–450, 2004.

[121] R. Ortega, A. Loria, P. J. Nicklasson, and H. Sira-Ramirez. *Passivity-based Control of Euler-Lagrange Systems*. Springer-Verlag, London, 1998.

[122] R. Ortega, A. van der Schaft, B. Maschke, and G. Escobar. Interconnection and damping assignment passivity-based control of port-controlled hamiltonian systems. *Automatica*, 38:585–596, 2002.

[123] P. G. Otanez, J.R. Moyne, and D.M. Tilbury. Using deadbands to reduce communication in networked control systems. In *American Control Conference, 2002. Proceedings of the 2002*, volume 4, pages 3015–3020 vol.4, 2002.

[124] P. G. Otanez, J. T. Parrott, J. R. Moyne, and D. M. Tilbury. The implications of ethernet as a control network. In *Proceedings of Global Powertrain Conference*, 2002.

[125] J. H. Park and H. C. Cho. Sliding mode control of bilateral teleoperation systems with force-reflection on the internet. In *Intelligent Robots and Systems, 2000. (IROS 2000). Proceedings. 2000 IEEE/RSJ International Conference on*, volume 2, pages 1187 –1192 vol.2, 2000.

[126] A. Peer. *Design and Control of Admittance-Type Telemanipulation Systems*. PhD thesis, Technische Universitaet Muenchen, 2008.

[127] A. Peer and Martin Buss. A new admittance-type haptic interface for bimanual manipulations. *IEEE/ASME Trans. on Mechatronics*, 13(4):416–428, August 2008.

[128] I. G. Polushin and H. J. Marquez. Stabilization of bilaterally controlled teleoperators with communication delay: an iss approach. *International Journal of Control*, 76(8):858–870, 2003.

[129] H. Pongrac, P. Hinterseer, J. Kammerl, E. Steinbach, and B. Färber. Limitations of human 3d-force discrimination. Technical report, CiteSeerX - Scientific Literature Digital Library and Search Engine [http://citeseerx.ist.psu.edu/oai2] (United States), 2006.

[130] V. M. Popov. *Hyperstability of Control Systems*. Springer-Verlag, 1973.

[131] G. A. Pratt and M. M. Williamson. Series elastic actuators. In *Intelligent Robots and Systems 95. 'Human Robot Interaction and Cooperative Robots', Proceedings. 1995 IEEE/RSJ International Conference on*, volume 1, pages 399 –406 vol.1, August 1995.

[132] M. M. Rahman, R. Ikeura, and K. Mizutani. Investigating the impedance characteristic of human arm for development of robots to co-operate with human operators. In *Systems, Man, and Cybernetics, 1999. IEEE SMC '99 Conference Proceedings. 1999 IEEE International Conference on*, volume 2, pages 676 –681 vol.2, 1999.

[133] G. J. Raju, G. C. Verghese, and T. B. Sheridan. Design issues in 2-port network models of bilateral remote manipulation. In *Robotics and Automation, 1989. Proceedings., 1989 IEEE International Conference on*, pages 1316–1321 vol.3, May 1989.

[134] M. Rank, Z. Shi, H. Müller, and S. Hirche. Quality-of-service control in visual-haptic presence systems. *Journal of Systems, Man, and Cybernetics, Part A-Systems and Humans*, 2012. to be published.

[135] D. Reintsema, K. Landzettel, and G. Hirzinger. *Advances in Telerobotics: Human System Interfaces, Control, and Applications*, chapter DLR's Advanced Telerobotic Concepts and Experiments for On-Orbit Servicing., pages 324–345. Springer, STAR series, 2007.

[136] P. Ridao, M. Carreras, E. Hernandez, and N. Palomeras. *Advances in Telerobotics: Human System Interfaces, Control, and Applications*, chapter Underwater Telerobotics for Collaborative Research, pages 347–359. Springer, STAR series, 2007.

[137] E. J. Rodriguez-Seda, D. Lee, and M. W. Spong. Experimental comparison study of control architectures for bilateral teleoperators. *Robotics, IEEE Transactions on*, 25(6):1304–1318, Dec. 2009.

[138] J. Rosen and B. Hannaford. Doc at a distance. *Spectrum, IEEE*, 43(10):34–39, Oct. 2006.

[139] H. E. Ross and E. E. Brodie. Weber fractions for weight and mass as a function of stimulus intensity. *The Quarterly Journal of Experimental Psychology Section A: Human Experimental Psychology*, 39(1), 1987.

[140] J.-H. Ryu, D. S. Kwon, and B. Hannaford. Stable teleoperation with time-domain passivity control. *Robotics and Automation, IEEE Transactions on*, 20(2):365–373, April 2004.

[141] J.-H. Ryu, C. Preusche, B. Hannaford, and G. Hirzinger. Time domain passivity control with reference energy following. *IEEE Transactions on Control Systems Technology*, 13(5):737–742, 2005.

[142] J. K. Salisbury. Active stiffness control of a manipulator in cartesian coordinates. In *Decision and Control including the Symposium on Adaptive Processes, 1980 19th IEEE Conference on*, volume 19, pages 95 –100, Dec. 1980.

[143] T. Schilling, editor. *Telerobotic Applications*. WIley Publishers, 1999.

[144] L. Sciavicco and B. Siciliano. *Modelling and Control of Robot Manipulators*. Springer-Verlag London, 2000.

[145] C. Secchi, S. Stramigioli, and C. Fantuzzi. Transparency in port-hamiltonian based telemanipulation. In *Intelligent Robots and Systems, 2005. (IROS 2005). 2005 IEEE/RSJ International Conference on*, pages 1844 – 1849, Aug. 2005.

[146] C. Secchi, S. Stramigioli, and C. Fantuzzi. Transparency in port-hamiltonian-based telemanipulation. *Robotics, IEEE Transactions on*, 24(4):903 –910, Aug. 2008.

[147] R. Sepulchre, M. Jankovic, and P. Kokotovic. *Constructive Nonlinear Control*. Springer-Verlag, 1 edition, 1997.

[148] C. Shahabi, A. Ortega, and M. R. Kolahdouzan. A comparison of different haptic compression techniques. In *Proceedings of the International Conference on Multimedia & Expo*, pages 657–660, Lausanne, Switzerland, August 2002.

[149] T. B. Sheridan and W. R. Ferrell. Remote manipulative control with transmission delay. *Human Factors in Electronics, IEEE Transactions on*, HFE-4(1):25 – 29, Sept. 1963.

[150] J. G. Snodgrass. *Experimental Sensory Psychology*, chapter Psychophysics, pages 17–67. 1975.

[151] J. E. Speich, L. Shao, and M. Goldfarb. Modeling the human hand as it interacts with a telemanipulation system. *Mechatronics*, 15(9):1127 – 1142, 2005.

[152] M. W. Spong and M. Vidyasagar. *Robot Dynamics and Control*. John Wiley and Sons, New York, 1989.

[153] M. A. Srinivasan, B. Eberman, H. Z. Tan, and B. Cheng. Human factors for the design of force-reflecting haptic interfaces. *ASME Dynamic Systems and Control Division*, 1:353–359, 1994.

[154] B. Stanczyk. *Developement and Control of an Anthropomorphic Teleoperator*. PhD thesis, Technische Universität München, Lehrstuhl für Steuerungs- und Regelungstechnik, 2006.

[155] B. Stanczyk and M. Buss. Development of a telerobotic system for exploration of hazardous environments. In *Intelligent Robots and Systems, 2004. (IROS 2004). Proceedings. 2004 IEEE/RSJ International Conference on*, volume 3, pages 2532 – 2537 vol.3, Sept.-2 Oct. 2004.

[156] E. Stoll, J. Letschnik, U. Walter, J. Artigas, P. Kremer, C. Preusche, and G. Hirzinger. On-orbit servicing. *Robotics Automation Magazine, IEEE*, 16(4):29 –33, December 2009.

[157] S. Stramigioli, A. van der Schaft, B. Maschke, and C. Melchiorri. Geometric scattering in robotic telemanipulation. *IEEE Transactions on Robotics and Automation*, 18(4):588–596, August 2002.

[158] M. A. Symmons, B. L. Richardson, and D. B. Wuillemin. Active versus passive touch: superiority depends more on the task than the mode. In *Touch, Blindness, and Neuroscience*, pages 179–185. UNED, 2004.

[159] K. Takei, T. Takahashi, J. C. Ho, H. Ko, A. Gillies, P. W. Leu, R. S. Fearing, and A. Javey. Nanowire active-matrix circuitry for low-voltage macroscale artificial skin. *Nature materials*, 9:821–826, 2010.

[160] K. Takei, T. Takahashi, J. C. Ho, H. Ko, A. G. Gillies, P. W. Leu, R. S. Fearing, and A. Javey. Nanowire active-matrix circuitry for low-voltage macroscale artificial skin. *Nature Materials*, Advance Online Publication, 2010.

[161] H. Z. Tan, N. I. Durlach, G. L. Beauregard, and M.A. Srinivasan. Manual discrimination of compliance using active pinch grasp: The role of force and work cues. *Perception and Psychophysics*, 57:495–510, 1995.

[162] H. Z. Tan, M. A. Srinivasan, B. Eberman, and B. Cheng. Human Factors for the Design of Force-Reflecting Haptic Interfaces. *Tan, Srinivasan, Eberman, & Chang, ASME WAM*, pages 1–11, 1994.

[163] K. P. Tee, E. Burdet, C. M. Chew, and T. E. Milner. A model of force and impedance in human arm movements. *Biological Cybernetics*, 90:368–375, 2004. 10.1007/s00422-004-0484-4.

[164] Tekscan. http://www.tekscan.com/ergonomic-grip-pressure-mapping.

[165] L. J. Tognetti. *Improved Design and Performancce of Haptic Two-Port Networks through Force Feedback and Passive Actuators*. PhD thesis, Georgia Institute of Technology, January 2005.

[166] N. Trawny and S. Roumeliotis. Indirect kalman filter for 3d attitude estimation. Technical report, Department of Computer Science & Engineering University of Minnesota, 2005.

[167] T. Tsuji, K. Goto, M. Moritani, M. Kaneko, and P. Morasso. Spatial characteristics of human hand impedance in multi-joint arm movements. In *Intelligent Robots and Systems '94. 'Advanced Robotic Systems and the Real World', IROS '94. Proceedings of the IEEE/RSJ/GI International Conference on*, volume 1, pages 423 –430 vol.1, September 1994.

[168] T. Tsuji, P. Morasso, K. Goto, and K. Ito. Human hand impedance characteristics during maintained posture. *Biological Cybernetics*, 72(6):475–485, May 1995.

[169] J. Vertut, A. Micaelli, P. Marchal, and J. Guittet. Short transmission delay on a force reflective bilateral manipulator. In *Proc. 4th Roman-Symposium, Poland*, 1981.

[170] X. Wang, B. Liang, C. Li, and W. Xu. The ground-based validation technology of teleoperation for space robot. *IEEE Conference on Robotics, Automation and Mechatronics*, pages 342 – 347, 2008.

[171] X. Wang, P.X. Liu, D. Wang, B. Chebbi, and M. Meng. Design of bilateral teleoperators for soft environments with adaptive environmental impedance estimation. In *Robotics and Automation, 2005. ICRA 2005. Proceedings of the 2005 IEEE International Conference on*, pages 1127 – 1132, april 2005.

[172] E. H. Weber. *Die Lehre vom Tastsinn und Gemeingefuehl, auf Versuche gegruendet.* Vieweg: Braunschweig, Germany, 1851.

[173] J. C Willems. Dissipative dynamical systems part i: General theory. *Archive for Rational Mechanics and Analysis*, 45(5):321 – 351, January 1972.

[174] A. Willig, K. Matheus, and A. Wolisz. Wireless technology in industrial networks. *Proceedings of the IEEE*, 93(6):1130 –1151, June 2005.

[175] B. G. Witmer and M. J. Singer. Measuring presence in virtual environments: a presence questionnaire. *Presence*, 7(3):225–240, 1998.

[176] H. Woo and D. Lee. Exploitation of the impedance and characteristics of the human arm in the design of haptic interfaces. *Industrial Electronics, IEEE Transactions on*, PP(99):1 –1, 2009.

[177] M. Wright, A. Green, and S. Baker. Limitations for change detection in multiple garbor targets. *Visual Cognition*, 7:237–252, 2000.

[178] X. D. Yang, W.F. Bischof, and P. Boulanger. Perception of haptic force magnitude during hand movements. In *Proceedings of the International Conference on Robotics and Automation*, pages 2061–2066, Pasadena, CA, USA, May 2008.

[179] Y. Yokokohji, T. Tsujioka, and T. Yoshikawa. Bilateral control with time-varying delay including communication blackout. In *Haptic Interfaces for Virtual Environment and Teleoperator Systems, International Symposium on*, volume 0, page 285, Los Alamitos, CA, USA, 2002. IEEE Computer Society.

[180] Y. Yokokohji and T. Yoshikawa. Bilateral control of master-slave manipulators for ideal kinesthetic coupling-formulation and experiment. *Robotics and Automation, IEEE Transactions on*, 10(5):605–620, Oct. 1994.

[181] X. Yu, J.W. Modestino, and X. Tian. The accuracy of gilbert models in predicting packet-loss statistics for a single-multiplexer network model. In *INFOCOM 2005. 24th Annual Joint Conference of the IEEE Computer and Communications Societies. Proceedings IEEE*, volume 4, pages 2602 – 2612 vol. 4, March 2005.

[182] M. H. Zadeh, D. Wang, and E. Kubica. Perception-based lossy haptic compression considerations for velocity-based interactions. *Multimedia Systems*, 13:275–282, November 2008.

[183] W-H. Zhu and S. E. Salcudean. Teleoperation with adaptive motion/force control. In *Robotics and Automation, 1999. Proceedings. 1999 IEEE International Conference on*, volume 1, pages 231 –237 vol.1, 1999.

[184] W-H. Zhu and S. E. Salcudean. Stability guaranteed teleoperation: an adaptive motion/force control approach. *Automatic Control, IEEE Transactions on*, 45(11):1951–1969, Nov 2000.

[185] M. Zinn, B. Roth, O. Khatib, and J. K. Salisbury. A new actuation approach for human friendly robot design. *The International Journal of Robotics Research*, 23(4-5):379–398, 2004.

Own related publications

[186] R. Bauernschmitt, E.U. Braun, M. Buss, F. Frohlich, S. Hirche, G. Hirzinger, J. Kammerl, A. Knoll, R. Konietschke, B. Kubler, R. Lange, H. Mayer, M. Rank, G. Schillhuber, C. Staub, E. Steinbach, A. Tobergte, H. Ulbrich, I. Vittorias, and Chen Zhao. On the role of multimodal communication in telesurgery systems. In *Multimedia Signal Processing, 2009. MMSP '09. IEEE International Workshop on*, pages 1–6, Oct. 2009.

[187] F. Brandi, R. Chaudhari, S. Hirche, J. Kammerl, E. Steinbach, and I. Vittorias. Perceptual haptic data reduction in telepresence and teleaction systems. *Multimedia Communication Technical Committee E-Letter*, 6(1):7–10, 2011.

[188] J. Kammerl, I. Vittorias, V. Nitsch, B. Faerber, E. Steinbach, and S. Hirche. Perception-based data reduction for haptic force-feedback signals using adaptive deadbands. *MIT Press Journals, Presence: Teleoperators and Virtual Environments*, 19(5):450–462, October 2010.

[189] E. Steinbach, S. Hirche, M. Ernst, F. Brandi, R. Chaudhari, J. Kammerl, and I. Vittorias. Haptic communications. *Proceedings of the IEEE, Special Issue on Frontiers of Audiovisual Communications: Converges of Broadband, Computing and Rich Media*, 100(4):937–956, April 2012.

[190] E. Steinbach, S. Hirche, J. Kammerl, I. Vittorias, and R. Chaudhari. Haptic data compression and communication. *Signal Processing Magazine, IEEE*, 28(1):87 –96, Jan. 2011.

[191] I. Vittorias, H. Ben Rached, and S. Hirche. Haptic data reduction in multi-dof teleoperation systems. In *Haptic Audio-Visual Environments and Games (HAVE), 2010 IEEE International Symposium on*, pages 1 –6, Oct. 2010.

[192] I. Vittorias and S. Hirche. The generalized scattering transformation for stable teleoperation with communication unreliabilities. In *Workshop on Network Induced Constraints in Control (NETCOC)*, September 2009.

[193] I. Vittorias and S. Hirche. Stable teleoperation with communication unreliabilities and approximate human/environment dynamics knowledge. In *American Control Conference (ACC), 2010*, pages 2791 –2796, July 2010.

[194] I. Vittorias and S. Hirche. Transparency of the generalized scattering transformation for haptic telepresence. In Astrid Kappers, Jan van Erp, Wouter Bergmann Tiest, and Frans van der Helm, editors, *Haptics: Generating and Perceiving Tangible Sensations*, volume 6191 of *Lecture Notes in Computer Science*, pages 183–188. Springer Berlin / Heidelberg, 2010.

[195] I. Vittorias and S. Hirche. Improved transparency of networked teleoperation through a dissipativity-based control approach. *IEEE Transaction on Robotics*, 2011. submitted.

[196] I. Vittorias, J. Kammerl, S. Hirche, and E. Steinbach. Perceptual coding of haptic data in time-delayed teleoperation. In *EuroHaptics conference, 2009 and Symposium on Haptic Interfaces for Virtual Environment and Teleoperator Systems. World Haptics 2009. Third Joint*, pages 208–213, March 2009.